UNIVERSITY OF INSUBRIA

Doctoral School of Biological and Medical Sciences

Ph.D in Neurobiology

CHARACTERIZATION OF THE NEOCORTICAL NETWORK EXCITABILITY WITH MULTIELECTRODE ARRAYS: ALTERATIONS IN MIGRAINE AND EPILEPSY MOUSE MODELS

Supervisor: *Dr. Lia Chiara Forti*

Co-supervisor: *Prof. Riccardo Fesce*

Coordinator: *Prof. Daniela Parolaro*

Ph.D. thesis of:

Albina Locarno

XXVI Cycle - 2010/2013

TABLE OF CONTENTS

Abstract

The neocortex is organized in repeating functional microcircuits, or modules, composed of various neuron subtypes. Each module performs basic signal transformations, which are then integrated with the activity of other modules in more extended brain areas (Lübke & Feldmeyer 2007). An ultimate goal of basic research is to unravel the information processing capability of this neocortical microcircuit and comprehensively understand higher cognitive functions. Luckily, the bewildering complexity of the microcircuits at the single cell level gives rise to surprisingly robust emergent activity patterns at the level of laminar and columnar local field potentials (LFPs). Although the precise correspondences between single cell activities and LFPs are still far from clear, multi-site LFP recording in the standardized slice preparation proves a suitable tool for comparing normal conditions to genetically altered situations based on native cortical microcircuitry.

In this work we assessed the potential of using micro-electrode arrays (MEA) to investigate several physiological properties of the mouse barrel cortex microcircuit by simultaneously recording from all the six cortical layers *ex vivo*. We describe a cortical-layer-specific pattern of response to electrical stimulation, and we report for the first time MEA recordings of the spontaneous recurrent activity in mice thalamocortical slices. MEA have enabled convenient analysis of activity-dependent changes of neuronal responses to electrical stimulation even at late developmental stages, which are less easily accessible to patch-clamp recordings.
More in detail, the two projects developed in this thesis aim at investigating the pathophysiology of two distinct episodic brain disorders by comparing genetic mouse models with their wild-type (WT) counterparts. This helps adding a little piece to the complex mosaic of cortical circuits studies. The two genetic mouse models employed are: the R192Q knock-in (KI) mouse, carrying a P/Q type Ca^{2+} channel mutation found in familial hemiplegic migraine type I, and the Synapsin I/II/III triple knockout (TKO) mouse, which shows an epileptic phenotype. Two different kinds of activity have been observed and analyzed: evoked activity in response to stimulation in layer 4 (by an isolated stimulus or a short train at 50 Hz), and spontaneous network activations ("up-states").

The first project concerns the investigation of the still unclear pathogenetic mechanisms of migraine, a complex neurological condition. Mutations in the gene encoding the pore-forming α1 subunit of voltage-gated $Ca_V2.1$ (P/Q-type) Ca^{2+} channels cause a rare subtype of migraine with aura: familial hemiplegic migraine type 1 (FHM1). KI mice carrying the R192Q FHM1 mutation show: increased P/Q-type current density in central neurons, increased strength of excitatory

synaptic transmission at synapses from pyramidal cell to fast-spiking interneuron, and unaltered inhibitory neurotransmission at the reciprocal fast-spiking interneuron to pyramidal cell synapses (Tottene et al., 2009). These differential effects suggest the episodic disruption of the excitation-inhibition balance as a possible cause of increased susceptibility to cortical spreading depression, the phenomenon that underlies migraine aura, and is a likely trigger of the migraine headache mechanisms. To test whether the differential alterations of neocortical excitatory and inhibitory synapses produce altered network activity, we recorded evoked and spontaneous LFPs from thalamocortical slices of matched WT and KI mice. Upon electrical stimulation in L4 with short 50 Hz trains, evoked LFPs are characterized by a negative peak that shows significantly larger short-term depression in KI mice. In both strains spontaneous field potential oscillations (up-states) start in layer 2/3 (L2/3), 4 (L4), or 5 (L5), and then propagate to the entire cortical column of origin and to nearby columns. Up-state frequency was significantly higher in KI than in WT mice, a larger percentage of events started in L2/3, and propagation from L2/3 to L5 was slower, while propagation in the reverse direction (L5 to L2/3) was faster. The strength of up-states was largest in L2/3 in KI, but not in WT slices. Overall, the analysis of evoked LFPs and spontaneous up-states revealed clearly different network excitability in WT and KI networks, suggesting stronger L2/3 excitability in KI mice.

The second part of this thesis reports a preliminary investigation of epilepsy pathogenetic mechanisms. Synapsins (Syn I, Syn II, and Syn III) are a family of synaptic vesicle phosphoproteins regulating synaptic transmission, development and plasticity, and SYN1/2 genes have been identified as major epilepsy susceptibility genes in humans. Syn I/II/III triple knockout (TKO) mice exhibit adult-onset epilepsy, so that the events that precede the seizures phase can be studied. Network activity has been demonstrated to be enhanced in the brain of these mice before the onset of epilepsy (Boido et al., 2010). Moreover, patch-clamp recordings from acute TKO cortico-hippocampal slices showed differential changes of excitatory and inhibitory transmission, and a deficit in tonic γ-amino-butyric acid (GABA) current, resulting in increased excitability of hippocampal pyramidal neurons (Farisello et al., 2013; Ketzef & Gitler, 2012). To test whether such changes influence the local network activity in the somatosensory cortex of pre-symptomatic young TKO mice, we recorded with MEAs evoked and spontaneous LFPs from thalamocortical slices of matched WT and TKO mice. A preliminary analysis shows that i) LFPs evoked by electrical stimulation in L4 display faster time-to-peak in all layers; ii) stimulation with short 50 Hz trains produces similar short-term depression and recovery from depression in all cortical layers in both strains, and ii) spontaneous up-states frequency is significantly higher in TKO mice.

In both projects, the experimental approach has fulfilled the expectations for MEA to generate new hypotheses about how known molecular and cellular alterations affect the neuronal network activity. Of course, further validation is needed, but the results presented here could be a good starting-point to unravel network dynamics alterations in diseases with a poorly understood etiology, such as episodic brain disorders. Our study paves the way to future electrophysiological studies combining MEA and patch-clamp recordings devoted to better clarifying the role of single neurons in neuronal ensemble activation.

1. INTRODUCTION

1.1 MEA recordings in the neocortex to investigate episodic brain disorders

The present study is focused on the description of cortical dynamics in healthy conditions and in the two most common episodic brain disorders: migraine and epilepsy. Although these pathologies have been observed and described for centuries, only in the past decades basic research studies have started to unravel the underlying molecular mechanisms, and in doing so they have also furthered our understanding of the mammalian brain physiology.

Electroencephalography (EEG) is one of the oldest and most widely used methods to investigate the electrical activity of the brain. EEG uses electrical leads placed all over the scalp to measure the collective electrical activity of the cerebral cortex. Since in a volume of brain tissue all currents, originated by neuronal activity, superimpose at any given point in space and generate a potential (with respect to a reference potential), the difference in potential between two locations yields a time-varying electric field that can be monitored by extracellular electrodes. Specifically, EEG measures the electric fields of thousands or millions of polarized neurons with similar spatial orientation. Pyramidal neurons of the cortex are thought to produce most of the EEG signal because they are well-aligned and fire together. EEG has excellent temporal resolution: it has been, and still is, a successful clinical tool to compare between healthy and pathological conditions, especially when millisecond-range temporal resolution is required, as in the case of epilepsy, where clear abnormalities appear on a standard EEG study (Markand, 2003). Another clinical use of the EEG is to study sleep and sleep disorders. However, EEG records lack discernible relationship with the activity of the contributing individual neurons. Indeed, because voltage fields of dipole[1]-like charge distributions decrease with the square of distance, activity from deep sources is more difficult to detect than currents near the skull (Buzsáki et al, 2012), so that EEG mainly samples electrical activity that occurs in the superficial layers of the cortex.

To characterize neuronal circuits at deeper locations, experimental recordings from brain slices are commonly employed (Buzsáki et al, 2012). Thanks to this *ex-vivo* preparation much is known about the individual neurons that, locally interconnected, constitute the microcircuits. The morphological and electrophysiological properties of these cells have been described, and several excitatory or inhibitory types have been identified (reviewed in DeFelipe et al., 2013; Ascoli et al., 2008). In

[1] An ideal electric dipole is defined by two charges of opposite polarity, separated by an infinitely small distance, r. The electric potential of a dipole falls off as $1/r^2$.

addition, paired and multiple simultaneous recordings from individual cells have been performed, providing important information on the interactions in such elementary circuits (reviewed in Gutnick & Crill 1995 and Lübke & Feldmeyer, 2007). Nevertheless, when we consider the role of microcircuits in larger units, such as layers and columns of the cerebral cortex, only multi-site extracellular recording techniques bear the promise to help us characterize and understand collective phenomena of neuronal populations. Microelectrode arrays (MEA) are among these well established methods, employed to study the dynamics of neural ensembles. Planar MEAs are devices utilized in biomedical and basic in vitro research to provide extracellular electrophysiological information about biological systems. A high spatial and temporal resolution is achieved as MEAs record the extracellular field potentials, called local field potentials (LFP), generated by the superposition of local transmembrane currents flowing through neuronal compartments of several neurons[2]. A variety of MEAs are available for electrophysiological measurements. In most commercially available systems (e.g., Multi Channel Systems GmbH, Germany; Panasonic Inc., Japan; Plexon Inc., USA), passive metal electrode arrays are exploited. These devices usually consist of 64 electrodes aligned on a glass or silicon substrate with externally positioned signal recording and filtering components (Jones et al., 2011).

In trying to elucidate the pathogenic aspects of migraine and epilepsy, brain slices have already been employed and cellular excitability dysfunctions have been described (Tottene et al, 2009; Farisello et al., 2013; see also paragraphs 1.3.5 and 1.4.1, respectively).

In migraine and epilepsy, as in other episodic neurological disorders, neurological function is impaired in the patient during an attack, while it is usually completely normal between attacks. Episodes are often triggered by mundane stimuli, such as hunger, emotions, diet, or hormones. Why these commonplace stimuli trigger episodes of neurologic impairment in some patients but not others is poorly understood. Most episodic neurological disorders are genetically complex, with unknown or polygenic inheritance, and the disease course seems to be driven by environmental influences rather than by genetic factors. In contrast, a number of episodic disorders exhibit Mendelian inheritance: in these rare disorders, which share a striking similarity with the complex disorders, single gene mutations are sufficient to cause disease. Most of these known mutations alter genes that encode membrane-bound ion channels, while others alter the genes of proteins that

[2] The extracellular potential, generated by transmembrane currents evoked by synaptic and spiking activity of neurons, can be divided into high- and low-frequency components, usually referred to as multiunit activity (MUA) and local field potential (LFP), respectively (Pettersen et al., 2007). The low-frequency component ($f \lesssim 300Hz$), or LFP, emphasizes synchronized postsynaptic activity of cortical pyramidal cells, which are aligned perpendicularly to the pial surface, creating a superposition of fields (Nunez & Srinivasan, 2006). Both excitatory (Mitzdorf, 1985) and inhibitory (Hasenstaub et al., 2005) postsynaptic potentials (PSPs) contribute significantly to LFP. Propagation of action potentials along axons, on the other hand, has been estimated to yield a minimal contribution to LFP (Mitzdorf, 1985).

regulate channel function or synaptic transmission. In general, dysfunctions at the synaptic and neuronal circuit levels likely underlie these disorders (Russell et al. 2013).

A promising way to access these neuronal networks alterations is using MEAs to measure electrical activity in genetic models of the diseases (Boido et al, 2010). MEAs record spontaneous and evoked LFPs from ensembles of neurons in acute cortical slices (Beggs & Plenz, 2003; Wirth & Luscher, 2004) and let us compare the network behavior of healthy cortical microcircuits with genetically modified ones. Figure 1.1 shows an example of evoked LFPs recorded simultaneously with a 60 channel MEA chip from a slice of rat barrel cortex. Electrodes are aligned in an 8x8 grid with empty corners; in this example, stimulation is in supragranular layers and each signal represents the near simultaneous discharge of a group of local principal neurons (Bakker et al., 2009). Since MEAs have proved suitable for providing insight into basic neural networks processes, this thesis is focused on the description of the deviations from normal excitability in a genetic model of migraine and in a genetic model of epilepsy through the characterization of the network behaviour with MEA slice recordings.

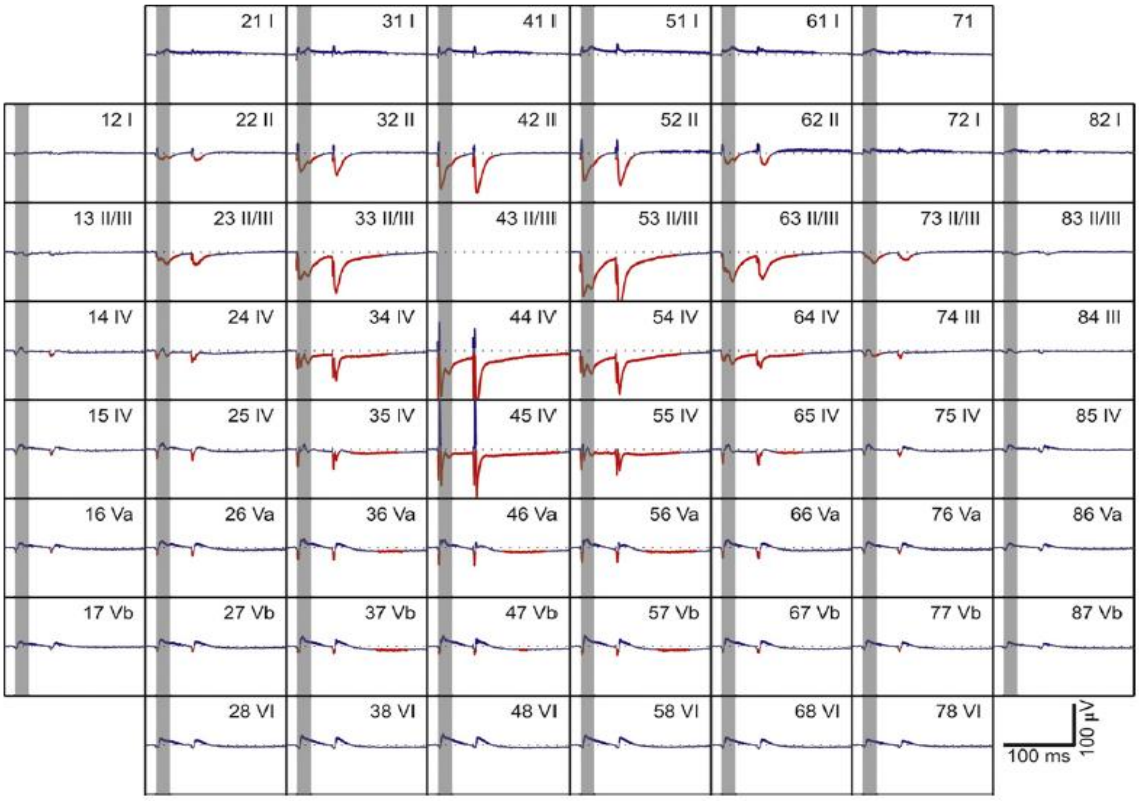

Figure 1.1. An example of evoked LFPs recorded simultaneously with a 60 channel MEA chip from a slice of rat barrel cortex. The vertical grey bars mark the first 20 ms of the first response. Negative voltages are highlighted in red if they fall below the noise threshold. Each trace is labelled with the channel number and the functional cortical layer. This information is obtained from photomicrographs made during the experiment. Taken from Bakker et al, 2009.

1.2 The neocortex: cells are organized in layers and columns

The neocortex, the furrowed gray matter overlying each brain hemisphere, constitutes nearly 80% of the human brain, and is composed of a variety of neuron subtypes interconnected (mostly within vertical columns) along up to six horizontal layers (Markram et al., 2004).

- Layer 1 (L1)[3] is the most superficial, located right beneath the pia mater, and consists of the dendrites of the cells located deeper in the cortex and of the axons that travel through or form connections in this layer.
- Layer 2 (L2) is comprised mainly of small spherical cells called granule cells.
- Layer 3 (L3) contains a variety of cell types, many of which are pyramidally shaped; the neurons located deeper in L3 are typically larger than those located more superficially.
- Layer 4 (L4), like L2, is made up primarily of granule cells (also named spiny stellate cells as they are star-shaped and with spiny dendrites) and is called the internal granule cell layer.
- Layer 5 (L5) contains mainly pyramidally shaped cells typically larger than those in L3 and has been subdivided into a cell-sparse layer 5A, containing mostly medium-sized pyramidal cells, and a cell-dense layer 5B containing pyramidal neurons of variable size.
- Layer 6 (L6) is a fairly heterogeneous layer of neurons. It blends into the white matter that forms the deep limit of the cortex and carries axons to and from the cortex.

Functionally, these layers can be divided into three groups: the supra-granular layers, L1-3, that contain the apical dendrites of neurons having their cell bodies in L5 and L6; the internal granular layer, L4, receiving thalamocortical connections from specific thalamic nuclei; and the infra-granular layers, L5 and L6, that contain the basal dendrites of neurons with cell bodies in L3 and L4. Laminar organization differs among different cortical regions. For example, sensory cortices have a more prominent L4 than the motor cortex. The latter feature can be understood in relation to thalamic connectivity. L4 is the main target of sensory information arriving from the thalamus. The motor cortex, which is primarily an output region of the neocortex, receives little sensory information directly from the thalamus (Amaral, 2000).

The neurons of the cortex, as elsewhere, can be broadly divided in two categories: projection neurons and local interneurons. Projection neurons have pyramidally shaped cell bodies. They are located mainly in layers 3, 5, and 6 and use the excitatory amino acid glutamate as their primary

[3] L1 is a major target of feedback connections between cortical areas and also receives input from subcortical nuclei. The existence of L1, specialized for the connection between distal dendrites and cortical and subcortical inputs, points to a general purpose of cortical lamination: generate a scaffold that constrains the way in which neurons can connect. This principle alone may be the reason why the brain makes such extensive use of cortical structures allowing neurons to connect with each other with the minimum use of wire (Douglas & Martin, 2004).

transmitter. Local interneurons use the inhibitory neurotransmitter γ-amino-butyric acid (GABA), constitute around 15% of the neurons in the neocortex (Beaulieu 1993; Fishell & Rudy, 2011), and are located in all layers where they do not generally create long range projections with their axon. Several types of GABAergic interneurons have been distinguished based on their morphological diversity, in particular their axonal arborization and, as a consequence, their postsynaptic targets. Some have axons that terminate on the cell bodies of target neurons (basket cells). Other interneurons have axons that terminate exclusively on the axons of target neurons; the multiple arrays of synaptic terminals formed by these GABAergic axons resemble a chandelier, and these cell types are called chandelier cells; Martinotti cells are still another type and target distal apical dendrites of pyramidal cells. Morphological differences and axonal targets are not the only differential properties of cortical inhibitory neurons: they can also be subdivided based on intrinsic electrophysiological properties, synaptic characteristics, and protein expression patterns (Ascoli et al., 2008; Fishell & Rudy, 2011; Isaacson & Scanziani, 2011). A large GABAergic neuronal population expresses the Ca^{2+}-binding protein parvalbumin (PV); some GABAergic neurons contain neuro-active peptides, such as somatostatin, cholecystokinin, or the opiate peptides. The neocortex also has a population of excitatory interneurons, located primarily in L4. These cells have a stellate plexus of dendrites, use the amino acid glutamate as a transmitter, and form synapses with neurons near the cell body. These excitatory interneurons are the primary recipients of sensory information received in the neocortex from the thalamus (Amaral 2000). The profile of inputs to a particular cortical neuron depends more on the distribution of its dendrites than on the location of its cell body.

Neurons in the neocortex are also distributed in functional, vertically oriented columns that traverse the layers. A cortical column is a recurring module of signal processing that would fit within a cylinder of 0.3 - 0.5 mm in diameter. Neurons within a particular column tend to have very similar response properties, presumably because they form a local processing network. The modular concept presumes that the neuronal network in a cortical column performs basic signal transformations, which are then integrated with the activity in other networks and more extended brain areas (Lübke & Feldmeyer, 2007). In rodents, a neocortical column of about 0.3 mm in diameter contains roughly 7,500 neurons: 100 neurons in L1; 2,150 in L2/3; 1,500 in L4; 1,250 in L5 and 2,500 in L6 (Markram et al., 2004).

All the behavioral functions of the brain—processing of sensory information, programming of motor and emotional responses, storing information (memory)—are carried out by specific patterns of interconnected neurons.

The thickness of the neocortex is always found to be between 2 and 4 mm. In other words: the number of neurons stacked on top of each other through the thickness of the cortex is remarkably similar in different cortical regions and in different species. Thus, what mainly differentiates the cerebral cortex of a human from that of a rat is not the thickness of the cortex or the organization of the cortical columns, but the total number of columns. The massive expansion of the surface area of the cerebral cortex in humans accommodates many more columns and thus provides greater computational power (Amaral, 2000).

1.2.1. The rodent primary somatosensory cortex: the barrel cortex

To understand how sensory signals from the periphery are transformed into electrical activity in the neocortex it is essential to elucidate the spatial-temporal dynamics of cortical signal processing and the underlying neuronal microcircuits. The ‘barrel’ field in the rodent somatosensory cortex, which processes sensory information arriving from the mysticial vibrissae, has become a quite attractive model system because here the columnar structure is clearly visible (Lübke & Feldmeyer, 2007). Since mice and rats are nocturnal animals, the whisker system is likely to have evolved to compensate for the poverty of visual information during much of a rodent’s life. The ‘barrel’ cortex is perhaps the most remarkable specialization of this sensory system: each whisker is represented by a discrete and well-defined structure in L4, called 'barrel'; and these L4 barrels are somatotopically arranged in an almost identical fashion to the layout of the whiskers on the snout. This barrel map is in large part genetically specified and forms early in development, so that even dramatic interventions such as peripheral lesions have little effect upon the somatotopic layout of the barrels. The functional organization, postnatal development, and experience-dependent plasticity of the primary somatosensory whisker cortex can therefore be examined in the context of an invariant anatomical somatotopic map (Petersen, 2007).

Depending on the criteria used, anywhere up to ~20 different interneuron subtypes have been described in the barrel cortex. Nonetheless, the most common subtypes can be broadly classified into six distinct categories: parvalbumin (PV)+ (*a*) chandelier or (*b*) basket cells, (*c*) somatostatin (SOM)+ Martinotti cells, (*d*) vasoactive intestinal protein (VIP)+ interneurons (bipolar, bitufted and multipolar cells), (*e*) Reelin+ (nonsomatostatin) interneurons, and (*f*) other poorly defined caudal ganglionic eminence-derived interneurons that do not express VIP or reelin. In total, the two most numerous populations of interneurons are the PV+ fast-spiking (FS) cells and the Martinotti cells. FS cells comprise ~40% of all GABAergic interneurons, and are the most prominent subtype across all cortical layers. They can be divided into two broad classes, basket cells and chandelier

cells, both of which express the Ca^{2+}- binding protein PV. Basket cells target the perisomatic domain of both excitatory and inhibitory neurons and are thought to be the strongest source of inhibition. On the other hand, chandelier cells target the axon initial segment. FS basket cells are by far the most common interneuron subtype and populate all layers except L1. Moreover, despite their common classification as a single interneuron subtype, their connectivity varies in accordance with their laminar position. In L5/6 this population innervates the pyramidal neurons that provide all cortical output. In L4 this population receives thalamic input, is thought to mediate thalamocortical (TC) feed-forward inhibition, and connects to the stellate cell population. In more superficial layers, basket cells provide inhibition to both L5 projecting pyramidal cells as well as commissural[4] and associative[5] projecting pyramidal neurons. FS basket cells also innervate other interneurons including other FS cells (reviewed in Fishell & Rudy, 2011). The second most prevalent inhibitory cell type within the barrel cortex can be loosely classified as Martinotti cells on the basis of their ascending axon and their expression of the neuropeptide SOM. Classically the term Martinotti cell was used for neurons with cell bodies located in L5/6 that send axons to L1. However, the cell bodies of this population, although biased toward deep layers, are present in all cortical layers except L1. This population is also characterized by their targeting distal dendrites and by the strong facilitation produced by the excitatory synapses they receive, a property that substantially influences their function (Silberberg & Markram, 2007). Strikingly, in contrast to the large amount of information that exists on the cellular properties of the various types of cortical inhibitory neurons, knowledge of the specific role that each of them plays in orchestrating cortical activity is extremely limited (Isaacson & Scanziani, 2011).

In the whisker-to-barrel cortex system, sensory information processing is already segregated in the brain stem, giving rise to the so-called lemniscal and paralemniscal pathways, which are relayed through the ventral posteromedial nucleus (VPM) and the posterior medial nucleus (POm) of the thalamus, respectively. These two thalamic nuclei provide feed-forward excitation to the neocortex, but have distinct projection targets in the barrel column. VPM projection neurons send axons to cortical layers 3, 4, 5B, and 6 of the related barrel columns, with the highest axonal density in L4. POm projection neurons send axons mainly to layers 5A and 1 as well as to the so-called septa between the barrels in L4 (Lübke & Feldmeyer, 2007). The lemniscal pathway leads to the so called ‘canonical’ circuit (reviewed in Douglas & Martin, 2004). Observed consistently across species, the canonical circuit provides a scheme for how information may flow vertically in the cortex in response to afferent input. In primary sensory areas, the starting point are intralaminar connections

[4] Commissural projection neurons: neurons that extend axonal projections within the cortex to the opposite hemisphere via the corpus callosum or the anterior commissure.
[5] Associative projection neurons: neurons that extend axonal projections within a single cerebral hemisphere.

between excitatory spiny neurons in L4, the primary target of thalamic input, which is relayed to L2/3 and then to L5 and L6, concomitant with feedback from L5 to L2/3 and L6 to L4 (Figure 1.2). Such vertical organization is linked horizontally by prominent projections within L2/3 and L5. Embedded within this large-scale wiring diagram are local microcircuits in which neurons receive prominent input from neighboring cells (Lübke & Feldmeyer, 2007). The canonical circuit is likely an oversimplified view of the vertical organization of a cortical column. Indeed, recent works have shown that all excitatory neuron types in a cortical column of somatosensory cortex are potentially innervated by at least 90 TC boutons. This can be regarded as the anatomical basis for the initial near-simultaneous representation of a sensory stimulus measured in different neuron types *in vivo*. In addition, excitatory neurons in L3, L5, and L6 have multiple subcellular TC innervation domains (Meyer et al., 2010a, 2010b; Wimmer et al., 2010).

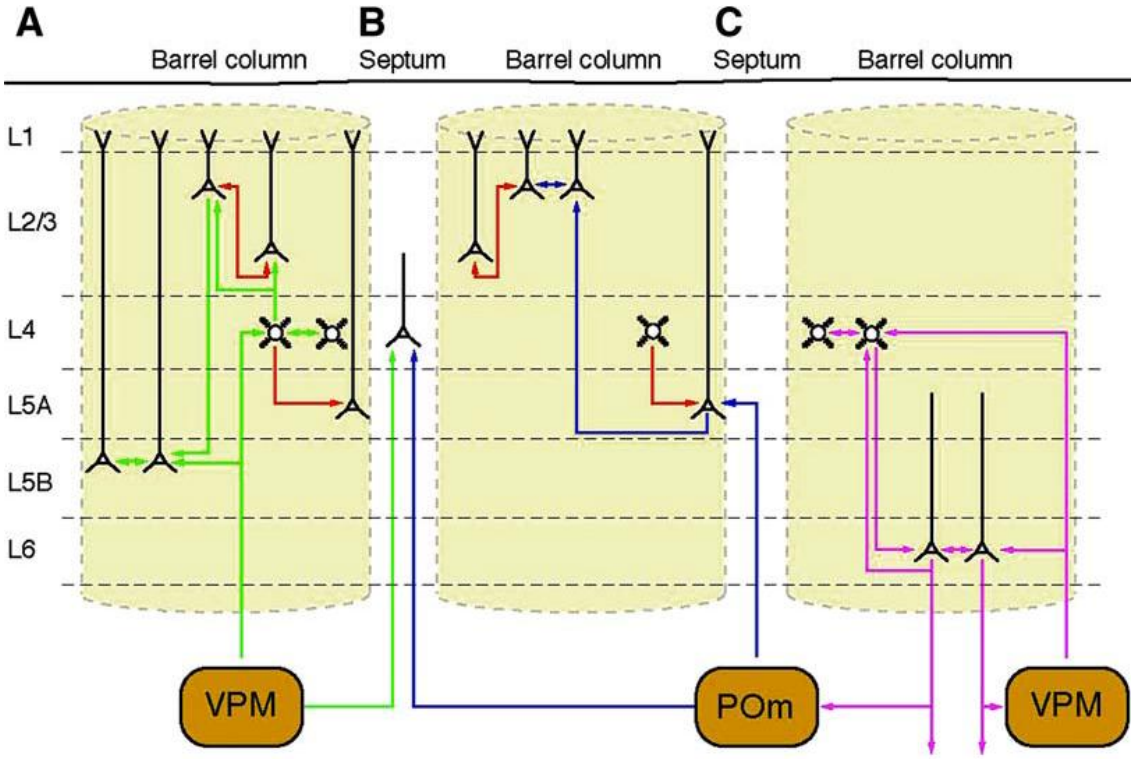

Figure 1.2. Simplified scheme of cortical microcircuits in the barrel cortex. A. The 'canonical' microcircuit receives lemniscal thalamic input from the ventroposterior medial nucleus (VPM) predominantly in L4 (and less in L5B). Information is relayed to L2/3 and then to L5. B. Intracortical microcircuits involved in the processing of signals arriving from the paralemniscal pathway (from posterior medial thalamic nucleus, POm, to L5A pyramidal neurons). C. Synaptic connections involved in the thalamo-cortical-corticothalamic feedback circuit among L4 spiny neurons, L6 pyramidal cells and the VPM. Barrel L4 spiny neurons are intrinsic elements of all three microcircuits. Green: 'canonical' microcircuit, blue: 'paralemniscal' pathway, red: intracortical microcircuits, violet: thalamocortical-cortico-thalamic loop. Taken from Lübke & Feldmeyer, 2007.

1.2.2. Excitation/inhibition balance in the cortex

The major mechanism by which neurons influence one another is by generating action potentials that produce postsynaptic potentials in target structures (Haider & McCormick, 2009). The interactions between GABAergic interneurons and glutamatergic principal cells are reciprocal: interneurons inhibit principal cells and are excited by them. The connectivity between these two neuronal classes is quite high: individual interneurons can inhibit >50% of principal cells located within ~100 µm and receive excitatory input from a large fraction of them (Silberberg & Markram, 2007; Fino et al., 2013). Thus, not only are GABAergic interneurons excited in proportion to the level of local network activity, but they directly influence it through their inhibitory feedback. This simple connectivity pattern is ubiquitous in cortex and forms the basis for so-called feedback or recurrent inhibition (Figure 1.3.A). Of course, not all cortical excitation received by inhibitory interneurons is locally generated. Cortical cells receive excitatory inputs via long-range axons originating from subcortical nuclei, as well as from other cortical regions and different cortical layers. These excitatory afferent inputs diverge onto both principal cells and interneurons, generating feedforward inhibitory circuits (Figure 1.3.B).

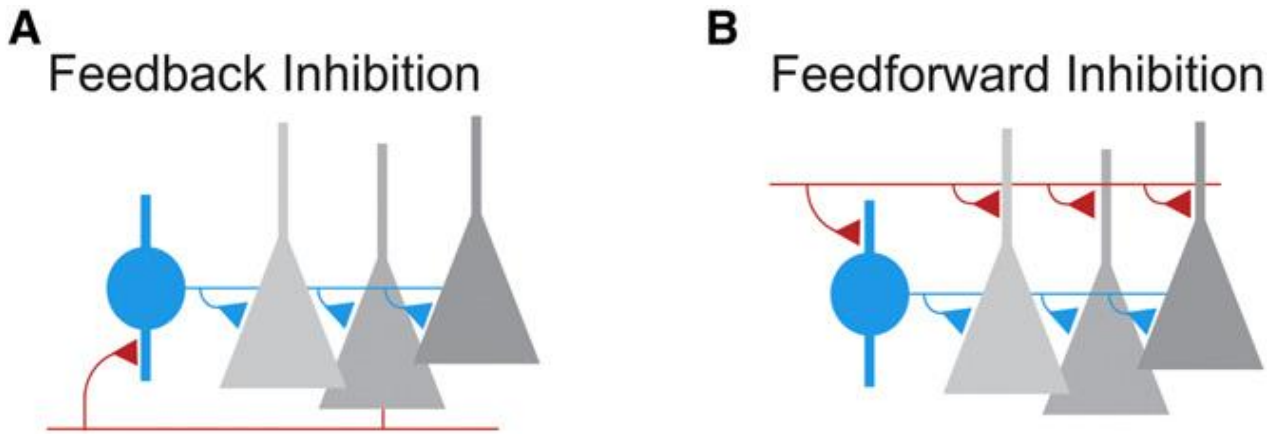

Figure 1.3. Feedback and Feedfoward Circuits are fundamental building blocks of cortical inhibition.
A. Feedback inhibition arises when cortical principal cells (gray) make excitatory synaptic contacts (red) on local interneurons (blue) that in turn form inhibitory synaptic contacts (blue triangles) on the principal cell population. B. Feedforward inhibition is generated when long-range excitatory afferent inputs (red) diverge onto both principal cells and local interneurons. Taken from Isaacson & Scanziani, 2011.

Interestingly, the same afferent fibers make stronger excitatory connections onto interneurons than they do on principal cells, thereby ensuring that even minimal levels of afferent input generate inhibition in cortical circuits (Gabernet et al., 2005). Together, these two simple inhibitory circuits, feedback and feedforward, represent fundamental building blocks of cortical architecture and

account for the fact that cortical excitation and inhibition are inseparable. GABAergic interneurons will be recruited no matter whether excitation is generated locally or received from distant sites. In addition to principal cells, GABAergic interneurons also make inhibitory contacts onto each other and the connectivity between interneurons is highly reciprocal. This mutual connectivity between interneurons is also poised to shape spatial and temporal features of cortical inhibition (Isaacson & Scanziani, 2011).

Synaptic excitation and inhibition are inseparable events in the cortex. Even the simplest sensory stimulus, such as a slight whisker deflection (Wilent & Contreras, 2005), a brief tone, an odor, or an oriented bar in the visual field lead to the concomitant occurrence of synaptic excitation and inhibition in sensory cortices. This co-occurrence of excitation and inhibition is not limited to activity generated by sensory stimuli. During spontaneous cortical oscillations, called ‘up- and down-states’ (see paragraph 1.5.2), for example, excitation and inhibition increase and decrease in parallel (Atallah & Scanziani, 2009; Haider et al., 2006). The corresponding changes in opposed synaptic conductances, impact the membrane potential and input resistance of the neuron and play a fundamental role in regulating neuronal output. In other words, excitatory and inhibitory conductances together govern the computations performed by cortical neurons. Ultimately, their respective strengths and their temporal relationship orchestrate cortical function in space and time (Isaacson & Scanziani, 2011). Therefore, a healthy cortex is a well-balanced cortex. This requires proper regulation of competing influences, from genes, to molecules, neurons, and networks of neurons, proper balance must be achieved in the relative number of excitatory and inhibitory neurons, the strength of excitatory versus inhibitory synapses, the intrinsic excitability of neurons, the tone of neuromodulators, and the expression of synapse-related proteins. Although diverse, these mechanisms share a common property: they all directly or indirectly affect the propensity of one action potential to cause another one. Thus, at the network level, balance may be viewed in terms of the efficacy of signal propagation through the cortex: such balance has surprising and important implications for the dynamics and function of large networks of neurons (Shew & Plenz, 2013).

As would be expected, the excitation/inhibition (E/I) counterbalancing forces are delicately regulated, and Hebbian and complex homeostatic mechanisms are set up by neurons to maintain this dynamic balance over a lifetime (reviewed in Turrigiano, 2011). However, how this E/I balance is established during development is largely unknown. Consistent with the central importance of E/I balance, a variety of neurological and psychiatric disorders are currently viewed as pathologies of brain excitability and are thought to involve or even be caused by disruption of this delicate

equilibrium. Among these pathologies are migraine, mental retardation, Rett syndrome, fragile X syndrome, autism spectrum disorders and epilepsy. A growing number of mutations in genes coding for proteins involved in neurotransmission (such as calcium channels, proton pumps, synaptic vesicle components, pre- and post-synaptic constituents) have been found in familiar cases of these pathologies (Poduri & Lowenstein, 2011; Rajakulendran et al., 2010).

Most of the known mutations involved in migraine and epilepsy affect proteins that are common to all neurons, raising the issue of how impairment of shared mechanisms can differentially affect excitatory and inhibitory tone and induce an E/I imbalance. In principle, small differences in the expression levels and post-translational processing of these proteins – and possible vicariating mechanisms - in distinct neuronal subpopulations can partly explain this phenomenon. However, these mutations are present since the earliest steps of neuronal development. Thus, defects of neurotransmission might primarily alter the development of neuronal circuits at a time when the excitatory and the inhibitory forces are not counterbalanced yet, thereby affecting the E/I balance in the mature organism. This would place the pathogenic mechanism very early in development, even though clinical signs might appear much later.

1.3 Neurobiology and pathophysiology of migraine

Migraine is a common disabling brain disorder (17% of females and 8% of males in the European population) with complex pathophysiology characterized by recurrent attacks of typically throbbing and unilateral, often severe headache, associated with other symptoms such as nausea, phonophobia, and photophobia. In one-third of patients the headache is preceded by transient neurological symptoms (“aura”) that are most frequently visual, but may involve other senses or can cause motor or speech deficits: this type of migraine is called migraine with aura (MA).

Most migraine attacks start in the brain, as suggested by the premonitory symptoms (e.g., difficulty with speech and reading, increased emotionality, sensory hypersensitivity) that in many patients may occur up to 12 h earlier and are highly predictive of the attack, and by the nature of typical migraine triggers: stress, sleep deprivation, oversleeping, hunger, and prolonged sensory stimulation. Moreover, psychophysical and neurophysiological studies have provided clear evidence that in the period between attacks migraineurs show hypersensitivity to sensory stimuli and abnormal processing of sensory information (Welch, 2005; Coppola et al., 2007; Aurora & Wilkinson, 2007; Vecchia & Pietrobon, 2012).

1.3.1 Mechanisms of migraine pain

A large body of indirect evidence supports the prevailing view that the development of migraine headache depends on the activation and sensitization of the trigeminovascular system (Dalkara et al., 2006). Within the skull, pain sensitivity is primarily restricted to the meningeal blood vessels, which are densely innervated by nociceptive sensory afferent fibers of the ophthalmic division of the trigeminal nerve (Pietrobon & Moskowitz, 2013). Activation of these fibers leads to sequential activation (and, in most patients, sensitization) of second and third order trigeminovascular neurons, in the trigeminal nucleus caudalis (TNC) and in specific thalamic nuclei, respectively, which in turn activate different areas of the brainstem and forebrain, resulting in pain and other symptoms of migraine; the bidirectional signaling between many of these areas contributes to the complexity of the symptoms. In several animal models, including non human primates, activation of the meningeal trigeminovascular afferents leads to activation of second order dorsal horn neurons in the TNC and the upper two metamers of the cervical spinal cord. Activation of the trigeminovascular afferents also leads to release of vasoactive neuropeptides contained in their peripheral nerve endings, including calcitonin gene-related peptide (CGRP), substance P (SP) and neurokinin A (NKA). In animal studies the neuropeptides released by trigeminal ganglion stimulation produce vasodilation of the meningeal vessels (mainly due to CGRP), plasma extravasation and mast cell degranulation with secretion of other proinflammatory substances in the dura, leading to neurogenic inflammation (Messlinger 2009).

Evidence that activation of the trigeminovascular system does occur in humans during migraine is provided by the observed increased level of CGRP in both the external and internal jugular blood during migraine attacks, brought back to normal levels after sumatriptan (an anti-migraine drug) treatment, in parallel with headache relief (Pietrobon, 2005a; Pietrobon and Striessnig, 2003). The maintenance of the severe prolonged pain of migraine headache involves sensitization of meningeal nociceptors and self-sustained sensitization of central neurons of the trigeminovascular system; the mechanism, still incompletely understood, may include alterations of descending endogenous pain modulatory pathways (Pietrobon, & Moskowitz, 2013). Although intracranial vasodilation is an appealingly simple explanation for migraine pain, this hypothesis has never been capable of explaining the wide range of symptoms that may precede, accompany, or follow the pain (Charles & Brennan, 2009; Dodick 2008). Indeed, multiple imaging studies have confirmed that vasodilation is not required for migraine headache, which to the contrary, begins during a cortical hypoperfusion phase and may end before the following hyperperfusion phase resolves.

1.3.2 Cortical spreading depression (CSD)

The nature and mechanisms of the primary brain dysfunction(s) leading to episodic activation of the trigeminovascular pain pathway remain incompletely understood and controversial. Given the wide genetic and clinical heterogeneity of migraine, several primary mechanisms presumably exist (Pietrobon & Moskowitz, 2013), but recent findings point to cortical spreading depression (CSD) as a key player in the pathogenesis of migraine (Pietrobon 2005a; Pietrobon and Striessnig, 2003). CSD can be induced in animals by focal stimulation of the cerebral cortex and consists in a slowly propagating (2-6 mm/min) wave of strong depolarization of neurons and glial cells that generates a transient neuronal intense spike activity as it progresses into the tissue, followed by long-lasting neuronal suppression (Charles & Brennan, 2009; Pietrobon, 2005a). The depolarization phase is associated with an initial transient vasodilation followed by an increase in regional cerebral blood flow (rCBF), whereas the phase of reduced neuronal activity is associated with a reduction in rCBF subsequent to a sustained vasoconstriction. Neuroimaging findings indicate that migraine visual aura is due to CSD (Pietrobon and Striessnig, 2003). Migraine visual aura frequently consists in a scotoma (an area of lost vision) with a scintillating border, that usually begins near the centre of vision as a twinkling star and then develops into an expanding circle that slowly move across the visual field towards the periphery. Changes in blood oxygenation level-dependent (BOLD) signals, observed using high field functional magnetic resonance imaging (fMRI) with near-continuous recording during visual aura in three patients, accompanied CSD. Moreover, magnetoencephalography has confirmed the presence of a CSD-like electrical activity during visual aura, as revealed by similarity with the changes in magnetic field induced by focal direct-current (DC) potential changes propagating across the cortex. These observations strongly suggest that an electrophysiological event, namely CSD, generates the aura in human visual cortex (Pietrobon 2005a, 2007). Interestingly, spreading cerebral perfusion changes have also been reported in migraine without aura (MO). This raises the possibility that CSD also occurs in MO patients but does not cause an aura because it originates in a clinically silent area of the cerebral cortex (Dalkara et al., 2006; Pietrobon, 2005a). Animal studies support the idea that CSD may also cause the migraine headache by inducing a large increase in the extracellular concentration of K^+ and H^+ ions, nitric oxide (NO), ATP, arachidonic acid, and prostaglandins (Pietrobon 2005a, 2007). Many of these substances are able to activate the meningeal trigeminovascular afferents, either directly or by causing perivascular inflammation (Figure 1.4; Charles & Brennan, 2009; Pietrobon, 2005a).

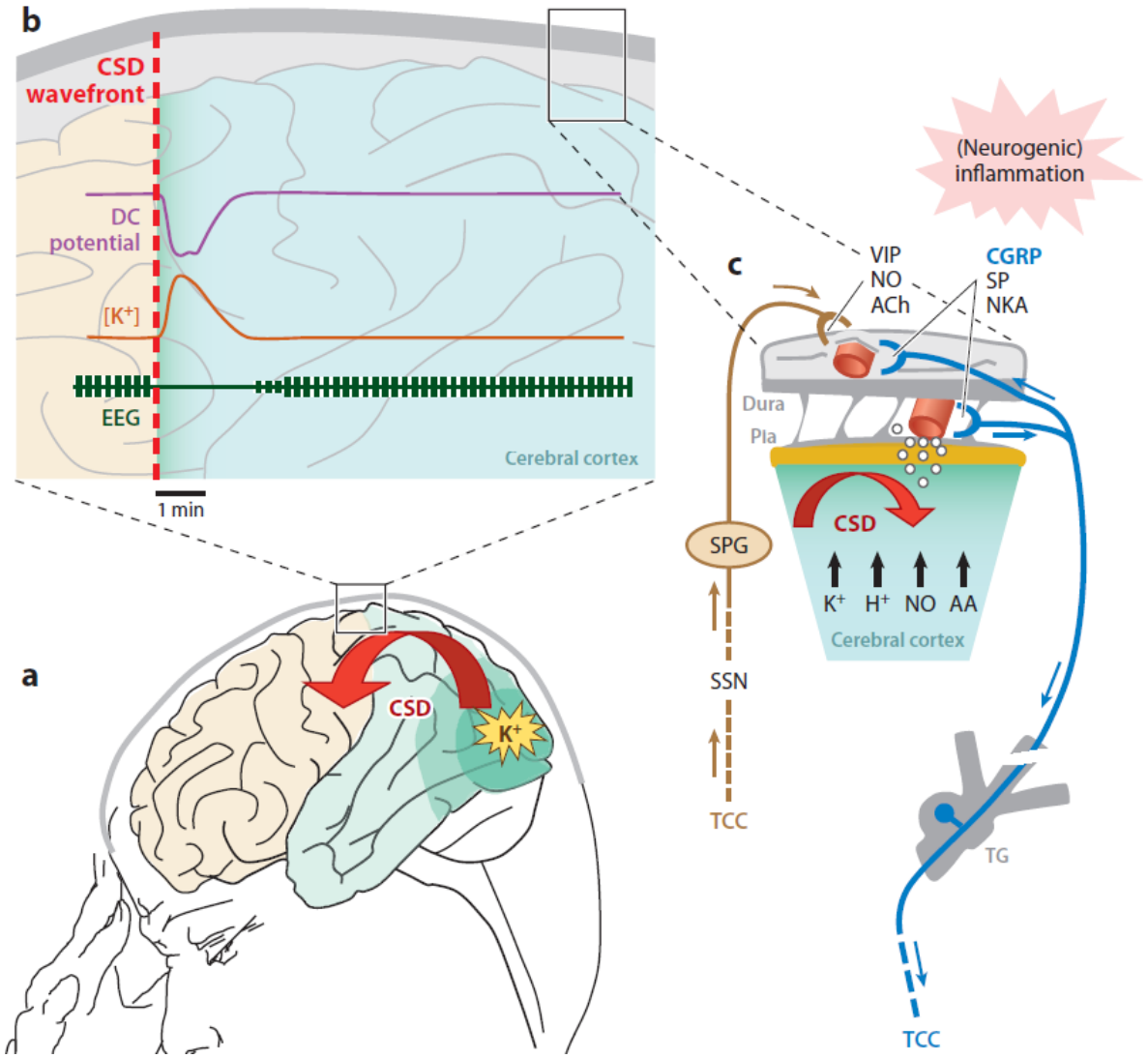

Figure 1.4. From cortical spreading depression (CSD) to trigeminovascular nociception. (*a*) CSD is believed to be ignited by local elevations of extracellular [K^+] above a critical level as a consequence of hyperactive neuronal circuits in the cerebral cortex. (*b*) CSD is a slowly propagating wave of strong neuronal and glial depolarization [see direct-current (DC) cortical potential trace] accompanied by depression of spontaneous and evoked electroencephalographic (EEG) activity and by a large increase in extracellular [K^+]. (*c*) Other noxious mediators (*open circles*), such as H^+, nitric oxide (NO), arachidonic acid (AA), and serotonin, are released during CSD, in addition to glutamate and other neurotransmitters. These substances are thought to activate trigeminal nociceptors innervating pial blood vessels and, via axon collaterals, dural trigeminal afferents, leading to activation of central trigeminovascular neurons in the trigeminocervical complex (TCC; *blue pathway*). Activation of the meningeal afferents leads to release of proinflammatory vasoactive neuropeptides, including calcitonin gene–related peptide (CGRP), substance P (SP), and neurokinin A (NKA), that may promote neurogenic inflammation in the dura and possibly sustain the activation of the trigeminovascular afferents and lead to their sensitization. Alternatively, mediators released by the CSD wave may lead to sensitization and ensuing activation of meningeal nociceptors. Also shown is a parasympathetic reflex involving activation of the superior salivatory nucleus (SSN) and the sphenopalatine ganglion (SPG) leading to release of vasoactive intestinal peptide (VIP), NO, and acetylcholine (ACh) from the meningeal parasympathetic efferents. TG: trigeminal ganglion. Adapted from Pietrobon & Moskowitz, 2013.

Five clinically used migraine prophylactic drugs, which are effective in reducing the frequency of migraine attacks with or without aura, suppress CSD susceptibility (Ayata et al., 2006). All these findings support the hypothesis that CSD may trigger migraine in patients with aura, as well as in patients that present attacks without aura (Pietrobon, 2007).

The mechanisms that make the brain of migraineurs susceptible to episodic "spontaneous" CSDs in response to specific triggers (which might coincide with known migraine triggers such as stress or intense, repetitive long lasting sensory stimulation) are unknown. Migraineurs are hypersensitive to any kind of sensory overload and there is strong evidence for altered cortical excitability and abnormal processing of sensory information in their brain in the period between migraine attacks (Aurora and Wilkinson, 2007; Coppola et al., 2007). The mechanisms underlying the interictal abnormalities in cortical activity are controversial and their relationship to susceptibility and/or occurrence of CSD is unclear. Regardless of whether CSD, as it is observed in animal models, is a trigger of a migraine attack in humans, it is clear that investigation of CSD can provide meaningful information about basic migraine mechanisms (Charles, 2010).

1.3.3 Disfunctional regulation of cortical excitability in migraineurs

Psychophysical and neurophysiological studies have provided clear evidence that in the period between attacks migraineurs show hypersensitivity to sensory stimuli and abnormal processing of sensory information, characterized by increased amplitudes and reduced habituation of evoked and event-related potentials (Brighina et al., 2009; Pietrobon & Moskowitz, 2013). To understand the primary mechanisms of migraine attacks, it seems essential to understand the mechanisms underlying the interictal abnormal processing of sensory information, how they are affected by migraine triggers, and the nature of the relationship between these mechanisms and susceptibility to CSD. The analysis of interictal cortical excitability using electrophysiology, transcranial magnetic stimulation (TMS), and fMRI has produced contradictory findings and interpretations regarding the mechanisms underlying the abnormal processing of sensory information (including trigeminal nociception) in migraineurs. Depending on the study, the cortex of migraineurs has been reported to be hyperexcitable, as a consequence of either enhanced excitation or reduced inhibition, or hypoexcitable (Pietrobon & Moskowitz, 2013). Recent TMS studies in MA patients point to deficient regulatory mechanisms of cortical excitability, rather than merely hypo- or hyperexcitability, and to the consequent impairment in dynamically maintaining the cortical E/I balance and preventing excessive cortical excitation, as the mechanisms underlying abnormal sensory processing (Antal et al., 2008; Conte et al., 2010; Siniatchkin et al., 2011). The molecular

and cellular mechanisms underlying the abnormal regulation of cortical function and its periodicity remain largely unknown. Possible hypothetical mechanisms include: alterations in the cortical circuits that dynamically maintain the E/I balance, essential for correctly processing sensory information and for preventing overexcitation (Shu et al., 2003), and alterations of cortical neuromodulation by serotonergic, noradrenergic, or cholinergic inputs from the brain stem. The extent to which some of the cortical and/or subcortical alterations are affected by disease duration (e.g., repetitive CSDs) is unclear. Equally unclear is the whether the abnormal processing of trigeminal nociceptive input reflects a primary dysregulation of central sensory processing or central sensitization persisting outside the attack (Pietrobon & Moskowitz, 2013).

1.3.4 Familial hemiplegic migraine type 1 (FHM1)

Migraine generally is a complex genetic disorder with polygenic multifactorial inheritance and recent genome-wide association studies have identified a few risk factors for both MA and MO that map within or near transcribed regions of potentially interesting genes. However, most of our present molecular understanding of migraine comes from studies of familial hemiplegic migraine (FHM), a rare, monogenic, autosomal dominant form of MA, characterized by onset in childhood and intermittent motor weakness or paralysis (often, but not always, unilateral) lasting for hours to days (Pietrobon, 2007; Pietrobon & Moskowitz, 2013). Three FHM causative genes have been identified, all encoding ion channels or transporters. Among them, familial hemiplegic migraine type 1 (FHM1) is caused by missense mutation in the *CACNA1A* gene, which is located at chromosome 19p13, and encodes the pore-forming α_{1A} subunit of human voltage-gated $Ca_V2.1$ (P/Q-type)[6] calcium channels (Vecchia & Pietrobon, 2012).

Voltage-dependent Ca^{2+} channels are multisubunit complexes composed of a pore-forming and voltage sensing α_1 subunit, and several auxiliary subunits[7] encoded by different genes. Although these auxiliary subunits modulate the properties of the channel complex, the pharmacological and electrophysiological diversity of Ca^{2+} channels arises primarily from the existence of multiple α_1 subunits (Catterall et al., 2005). The α_1 subunit is composed of about 2000 amino acid residues

[6] According to the rational nomenclature of voltage gated calcium channels (Ertel et al., 2000), Ca^{2+} channels are named using the chemical symbol of the principal permeating ion (Ca) with the principal physiological regulator (voltage) indicated as a subscript (Ca_V). The numerical identifier corresponds to the Ca_V channel α_1 subunit gene subfamily (1 to 3 at present) and the order of discovery of the α_1 subunit within that subfamily (1 through *n*). The complete amino acid sequences of these α_1 subunits are more than 70% identical within a subfamily but less than 40 % identical among subfamilies. According to this nomenclature, the Ca_V2 subfamily ($Ca_V2.1$ through $Ca_V2.3$) includes channels containing α_{1A}, α_{1B}, and α_{1E}, which mediate P/Q-type, N-type, and R-type Ca^{2+} currents. The different α_1 subunits are expressed at different sites, where they mediate different physiological processes (Catterall et al., 2005).

[7] Auxiliary subunits of Ca_V channels include β, $\alpha_2\delta$ and in some cases γ subunits.

organized in four homologous domains (I-IV), each consisting of six-transmembrane α helices (S1 through S6) and a membrane-associated P loop between S5 and S6 (Catterall et al., 2005). The S4 segment has been shown to play a major role in voltage sensing, whereas the P loop between S5 and S6 in each domain forms the pore. Mammalian α_1 subunits are encoded by at least ten distinct genes (Vecchia & Pietrobon, 2012).

$Ca_V2.1$ channels are located in presynaptic terminals and somatodendritic membranes throughout the mammalian brain. They are expressed in all brain structures that have been implicated in the pathogenesis of migraine and/or migraine pain, including the cerebral cortex, the trigeminal ganglia, and brainstem nuclei involved in the central control of nociception, and their expression is particularly high in the cerebellum (Pietrobon & Striessnig, 2003). $Ca_V2.1$ channels play a prominent role in initiating action potential-evoked neurotransmitter release at central nervous system synapses (Pietrobon, 2005b; Catterall & Few, 2008). At many central synapses P/Q-, N- and R-type Ca^{2+} channels cooperate in controlling neurotransmitter release, but P/Q-type channels have a dominant role, partly because of a more efficient coupling to the exocytotic machinery. Fast synchronous release is elicited by local Ca^{2+} transients produced by the opening of a few Ca^{2+} channels, located in close proximity to the Ca^{2+} sensors on readily releasable vesicles, through specific interactions with multiple proteins of the active zones (Catterall & Few, 2008). P/Q channels are involved in synaptic transmission at the main synapses of the neuronal microcircuits in the cerebral cortex. Excitatory synaptic transmission at pyramidal cell synapses in various cortical areas predominantly depends on P/Q-type Ca^{2+} channels (Tottene et al, 2009; Sessolo et al., 2011). The pharmacology of Ca^{2+} channels initiating inhibitory neurotransmission in the cortex has only been investigated at the synapses between fast-spiking (FS) interneurons, and SOM+ interneuron (Martinotti cells) and pyramidal cells in L2/3; neurotransmission was found to be predominantly dependent on P/Q-type Ca^{2+} channels (Tottene et al., 2009; Sessolo et al., 2011).

All the 21 FHM1 missense mutations, reported so far, result in substitutions of conserved amino acids in important functional regions of the $Ca_V2.1$ α_1 subunit (Figure 1.5; de Vries et al., 2009). Occasionally, hemiplegic migraine patients are encountered outside FHM1 families, although they may display the clinical symptoms of FHM1 (Pietrobon, 2007).

Typical FHM1 attacks are characterized by unilateral and pulsating moderate-to severe headache (lasting 4 to 72 hours), preceded by the obligatory motor aura and often accompanied by nausea, phonophobia and photophobia (Pietrobon, 2007). Nearly always, three to four kinds of aura symptoms are present in FHM1 attacks (typically in the temporal order: visual, sensory, motor, aphasic), and they last longer than in MA (in MA they rarely exceed 60 minutes duration). Usually MA only exhibits visual symptoms, but the appearance and progression of the visual percept are

similar in MA and FHM1. Also the duration of the headache is usually longer in FHM1 than MA, but all other headache characteristics are similar. In addition to typical FHM1 attacks, some patients can have atypical severe attacks followed by fever, aphasia, prolonged hemiplegia lasting several days, impairment of consciousness or confusion, and in the more severe cases, coma and seizures. Moreover, about 20% of FHM1 families show permanent cerebellar symptoms of progressive cerebellar ataxia and/or nystagmus and/or dysarthria (Pietrobon, 2007). Emotional stress and minor head trauma are among the most common triggers of FHM1 attacks (Pietrobon, 2007). FHM1 can be considered a model for the common forms of migraine because the headache and aura features, apart from the hemiparesis, are identical and FHM1 patients have, in addition to FHM attacks, also attacks of common non-hemiplegic migraine (de Vries et al., 2009; Pietrobon, 2007). The study of FHM mechanisms may thus provide unique insights into the pathophysiology of migraine.

1.3.5 Functional consequences of the FHM1 mutations

The functional consequences of 13 FHM1 mutations have been investigated by expressing recombinant $Ca_V2.1$ channels in a heterologous expression system (Pietrobon, 2013). Five of these mutations have also been analyzed in transfected neurons from $Ca_V2.1$ $\alpha_1^{-/-}$ mice expressing human $Ca_V2.1$ α_1 subunits (underlined in Figure 1.5; Pietrobon 2010a). Nevertheless, to be able to draw meaningful conclusions regarding the neurophysiological processes involved in the pathogenesis of FHM1, it is essential to study these processes in neurons expressing the channels at their native endogenous level. Therefore, the effect of mutations R192Q and S218L on neuronal $Ca_V2.1$ channels has also been analyzed in various neurons of FHM1 knock-in mice, in which the mutant Ca^{2+} channels are endogenously expressed.

We will mainly focus on the R192Q mutation, consisting in the substitution of a positively charged arginine with a neutral, non polar glutamine in the S4 segment of domain I, which forms part of the voltage sensor. The R192Q FHM1 mutation induces in patients pure attacks of hemiplegic migraine with neither more severe symptoms (e.g fever, seizures, coma), nor cerebellar neurological dysfunctions (Pietrobon, 2005b). In 2004 van den Maagdenberg et al. reported the generation of a knock-in (KI) mouse obtained by introducing the human R192Q FHM1 mutation at the corresponding position in the mouse orthologous *cacna1a* gene, by homologous recombination. The homozygous R192Q KI mice were healthy and did not exhibit any overt phenotype. Moreover, the expression of the mutant $Ca_V2.1$ α_1 protein was not increased and no apparent brain cytoarchitectural abnormalities were observed.

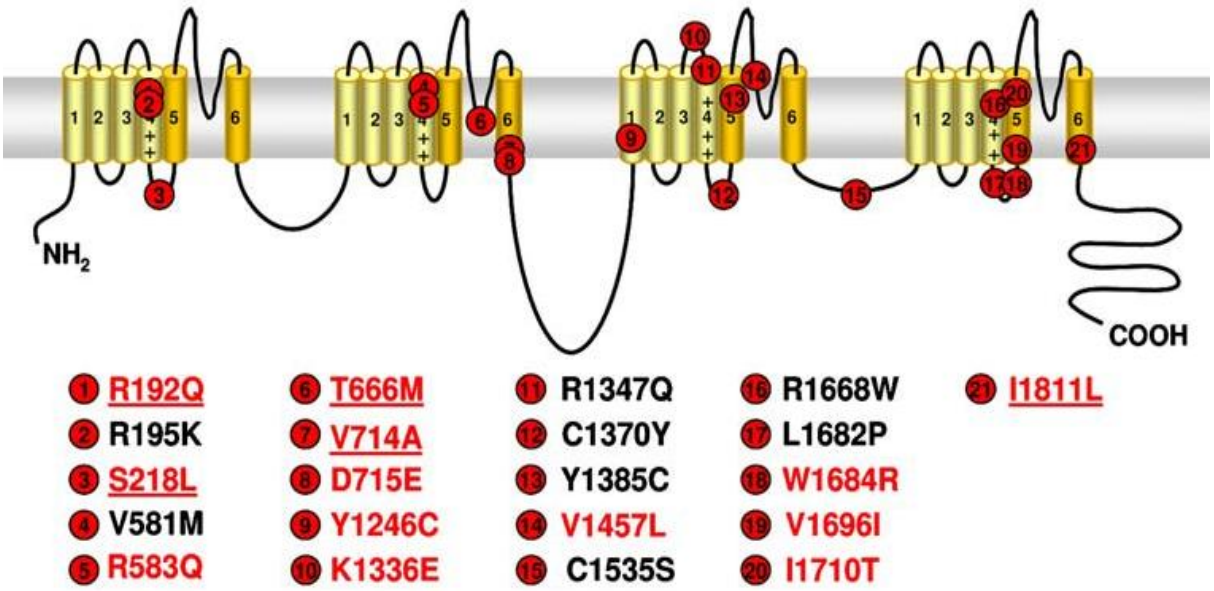

Figure 1.5. Location of human FHM1 mutations in the secondary structure of the $Ca_V2.1\alpha1$ subunit.
The mutations in red are those whose effects on the biophysical properties of recombinant $Ca_V2.1$ channels have been studied in heterologous expression systems; the underlined mutations have also been studied in transfected neurons from $Ca_V2.1-/-$ mice expressing human $Ca_V2.1$ α1 subunits. From Pietrobon 2010a.

Consequences on channel biophysical properties. The analysis of eight FHM1 mutations on the single channel properties of mutant recombinant human $Ca_V2.1$ channels and on the P/Q-type Ca^{2+} current in neurons of FHM1 knock-in mice revealed a consistent gain-of-function phenotype, with an increased Ca^{2+} influx through single human $Ca_V2.1$ channels, mainly due to increased channel open probability and channel activation at lower voltages (Pietrobon, 2010b). Moreover, the investigation of the effect of five different FHM1 mutations on the modulation of recombinant human $Ca_V2.1$ channels by G proteins, revealed a consistent reduction of G-protein mediated channel inhibition (Pietrobon, 2013), an effect that may lead to further enhancement of Ca^{2+} influx through mutant channels during neuromodulation.

Consequences of the R192Q mutation on neurotransmission at different cerebral cortex synapses. The analysis of cortical excitatory synaptic transmission in neuronal microcultures and at L2/3 pyramidal cells synapses in brain slices from R192Q KI mice, revealed enhanced excitatory neurotransmission, due to enhanced action potential-evoked Ca^{2+} influx through mutant presynaptic P/Q Ca^{2+} channels and enhanced probability of glutamate release (Tottene et al., 2009). Short-term synaptic depression during trains of action potentials was also enhanced. Neither amplitude, nor frequency, of miniature excitatory postsynaptic currents were altered, indicating the absence of homeostatic compensatory mechanisms at excitatory synapses onto pyramidal cells (Tottene et al., 2009). In striking contrast with the enhanced glutamatergic transmission, paired recordings of fast

spiking (FS) inhibitory interneurons and L2/3 pyramidal cells in acute cortical slices revealed that the inhibitory GABAergic transmission at FS synapses, though also initiated by P/Q Ca^{2+} channels, was not altered in R192Q KI mice, (Tottene et al., 2009). The demonstration that FHM1 mutations may differently affect synaptic transmission, and short-term synaptic plasticity, at different cortical synapses strongly suggests that the neuronal circuits that dynamically adjust the balance between excitation and inhibition during cortical activity are altered in FHM1 (Tottene et al., 2009). Functional alterations in these circuits are expected to lead to abnormal processing of sensory information (Shu et al., 2003; see paragraph 1.4.3).

Consequences of the R192Q mutation on neurotransmission at the excitatory calyx of Held synapse. The giant synapse of the auditory system formed by the presynaptic calyx of Held terminal and the postsynaptic neurons of the medial nucleus of the trapezoid body (MNTB) has also been investigated. In mutant R192Q KI mice $Ca_V2.1$ channel activation shifted toward lower voltages at the calyx of Held, similar to cortical pyramidal cells; however, such shift did not alter the AP-evoked Ca^{2+} current at the calyx, or the excitatory evoked post-synaptic currents (EPSCs) in postsynaptic neurons (Inchauspe et al., 2010). This was explained as a result of the duration of APs, shorter at MNTB terminals than at cortical pyramidal cells. However, short-term depression of EPSCs induced by repetitive stimulation of afferent axons to the MNTB at various frequencies recovered significantly faster in R192Q KI mice than in WT mice. Such faster recovery was prevented by the Ca^{2+} chelator EGTA-AM, pointing to enlarged residual Ca^{2+} as a key factor in accelerating the replenishment of synaptic vesicles (Inchauspe, 2012).

Consequences on CSD generation. The investigation of experimental CSD, elicited either by electrical stimulation of the cortex in vivo or high KCl in cortical slices, revealed a lower threshold for CSD induction and an increased velocity of CSD propagation in R192Q and S218L knock-in compared to WT mice (van den Maagdenberg et al., 2004; Tottene et al., 2009). Moreover, a single CSD, elicited by brief epidural application of high KCl, produced more severe and prolonged motor deficits (including hemiplegia) in FHM1 KI mice, and, readily propagated into the striatum, in contrast with WT mice (Pietrobon, 2013). The much higher propensity of CSD to propagate to the striatum in FHM1 mutants compared to WT mice may explain their motor deficits and the hemiplegia typical of FHM1 aura. The strength of CSD facilitation as well as the severity of the post-CSD neurological motor deficits and the propensity of CSD to propagate into subcortical structures in R192Q and S218L knock-in mice were all in good correlation with the degree of

$Ca_V2.1$ channel function enhancement and the severity of the clinical phenotype produced by the two FHM1 mutations (van den Maagdenberg et al., 2004; Pietrobon, 2013).

It has been shown that the enhanced glutamate release at synapses onto cortical pyramidal cells can explain the facilitation of experimental CSD in FHM1 KI (Tottene et al., 2009). In fact, the facilitation of CSD in acute cortical slices of R192Q KI mice was completely eliminated (both CSD threshold and velocity became similar to those in WT slices) when glutamate release at pyramidal cell synapses was brought back to WT values by partially inhibiting P/Q channels (Tottene et al., 2009). The data are consistent with and support a model of CSD initiation in which $Ca_V2.1$-dependent release of glutamate from cortical pyramidal cell synapses and activation of NMDA receptors (and possibly postsynaptic $Ca_V2.1$ channels) play a key role in the positive feedback cycle that ignites CSD (Tottene et al., 2009; Pietrobon, 2005a). This model and in general the specific requirement for $Ca_V2.1$ channels in the initiation and propagation of CSD (induced by electrical stimulation or brief pulses of high K^+) are further supported by the findings that i) in the "leaner" and "tottering" spontaneous mouse mutants, that carry loss-of-function mutations in *cacna1a*, the *in vivo* electrical threshold for CSD initiation was higher and the CSD velocity smaller than in WT mice (Pietrobon, 2010b) and ii) after blockade of either the P/Q-type Ca^{2+} channels or the NMDA receptors, CSD could not be induced in cortical slices of WT mice (Pietrobon, 2007); in contrast, blockade of N- or R-type Ca^{2+} channels had only a small inhibitory effect on CSD threshold and velocity of propagation (Pietrobon, 2013).

As a whole, the studies of experimental CSD in FHM1 knock-in mice strengthen the view of CSD as a key player in the pathogenesis of migraine. In migraineurs, CSD is not induced by experimental depolarizing stimuli, but arises "spontaneously" in response to specific triggers, that somehow create in the cortex conditions for initiation of the positive feedback cycle that overwhelms the regulatory mechanisms controlling cortical $[K^+]_o$ and ignites CSD. Insights into how this might occur have been provided by the differential effect of FHM1 mutations on cortical excitatory and inhibitory synaptic transmission (Tottene et al., 2009) suggesting altered regulation of the cortical excitatory–inhibitory balance in FHM1. It has been hypothesized that this dysregulation may lead in certain conditions (e.g. in response to migraine triggers such as intense, prolonged sensory stimulation) to disruption of the excitatory–inhibitory balance and hyperactivity of cortical circuits, mainly due to excessive recurrent excitation, that may create the conditions for the initiation of "spontaneous" CSDs (e.g. by increasing the extracellular $[K^+]$ above a critical value) (Tottene et al., 2009; Vecchia & Pietrobon, 2012).

Impairment of the cortical circuits that dynamically adjust the excitatory–inhibitory balance during cortical activity, due to excessive recurrent glutamatergic neurotransmission, might also underlie

the abnormal regulation of interictal cortical function in some common migraine subtypes, for which indirect evidence points to enhanced cortical glutamatergic neurotransmission (Siniatchkin et al., 2011) and enhanced cortico-cortical or recurrent excitatory neurotransmission (Pietrobon, 2013). Some of the susceptibility loci for MA and MO recently identified in genome-wide association studies also appear consistent with the idea of migraine as a disorder of glutamatergic neurotransmission and/or dysregulated brain excitatory–inhibitory balance. Given the wide clinical and genetic heterogeneity of migraine, different molecular and cellular mechanisms, that remain largely unknown, may well underlie the impaired regulation of brain function and the susceptibility to CSD in different migraineurs (Vecchia & Pietrobon, 2012). The conclusions regarding the functional consequences of FHM1 mutations derived from the functional analysis of R192Q and S218L knock-in mice (figure 1.6: gain-of function of cortical pyramidal cell $Ca_V2.1$ channels with consequent enhancement of cortical glutamatergic synaptic transmission causing facilitation of CSD) provide a coherent picture of molecular and cellular mechanisms that may produce increased susceptibility to CSD and thus explain the aura symptoms in FHM1 patients. Thus, most likely, the conclusions are valid for all FHM1 mutations, given that the aura phenotype is common to all FHM1 patients.

Consequences of the R192Q mutation on trigeminal ganglion neurons and meningeal nociceptors.

The expression of specific $Ca_V2.1$ splice variants and/or auxiliary subunits in different neurons might underlie the recent finding of a differential effect of the R192Q mutation on gating activation of native P/Q-type Ca^{2+} channels in different trigeminal ganglion (TG) neurons of KI mice (Fioretti et al., 2011). The functional analysis of TG neurons and dural afferents in R192Q KI mice showed that i) the FHM1 mutations may lead to enhanced P/Q Ca^{2+} current in certain TG neurons without affecting the P/Q current in other TG neuron subtypes, including small-capsaicin-sensitive dural afferents; and ii) the FHM1 mutations do not alter the functional properties of small capsaicin-sensitive peptidergic dural afferents, including CGRP release from their peripheral terminals at the dura (Pietrobon, 2013). However, FHM1 mutations lead to several function enhancements at the TG level: increased evoked CGRP release from intact trigeminal ganglia (Fioretti et al., 2011) and CGRP release, both basal and evoked, from cultured TG neurons (Ceruti et al., 2011) of R192Q KI mice, suggest that CGRP-mediated intraganglionic crosstalk among neurons and between neurons and satellite glial cells could promote and maintain a neuron–glia inflammatory cycle that might contribute to peripheral trigeminal sensitization (Pietrobon, 2013). Inflammatory mediators can sensitize TG neurons and act back on glial cells further activating them (Vecchia & Pietrobon, 2012, and references therein). If similar phenomena occur in the TG in vivo upon prolonged

elevations of CGRP, the enhanced intraganglionic CGRP release, measured in KI mice suggests, that FHM1 mutations might facilitate peripheral sensitization at the ganglion level. Actually, some evidence does suggest facilitation of CGRP-mediated neuron-glia crosstalk following exposure to proinflammatory stimuli in cultured TG neurons from juvenile R192Q KI mice (Ceruti et al., 2011). Based on these findings, FHM1 mutations have been suggested to possibly originate a basal inflammatory milieu within the trigeminal ganglion.

Taken together these findings have important general implications for familial migraine mechanisms, in that neuron subtype-specific (and/or subcellular compartment-specific) alterations of $Ca_V2.1$ channels and/or AP-evoked Ca^{2+} influx may help to explain why a mutation in a Ca^{2+} channel that is widely expressed in the nervous system (Pietrobon, 2005b) produces the specific neuronal dysfunctions leading to migraine.

As a whole, the functional analysis of FHM1 KI mouse models supports the view of migraine as a disorder of brain excitability characterized by deficient regulation of the cortical E/I balance, gives insights into the possible underlying molecular and cellular mechanisms and their relationship to CSD susceptibility, and strengthens the view of CSD as a key migraine trigger.

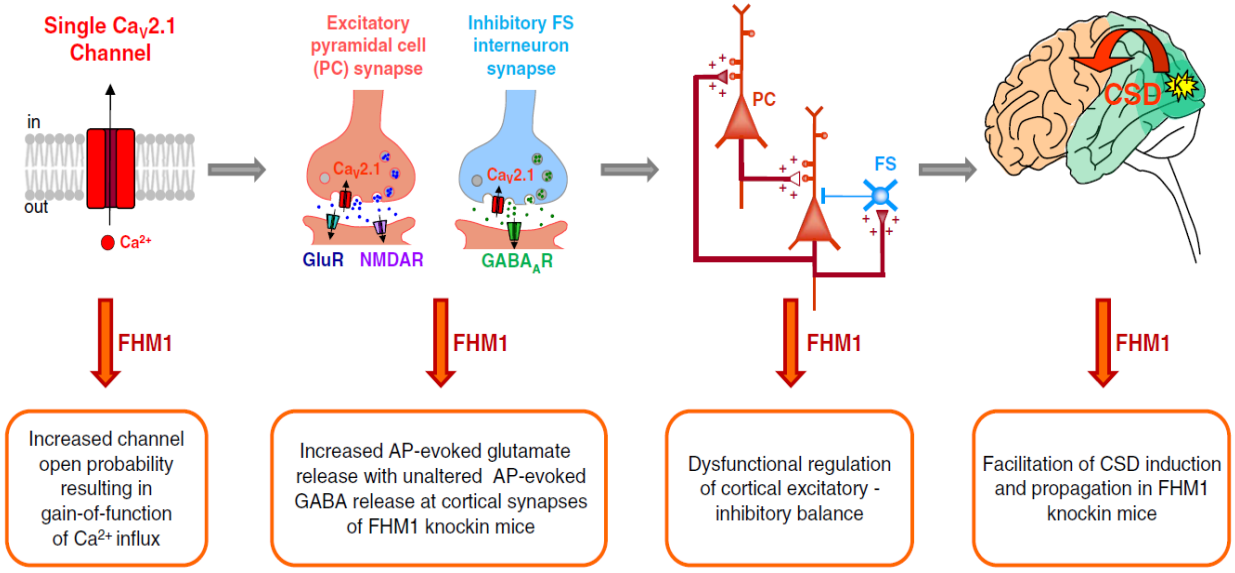

Figure 1.6. Functional alterations in the cerebral cortex of an FHM1 KI mouse model. Action potential (AP)-evoked glutamate release and excitatory synaptic transmission at pyramidal cell (PC) synapses are increased, due to increased AP-evoked Ca influx through presynaptic $Ca_V2.1$ channels consequent to the increased open probability and activation at lower voltages of mutant compared to WT channels. In striking contrast, AP-evoked GABA release and inhibitory synaptic transmission at fast spiking (FS) interneuron synapses are unaltered. The differential effect of the FHM1 mutation on excitatory and inhibitory synaptic transmission very likely results in dysfunctional regulation of the cortical excitatory–inhibitory balance. Experimental cortical spreading depression (CSD) is facilitated, as revealed by a decreased threshold for CSD induction, an increased rate of CSD propagation and an increased propensity to propagate into subcortical structures. Taken from Pietrobon 2013.

An interesting open question is why overexcitation and neuronal hyperactivity in migraine produce a CSD and not an epileptic discharge. Indeed, local neuronal hyperactivity has been proposed to initiate epileptic discharge in slice models by progressively recruiting a synchronous discharge via recurrent excitatory collaterals and $[K^+]_o$ accumulation. The initiation mechanisms of CSD and seizure may well be similar, and their evolution different, depending on whether the neuronal hyperactivity, and $[K^+]_o$ increase, exceed a critical level that induces depolarization block and prevents firing; this hypothesis would look at CSD as ''a poorly controlled seizure'' in which $[K^+]_o$ regulation is completely disrupted. Similar mechanisms are likely to be involved in initiation of CSD and seizures since (1) comorbidity between migraine and epilepsy has been established, (2) some antiepileptic drugs are effective in migraine prophylaxis (Ayata et al., 2006), (3) migraine and epilepsy have various trigger factors in common, and (4) mutations in all three known FHM genes can cause seizures (Welch, 2005; Pietrobon, 2007).

1.4 Neurobiology and pathophysiology of epilepsy

Epilepsy is an episodic disorder of circuit excitability that affects 1%–2% of the population (including one in 200 children), and presents as recurrent, unprovoked seizures[8], with potentially devastating effects. Though the causes of epilepsy are diverse and heterogeneous, epilepsy is considered a highly genetic and in many cases heritable condition (Poduri & Lowenstein, 2011).
Particularly at the genetic level, the process of epileptogenesis is bewildering complex with many contributory elements. Indeed, so intricately is normal brain function dependent on the proper mix of receptors, channels, chemical environment and other factors that it may appear a miracle that so many animals are able to function at all, and that not many more among us are subject to epilepsy. In principle, any abnormality in gene expression or molecular environment, which appears to be associated with clinical or electrophysiological evidence of epileptogenesis, may represent one of three possibilities:

- it may constitute a causative factor,
- it may be a response to other epileptogenic factors
- it may be a noncontributory, incidental finding.

It is often difficult to classify each abnormality to one of these three classes. To clarify the behavior of the whole, it would be necessary to understand how all the constitutive parts come together, first at the neuron level and then at the network level (Hsu et al., 2008).

[8] An epileptic seizure is a transient occurrence of signs and/or symptoms due to abnormal excessive or synchronous neuronal activity in the brain (definitions of epileptic seizure and epilepsy in the special article of Fisher et al., 2005).

Epileptic syndromes, including idiopathic epilepsies, have a large genetic component. In the last decades, mutations in various subunits of a number of ion channels, including voltage-gated channels, as well as $GABA_A$, AMPA and nicotinic receptors, have been found to play major roles in the pathogenesis of several epileptic syndromes. However, the number of potential genes whose mutations are associated to epilepsy is much larger. Some of these genes are involved in neuronal development and migration, synaptogenesis, neurotransmitter release and synaptic plasticity. Accordingly, large families of proteins involved in synaptic vesicle (SV) trafficking and exo-endocytosis (over 140 gene products) could be involved in epilepsy. Although a large number of these genes have been inactivated in animal models to uncover the physiological role of the respective encoded proteins, only few mutants have been reported to exhibit an epileptic phenotype. A severe epileptic phenotype was found in genetically altered mice lacking members of the synapsins (Syns) and SV2 families of SV proteins, whereas epilepsy was not observed in mouse mutants deleted for other SV or presynaptic plasma membrane proteins (Giannandrea et al., 2013).

1.4.1 The triple synapsin knock-out mouse: an epilepsy model

Studying epileptogenesis in a genetic mouse model can provide information on the mechanisms that promote the conversion of a normal brain into one chronically prone to seizures. The epileptic mouse models supply an opportunity to experimentally probe the properties of networks of neurons *in vitro*, and have provided substantial information concerning their synaptic deficits.

Synapsins (Syns) are the most abundant family of neuron-specific, SV-associated, phosphoproteins, working as multitask regulators of neuronal development and functioning. In mammals the family comprises three members encoded by distinct genes (*SYN1*, *SYN2* and *SYN3*, respectively located on chromosomes X, 3 and 22) that in turn give rise to various splicing isoforms. In the central nervous system, the vast majority of neurons express at least one Syn isoform, somehow involved in synaptic transmission and plasticity. However, the functions of these proteins are not fully understood to date (Chiappalone et al., 2009).

Syns control multiple steps of the SV life cycle and have been proposed to contribute to the clustering of SVs and to their attachment to the actin-based cytoskeleton (Benfenati et al., 1992; Ceccaldi et al., 1995; Valtorta et al., 1992a; Valtorta et al., 1992b). A consistent amount of data implicates Syns in neuronal development, from the early stages of neurite sprouting to the regulation of synapse formation and refinement.

Recent evidence indicates that the genes encoding for Syn I and II are epilepsy susceptibility genes in mouse and humans: (i) although knock-out (KO) mice for single or multiple Syn isoforms do not

display overt alterations in neuroanatomy and behavior, all mutants (Syn I, II, I/II and I/II/III KO), except single Syn III KO, exhibit early onset (2 months of age) spontaneous and sensory stimuli-evoked epileptic seizures with severity proportional to the number of inactivated genes (Cesca et al., 2010); (ii) a nonsense mutation of *SYN1* was identified in a family affected by X-linked syndromic epilepsy (Garcia et al., 2004); and (iii) *SYN2* has been found as one of the major neural genes contributing to sporadic epilepsy predisposition and *SYN2* polymorphisms were found to affect epileptogenesis and the response to anti epileptic drugs in humans (Cesca et al., 2010).

The causal link between Syn deficiency and the epileptic phenotype is under study. The reported depletion of the SV reserve pool (RP) in inhibitory terminals with Syn deletion may play a role (Gitler et al., 2004). It has been hypothesized that synaptic depression at inhibitory neurons during repetitive stimulation may contribute to seizure development by causing an imbalance between the excitatory and inhibitory systems. Indeed, inhibitory GABAergic interneurons often experience high frequency firing, so that GABA release may be particularly sensitive to the integrity of the Syn-dependent SV RP. Impaired GABAergic function has been reported in Syn I-/- mice, with decreased size of both reserve and readily-releasable pools (RRP) and high susceptibility to synaptic depression (Chiappalone et al., 2009). Such impairment in the inhibitory systems is accompanied by an increased size of the RRP in glutamatergic terminals, which further enhances the imbalance between excitatory and inhibitory activity and leads to network hyperexcitability and eventually to the generation of seizures (Chiappalone et al., 2009). Similar findings, with Syns deletion differentially affecting excitatory and inhibitory neurotransmission and toning down basal inhibitory responses, were observed in cultured neurons from newborn Syn I,II,III-/- (triple-knockout, TKO) mice (Gitler et al., 2004).

Synapsin TKO mice exhibit adult-onset epilepsy, which makes it possible to characterize events and changes as presumably preceding the onset of seizures or following it. Since reduced inhibition is expected to enhance brain excitability, the described deficit in inhibitory transmission has been directly linked with the epileptic nature of the Syn KO mice (Chiappalone et al. 2009; Boido et al. 2010). Nevertheless, if this congenital reduction in inhibitory transmission were the underlying cause for epilepsy in these mice, it is unclear why young TKO mice are asymptomatic. It seems fairer to propose that the genetic lesion exerts long-term progressive effects extending well into adulthood. Indeed, network activity is enhanced in the brains of young TKO mice before the onset of epilepsy (Boido et al. 2010; Farisello et al. 2013), suggesting that functional changes occurring during the latent period are necessary to initiate epilepsy. Moreover, contrary to prevailing epileptic models, GABAergic transmission is enhanced in the brains of adult epileptic TKO mice (see below; Ketzef & Gitler, 2012).

MEA recordings have been used to characterize neuronal hyperexcitability in acute hippocampal slices of Syn TKO mice at various developmental stages. Because of the rare occurrence of spontaneous epileptic discharges, interictal and ictal activities were studied from 3/4-weeks and 1-year-old WT and TKO mice in the presence of the convulsant 4-aminopyridine (4-AP). Syn deletion was associated with a higher propensity to 4-AP induced epileptic paroxysms, that appeared before the onset of epilepsy and consolidated with age. In 1-year-old mice, ictal seizures were not produced in WT slices, but persisted in TKO slices, in parallel with the course of the epileptic phenotype. Such hyperexcitability was attributed to a generalized increase in excitatory and inhibitory inputs and was ameliorated by acute treatment with the synaptic vesicle-targeted antiepileptic drug levetiracetam through a selective enhancement of the inhibition/excitation ratio (Boido et al., 2010).

To clarify the role of Syns in neurotransmission and epileptogenesis, synaptic and extrasynaptic alterations have been examined with patch-clamp recordings from the CA1 region of acute hippocampal slices from 1-month-old presymptomatic and 6-month-old epileptic TKO mice and age-matched controls. A strong imbalance between basal glutamatergic and GABAergic transmission was found in TKO mice, showing increased evoked excitatory postsynaptic current and impaired evoked inhibitory postsynaptic current amplitude. This imbalance was accompanied by a parallel derangement of short term plasticity paradigms, with enhanced facilitation of glutamatergic transmission in the presymptomatic phase and milder depression of inhibitory synapses in the symptomatic phase. Interestingly, a lower tonic $GABA_A$ current - due to impaired GABA release - is responsible for the more depolarized resting potential found in TKO CA1 neurons, which makes them more susceptible to firing. All these changes preceded the appearance of epilepsy, suggesting that the distinct changes in excitatory and inhibitory transmission due to the absence of Syns initiate the epileptogenic process (Farisello et al., 2013). This study showed impairment of phasic inhibition in the hippocampus that persisted into adulthood, and weaker tonic inhibition at all ages; in contrast in the entorhinal cortex inhibitory transmission is initially reduced and subsequently strengthened with respect to control mice, while tonic inhibition is transiently enhanced (Ketzef & Gitler 2012). The differences between the hippocampus and the entorhinal cortex might be due in part to spared local recurrent connections in the horizontal cortico-hippocampal slice preparation, which let synchronized activity propagate in the entorhinal cortex. Therefore, seizure activity may entail interplay between reciprocally interconnected cortical and subcortical areas, as has been proposed by Farisello et al. (2013).

To summarize, inhibitory transmission is initially reduced, and possibly subsequently enhanced, so that the E/I balance in adult epileptic TKOs may be inverted in favour of inhibition, although with

regional differences. However, the dynamic pattern of the E/I balance (tonic, phasic, and degree of activity-dependent depression) may be even more relevant than overall E/I balance. Indeed, long-term alterations in depression kinetics of excitatory and inhibitory synaptic transmission have been observed, illustrating adaptations in synaptic properties (Farisello et al., 2013; Ketzef & Gitler, 2012). Moreover, age-dependent acceleration of the action potential did not occur in TKO cortical pyramidal neurons, suggesting wide-ranging secondary changes in brain excitability. Overall, although congenital impairments in inhibitory transmission may initiate epileptogenesis in the Syn TKO mice, secondary adaptations are crucial for the establishment of an epileptic network (Ketzef & Gitler, 2012).

This is consistent with the delay in the onset of epilepsy, which has also been observed in other genetic models as well as in patients with known mutations, suggesting that developmental changes in network activity may be instrumental in defining the timing of seizure onset. Considering current progress in therapeutic sequencing and the advent of tailored personalized medicine, prior knowledge of the expected delay in the onset of genetic epilepsy may provide a critical window of opportunity to avert its onset in affected individuals. This realization stresses the utility of genetic animal models as test beds for probing the complex process of epileptogenesis.

1.5 Network electrical activity

A biological neural network, or circuit, is a functional entity of interconnected neurons whose activation defines a recognizable sequential pathway, and that is able to regulate its own activity using feedback loops. The basic kinds of connections between neurons are chemical synapses and electrical gap junctions. Excitatory and inhibitory synaptic transmission produce, respectively, excitatory post-synaptic potentials (EPSPs) and inhibitory post-synaptic potentials (IPSPs). One principle of neuronal operation is neural summation, i.e. potential changes at the post-synaptic membrane will sum up in the cell body. If the resulting depolarization at the emergence point of the neuron axon trespasses a threshold, an action potential will occur and travel down the axon to the terminal endings to transmit a signal to other neurons. Changes in synaptic function may have major impact on neural summation and network activity (Kandel & Siegelbaum, 2000).

As the purpose of the present study is the characterization of both evoked and spontaneous activity of a cortical network in pathological conditions, we will focus on two basic phenomena that are relevant for this study: i) short-term synaptic plasticity, which is known to be altered in migraine and epilepsy, and ii) the spontaneous up- and down-states of cortical neuronal networks (see paragraph 1.6.2).

1.5.1 Synaptic plasticity: short- and long-term

Primary functions of the brain are transmitting, processing and storing information about the body and the environment. Moreover, brains have the ability to change in response to experience and use, thanks to learning and memory processes that occur in neuronal circuits on long time scales (hours to days), and thus are able to remember patterns in the sensory world, refine movements, predict and obtain reward, and even recover function after injury.

Neurons are the computational engines of the brain, connected through synapses that let information flow among them. Synapses conduct signals in an ever-changing manner, depending on the past history of their activation, a process known as "synaptic plasticity". Diverse types of synaptic plasticity, operating on different timescales, are thought to represent the basic cellular mechanisms that contribute to network plasticity implementation and, ultimately, provide the flexibility of brain function. Long-term changes in the transmission properties of synapses provide a physiological substrate for learning and memory, whereas short-term changes support a variety of computations necessary for neural network activity and information processing (Abbott & Regehr, 2004).

Long-term synaptic plasticity. A major goal of neuroscience has been to understand the cellular and molecular plasticity mechanisms that underlie the learning and memory processes. Neuronal long-term plasticity can take many forms, including changes in intrinsic excitability, structural changes that result in synapse formation or elimination, and alterations in the strength of existing synapses (Feldman 2009). Long-term synaptic plasticity is thought to require gene expression and new protein synthesis (Citri & Malenka, 2008).

Neural systems are thought to obey Hebbian or anti-Hebbian learning rules (Hebb, 1949; Kullmann & Lamsa, 2008), implemented through correlated or anti-correlated activity, respectively, of their neuronal synaptic connections. Hebbian learning rules can be summarized by the phrase "cells that fire together, wire together." In the simplest formulation, if a neuron consistently fires while its target neuron is activated then the interposed synapse is strengthened by a small factor. Such a learning rule represents long-term potentiation (LTP). Conversely, if firing of one neuron does not coincide with firing of its target, then the connection is weakened. Such a learning rule represents long-term depression (LTD). When a synapse possesses both Hebbian LTP and LTD it is said to display "spike-timing dependent plasticity" (STDP). These learning rules are competitive associative rules. Different synapses may present variable combinations of LTP and LTD phenomena, and may even display inverse regulation of such processes: for example, in anti-Hebbian plasticity, LTP requires for its induction simultaneous presynaptic depolarization (i.e.,

firing of the presynaptic neuron) and postsynaptic hyperpolarization (lack of activity in the post-synaptic neuron). Hebbian or anti-Hebbian forms of plasticity enable specific synapses to be strengthened or weakened based on associative aspects, i.e. the correlated, or inversely correlated, pattern of activity between the pre- and postsynaptic cell. Non-Hebbian forms of plasticity, such as homeostatic plasticity (Turrigiano 2011), have also been demonstrated to operate to maintain stable neuronal function and an adequate margin of positive/negative modulation despite marked changes in sensory driven or local network activity. This can be achieved either by global adjustment of synaptic strength or excitability across an individual neuron, or by network-wide modification of the E/I balance.

Short-term synaptic plasticity. Neurons fire at frequencies ranging from less than one per second (1 Hz) to several hundred Hz. Changes in firing rate induce different forms of synaptic plasticity that alter the amplitude of both synchronous and asynchronous components of the synaptic response (Zucker & Regehr, 2002; Catterall & Few, 2008). Short-term synaptic plasticity, which occurs on a timescale of milliseconds to minutes, regulates the activity of neural networks and information processing in the nervous system either through synaptic enhancement (three processes have been described: facilitation, augmentation, and post-tetanic potentiation, PTP, over time scales ranging from ms to tens of seconds), or synaptic depression (Zucker & Regehr, 2002; Catterall & Few, 2008). The molecular mechanisms mediating the various forms of short-term plasticity are still a topic of debate, but all of them are sensitive to Ca^{2+} (Zucker & Regehr, 2002).
Short-term synaptic enhancement has two mechanistic elements: (1) the source and regulation of the residual Ca^{2+} that initiates the process and (2) the effector mechanism(s) that respond to residual Ca^{2+} and enhance neurotransmitter release. A major effector mechanism of residual Ca^{2+} has been proposed to contribute synaptic facilitation: occupancy of high-affinity Ca^{2+} buffers. These presynaptic Ca^{2+} buffers are partially occupied by residual Ca^{2+} remaining after an action potential. Thus, when another action potential follows in close succession, more of the entering Ca^{2+} remains free and available to act on the normal Ca^{2+} sensor(s) for neurotransmitter release, presumably the synaptotagmins (Catterall & Few, 2008). Augmentation and PTP require longer trains of stimuli than facilitation, as the contributions of single stimuli are minimal, but they have longer decay time constants (protein phosphorylation and cytoskeletal rearrangement may be implied) and therefore add up during repetitive activation (Zucker & Regehr, 2002).

Short-term synaptic depression reduces the strength of synaptic transmission during repeated stimuli, whether delivered as closely paired stimuli (paired-pulse depression) or as trains of stimuli.

It is thought that depression primarily results from depletion of the pool of readily releasable vesicles in the presynaptic terminal (Zucker and Regehr, 2002). However, physiological studies show that vesicle depletion does not fully account for rapid synaptic depression at some synapses (Catterall & Few, 2008). Decreased release probability caused by decreased Ca^{2+} entry, or changes downstream of Ca^{2+} entry have been proposed, and changes in the availability of postsynaptic receptors can also occur. Therefore, like in the case of facilitation, augmentation, and PTP, multiple mechanisms contribute to synaptic depression, and their roles remain under debate (Catterall & Few, 2008). A crucial aspect is that molecular mechanisms involved in both facilitation and depression are initiated by synaptic activation, and the overall prevalence of synaptic enhancement or weakening depends on the mode and intensity of activation of the secretory machinery.

1.5.2 Up-states

Brain synchronous rhythms in EEG recordings. Cortical neurons receive the great majority of their synaptic inputs from neurons within the local network (<1 mm distant) (Binzegger et al., 2004). As a consequence of this dense, local connectivity the cortex exhibits spontaneous, persistent activity in the absence of any external stimulation (Buzsaki, 2010; Poulet & Petersen, 2008). This ongoing activity is revealed by the rhythmic and synchronous oscillation of the membrane potential of populations of neurons; it is present during active behavior, quiet resting, sleep and anesthesia; and can be detected with scalp electrodes as a component of the EEG. The spatial and temporal patterns of spontaneous activity in the cortex markedly differ across the various physiological conditions; EEG records, as time dependent signals, are decomposed into five main frequency bands, ranging from low frequency delta (< 4 Hz) and theta (4–8 Hz) waves, commonly found during slow-wave sleep, through alpha (8–12 Hz) and beta (13–30 Hz) waves, associated with an awake and alert brain, to gamma waves (30-100 Hz), associated with intense multimodal information processing.

Slow oscillations described with intracortical recordings of LFPs, multi-unit activity, intracellular and optical recordings. The most well-studied pattern of recurrent network activity is the typical "slow" (<1 Hz) oscillation, characterized by a rhythmic alternation between activated and deactivated states (Haider & McCormick, 2009). The cortical slow oscillation was first described in studies of anesthetized rat auditory (Metherate & Ashe, 1993) and cat association cortex *in vivo* (Steriade et al., 1993), where rhythmic oscillations of the LFP, approximately once every second or two, were seen mirrored in the membrane potential of nearby neurons. This rhythmic cycle of depolarization and hyperpolarization survived thalamic lesions and transection of the corpus

callosum (Steriade et al., 1993), and occurs in slices of many cortical regions (Sanchez-Vives & McCormick, 2000; Mao et al., 2001; Shu et al., 2003), indicating that the core mechanisms of its generation exist in local cortical circuits. Similar epochs of depolarization and hyperpolarization were found in striatal and corticostriatal neurons of anesthetized rodents, where it results from synaptic bombardment originating in cortical networks (reviewed in Wilson, 2008). Importantly, this type of activity occurs not only in anesthesia but also naturally during slow wave sleep (Steriade et al., 2001) and may even occur during quiet waking (Petersen et al., 2003; Poulet & Petersen, 2008). The two states of the slow oscillation are also called "up-state" (the synaptically mediated depolarization and action potentials), and "down-state" (the decrease of synaptic inputs, leading to membrane hyperpolarization and cessation of firing). Up-states, or active states of the slow oscillation, are seen simultaneously in the somatic, dendritic, and proximal axonal membrane potential of single neurons and in the local cortical network reflected in the LFP (Haider et al., 2006; Kerr et al., 2005; Sanchez-Vives & McCormick, 2000; Steriade et al., 1993; Waters & Helmchen, 2006).

Up-states are generated intrinsically in the neocortex (Steriade et al., 1993; Sanchez-Vives & McCormick 2000; Chauvette et al., 2010) and can recruit subcortical targets other than the stiatum, such as the thalamus (Rigas & Castro-Alamancos, 2007). The activity of cortical networks during up-states resembles activity during activation, and this has raised the hypothesis that up-states may be equivalent to activated states typical of arousal. During an up-state, the membrane potential of an individual cortical neuron is characterized by depolarization of 15–25 mV, a modest increase in membrane conductance, and irregular action potential firing driven by irregularity in the depolarizing potentials that reach action potential threshold. This firing irregularity is also an important hallmark of neuronal activity in awake, behaving animals. Many studies have demonstrated that activity in the local network generates the depolarized and moderately variable (standard deviation of 2–3 mV) membrane potential of the up-state (Petersen et al., 2003; Sanchez-Vives & McCormick, 2000) through an interaction of inhibitory and excitatory synaptic potentials (Haider et al., 2006; Shu et al., 2003). Long-range connections play a key role in the communication, propagation, and synchronization of this locally generated activity (Haider & McCormick, 2009).

High-frequency oscillations in cortical networks have been linked to a variety of cognitive and perceptual processes. Spontaneous oscillations in the β and γ range (10–80 Hz) emerged during simultaneous intracellular and LFP recordings of up-states from slices of ferret cerebral cortex in the absence of additional pharmacological or electrical stimulation (Compte et al., 2008), indicating that neuronal synchronization at these frequencies is generated in the local cortical circuit.

Origin of up-states. High-density EEG recording in humans revealed that the slow oscillation spread over the cortex as traveling waves that may originate at different sites, but typically in prefrontal-orbitofrontal regions (Massimini et al., 2004). But how does activity originate during silent state, when no action potentials are generated by neocortical neurons? Three hypotheses on the origin of the up-states in local networks have been proposed (Chauvette et al., 2010):

- spontaneous release hypothesis: spontaneous (action potential independent) transmitter release in large neuronal populations occasionally depolarizes some cells to the firing threshold, thus initiating an active state in the network (Timofeev et al., 2000). The ‘‘spontaneous release’’ hypothesis predicts that activity may start in any neuron, although cells receiving largest excitatory convergence will have higher probability of being activated before the others.
- L5 neurons hypothesis: suggests that transition from silence to activity is mediated by intrinsic membrane potential oscillations of L5 pyramidal neurons, which remain more depolarized because of their intrinsic or synaptic properties and generate some spikes between the active states when other cortical neurons are silent (Sanchez-Vives & McCormick, 2000). Once initiated by L5 neurons, activity then propagates to other cortical layers. The ‘‘L5 neuron’’ hypothesis predicts that activity always originates in these neurons, whereas it appears later in other cells.
- Selective synchronization hypothesis: transitions from silent to active states are attributed to the selective synchronization of spatially structured "attractor" neuronal ensembles involving a small number of cells (Cossart et al., 2003). The ‘‘selective synchronization’’ hypothesis predicts that even during the silent states, some neurons of the network still generate irregular spontaneous firing.

More recent studies provided controversial results. Intracortical recordings from epileptic patients demonstrated that active states originate in superficial layers (Cash et al., 2009). However, optical and patch-clamp recordings from L2/3 neurons from visual and somatosensory cortex of healthy rats demonstrated very low firing rates of these neurons, making them unlikely candidates for active state initiation (Waters & Helmchen 2006). Extracellular unit recordings from L5 neurons revealed that each neuron has its unique spiking pattern, that contradicts the idea of stochastic origin of active states (Timofeev et al., 2000; Cossart et al., 2003), but supports the hypothesis that particular sets of neurons start the active state (Sanchez-Vives and McCormick 2000).

A clearer picture derives from combined multisite LFP, extracellular multiunit, and intracellular recordings from closely located neurons in the cat neocortex during natural slow-wave sleep and anesthesia-induced slow oscillation: in local networks subthreshold activity was shown to originate

first at variable neurons and depths, but activation of large pyramidal cells from deep layers was more likely to occur first, probably due to the large excitatory convergence on these cells (Chauvette et al., 2010). Given the large dendritic tree of L5 neurons, there might be a higher probability that spontaneous synaptic inputs sum up and lead to firing in these cells than in neurons in other layers.

Role of cortical layers in the initiation and propagation of up-states. To reveal how specific layers contribute to the initiation and propagation of self-generated recurrent activity a combination of voltage-sensitive dye imaging, LFP, and intracellular recording in thalamocortical connected slices of rat barrel cortex have been performed. A single thalamic input typically triggers an up-state that initiates within a column following a sequence of L4 → L2/3 → L5, and then propagates via L2/3 and L5 to neighboring columns. However, L5, but not L2/3, is crucial for the spread of excitation both within a column and across columns. L5 can sustain and propagate activity to neighboring columns in the absence of L2/3. Conversely, L2/3 cannot sustain activity in the absence of the underlying L5, and often fails to propagate activity to neighboring columns. In other words, L5 amplifies activity in local L2/3 networks and distributes it over many columns within the primary sensory cortex (Wester & Contreras, 2012).
A further confirmation of the specific role of L5 neurons in sustaining and propagating up-states comes from a recent *in vivo* study using optogenetic activation of infragranular or supragranular neurons. Infragranular optogenetic activation generated network activity that resembled spontaneous up-states, whereas photoinhibition of these same neurons substantially attenuated ongoing up-states. In contrast, light activation and inhibition of supragranular cells had modest effects on spontaneous slow activity (Beltramo et al., 2013). The authors also proposed that the differential role of L5 and L2/3 neurons in low-frequency activity is linked to the better ability of L5 excitatory neurons to propagate depolarization through the cortical network.

Synaptic and cellular mechanisms that control up-states: role of the E/I balance, of intrinsic neuronal properties, of external inputs and synaptic and glial modulation. Several mechanisms have been proposed to control slow oscillations, including excitatory-inhibitory interactions (Shu et al., 2003), neuronal intrinsic properties, and the modulation of synaptic transmission (Steriade et al., 1993). Several lines of evidence confirm that both excitatory and inhibitory neurons participate in the firing during up-states. The first study that presented a detailed description of slow oscillations (Steriade et al. 1993) reported firing of both excitatory and inhibitory neurons (fast-spiking interneurons) during up-states, and this was confirmed later. Furthermore, both excitatory and

inhibitory synaptic potentials coexist during up-states *in vivo* as well as *in vitro* (Sanchez-Vives & McCormick 2000; Steriade et al., 2001; Wilson, 2008).

Up-states are generated by recurrent excitation within local circuits and may terminate spontaneously because of synaptic depression and/or build-up of activity-dependent potassium conductances (Sanchez-Vives & McCormick, 2000; Timofeev et al., 2000; Shu et al., 2003). During cortical up-states, neurons also receive barrages of GABAergic[9] inputs (Sanchez-Vives & McCormick, 2000; Shu et al., 2003), which produce an inhibitory conductance that scales proportionally with the degree of recurrent excitation (Shu et al., 2003; Haider et al., 2006). Phase transitions between up- and down-states can also be triggered by sensory input *in vivo* (Petersen et al., 2003) and synaptic stimulation *in vitro* (Shu et al., 2003; MacLean et al., 2005; Rigas & Castro-Alamancos, 2007). It has been suggested that the precise balance between excitation and inhibition is critical for stabilizing persistent activity, and that afferent stimuli can turn off persistent activity by tipping the balance in favor of inhibition (Shu et al., 2003). The importance of fast GABAergic inhibition in controlling persistent activity is supported by the fact that blocking $GABA_A$ receptors transforms up-states into epileptiform bursts (Sanchez-Vives & McCormick, 2000; Shu et al., 2003). Examination of the role of inhibition through $GABA_A$ and $GABA_B$ receptors in controlling up-states recorded in L3 principal neurons of the rat entorhinal cortex *in vitro*, suggest that, while $GABA_A$ receptor-mediated inhibition is critical for balancing up-states, GABAergic inhibition via $GABA_B$ receptors provides a powerful mechanism for the afferent-driven termination of persistent network activity (Mann et al., 2009).

Although pharmacological studies have shown the importance of synaptic modulation on slow oscillations, it is not known whether endogenous cellular systems capable of modulating synaptic transmission have a role in shaping this cortical rhythm (Haider & McCormick, 2009).

Gliotransmission, the release of molecules from astrocytes, regulates neuronal excitability and synaptic transmission in situ (Bacci et al., 2002). Recent experiments showed that the attenuation of gliotransmission leads to reduced cortical slow oscillations. These data provide a demonstration that the output of a neuronal network relies on the coordinated activity of an electrically excitable neuronal system in concert with an electrically inexcitable glial cell system, in which synaptic

[9] GABAergic inhibition is mediated via two distinct types of receptor, $GABA_A$ and $GABA_B$ receptors, responsible for fast and slow inhibition, respectively.

connectivity generates the rhythm that is tuned by glial dependent neuromodulation (Fellin et al., 2009).

Since it has been reported that excitation and inhibition balance each other both during spontaneous and sensory activated cortical activity (Haider et al. 2006; Shu et al. 2003; Compte et al. 2008), the slow oscillatory activity can provide a model to investigate the E/I imbalance in the course of network dysfunctions, such as in epilepsy and in migraine.

2. AIM OF THE PROJECTS

The two studies presented in this thesis aim at characterizing the alterations of network electrical excitability in the barrel cortex of two genetic mouse models of two distinct episodic brain disorders, by comparing model animals with their matched wild type (WT) counterparts using micro-electrode array (MEA) recordings from thalamocortical brain slices.

The two projects observe and analyze i) local field potentials evoked by stimulation in layer 4, either with an isolated stimulus or with a short train of stimuli, and ii) extracellular voltage signals arising from spontaneous synchronous neuronal activations (up-states).

In detail, two genetic mouse models of the two most common episodic neurological disorders, both known to develop distinct alterations at excitatory and inhibitory synapses, are analyzed:

- knock-in mice (KI) carrying the R192Q mutation in the CACNA1A gene coding for the P/Q Ca^{2+} channel subtype, which is found in familial hemiplegic migraine type 1 (FHM1) patients. FHM1 KI mice show: increased P/Q-type current density in central neurons, increased strength of excitatory synaptic transmission at pyramidal cell to fast-spiking interneuron synapses in layer 2/3 of the somatosensory cortex, and unaltered neurotransmission at the reciprocal inhibitory synapses (Tottene et al., 2009). These distinct effects of the FHM1 mutation suggest that an episodic disruption of the excitation-inhibition balance may subtend the increased susceptibility to cortical spreading depression, the phenomenon underlying migraine aura and a likely trigger of the migraine headache mechanisms. We record evoked and spontaneous LFPs in thalamocortical slices of matched WT and KI mice to test the hypothesis that the distinct alterations at excitatory and inhibitory synapses produce an altered network activity in the KI barrel cortex;

- synapsin I/II/III triple knockout (TKO) mice, which exhibit adult-onset epilepsy. Patch-clamp recordings from acute TKO cortico-hippocampal slices before the appearance of epilepsy showed a strong imbalance in excitatory and inhibitory transmission, and a deficit in tonic γ-amino-butyric acid current, causing increased excitability of hippocampal pyramidal neurons (Farisello et al., 2013). We record evoked and spontaneous LFPs from thalamocortical slices of WT and TKO mice to test the hypothesis that the distinct changes in excitatory and inhibitory transmission, due to the absence of synapsins, influence the local network activity in the somatosensory cortex of pre-symptomatic young TKO mice.

3. MATERIALS AND METHODS

3.1 Animals

The two projects were performed using two different genetically modified C57Bl/6J mouse and their wild-type (WT) C57Bl/6J counterparts.

Experiments described in Results (I) were performed using WT mice and homozygous knock-in (KI) mice carrying the $Ca_V2.1$ R192Q FHM1 mutation with the same genetic background. KI mice from 17- to 29-day-old (P17-P29) of either sex together with age-matched WT were used. For confirmatory genotyping, DNA was extracted from tail and analyzed by PCR using the previously described primers (van den Maagdenberg et al., 2004).

Experiments described in Results (II) were performed using WT mice and homozygous Syn I/II/III triple knock-out (TKO) mice kindly provided by Drs. H.T. Kao (Brown University, Providence, RI, USA) and Paul Greengard (The Rockefeller University, NY, USA). Genotyping of mice for all experiments was performed by PCR analysis as described earlier (Gitler et al., 2004). TKO mice from 24- to 36-day-old (P24-P36) of either sex together with age-matched WT were used.

Mice were housed under constant temperature (22±1 °C), humidity (50%) and acoustic isolation conditions with a 12-h light/dark cycle, and were provided with food and water *ad libitum*. The two studies were performed using both male and female mice, and summary data show results from both sexes. Experiments from WT and mutant animals of similar age were alternated on a daily basis. All experimental procedures were carried out in accordance with the international guidelines from the European Community Council Directive 86/609 on the ethical use of animals, and the Italian Animal Welfare Act, and approved by the local authority veterinary service.

3.2 Thalamocortical acute slice preparation and maintenance

Acute thalamocortical slices of the barrel cortex were prepared from P17-P29 or P24-P36 mice, for the first and the second project, respectively. The animals were decapitated after deep anaesthesia with halothane (Sigma-Aldrich, Milan, Italy; 0.25 ml in 1 l for 1-2 min); the brain was quickly removed and kept in ice-cold (2-3°C) standard bicarbonate-buffered solution ("BBS"), containing (mM): 125 NaCl, 2.5 KCl, 2 $CaCl_2$, 1 $MgCl_2$, 26 $NaHCO_3$, 1.25 NaH_2PO_4, 10 glucose, at pH 7.4 when bubbled with 95% O_2 and 5% CO_2. The brain was then dissected as described in Agmon and Connors (1991). Briefly, the brain anterior to the tectum was removed and placed on a 10° plexiglass ramp. The tissue was placed with the ventral face toward the plexiglass slide and the

anterior end downhill (Figure 3.1A). Throughout this and the following procedures the exposed brain surface was frequently irrigated with ice-cold BBS. A hand-held single edge razor blade was used to make a vertical cut through the tissue at an angle of 55° to the right of the posterior-to-anterior axis at about its anterior one-third point (Figure 3.1B). The plane of cut was thus determined by two angles: the ramp tilt angle of 10° and the blade rotation angle of 55°. The tissue rostral to the cut was discharged. The remaining tissue was lightly blotted on filter paper and glued with cyanoacrylate glue onto the stage of a vibratome (Leica, Germany) with the cut surface down and the pial surface toward the blade (Figure 3.1C). The glue was allowed a few seconds to dry and then the tissue was totally immersed in an ice-cold (2-3°C) solution containing (mM): 130 potassium gluconate, 15 KCl, 0.2 ethylene glycol-bis (2-aminoethyl ether)-N,N,N´,N´-tetraacetic acid (EGTA), 20 N-2-hydroxyethyl piperazine-N-2-ethanesulphonic acid (HEPES), 25 glucose, 2 Na-kynurenate, $5 \cdot 10^{-5}$ minocycline, adjusted to pH 7.4 with NaOH (Dugué et al., 2005). A few (depending on brain size) slices were cut and discarded. The remaining tissue was cut into 350 µm-thick slices. Before recording, slices were maintained for 30 min at 32°C in oxygenated BBS, and thereafter maintained at room temperature in the same solution until use.

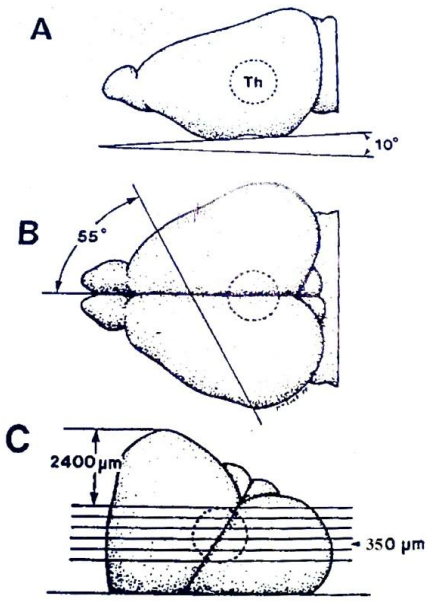

Figure 3.1. Preparation of the thalamocortical slice.
A. Brain laid on the ramp. Th, approximate location of the thalamus. B. Dorsal view, showing angle of initial cut. C. Brain on vibratome stage. Approximate position of collected slices. Adapted from Agmon & Connors (1991).

3.3 MEA recordings

Extracellular electrical field potentials were recorded using 60 planar electrodes of titanium nitride (TiN) arranged in an 8x8 array (200 µm inter-electrode distance) with empty corners (MEA chip; Multichannel Systems, Reutlingen, Germany). Electrodes (diameter: 30 µm) in the MEA layout covered a square area of ~1.4x1.4 mm^2 (Figure 3.2B). The MEA amplifier (MEA1060 Up) recorded signals in the 10 Hz - 3 kHz frequency band (gain: 1200), and was connected to a 12-bit, 64-

channels data acquisition board (NI 6071E, National Instruments) and a personal computer. Signals were acquired at 2-10 kHz with a home-made routine written in C in the Win-CVI environment, and stored in binary format for later analysis with MATLAB. Notice that with our filter settings the amplifiers recorded voltage traces which included both lower frequency components, usually classified as "local field potentials" (LFPs), mostly reporting the presence of post-synaptic potentials, and higher frequency components, typically reporting the occurrence of spikes (normally referred to as multi-unit activity; see footnote page 7).

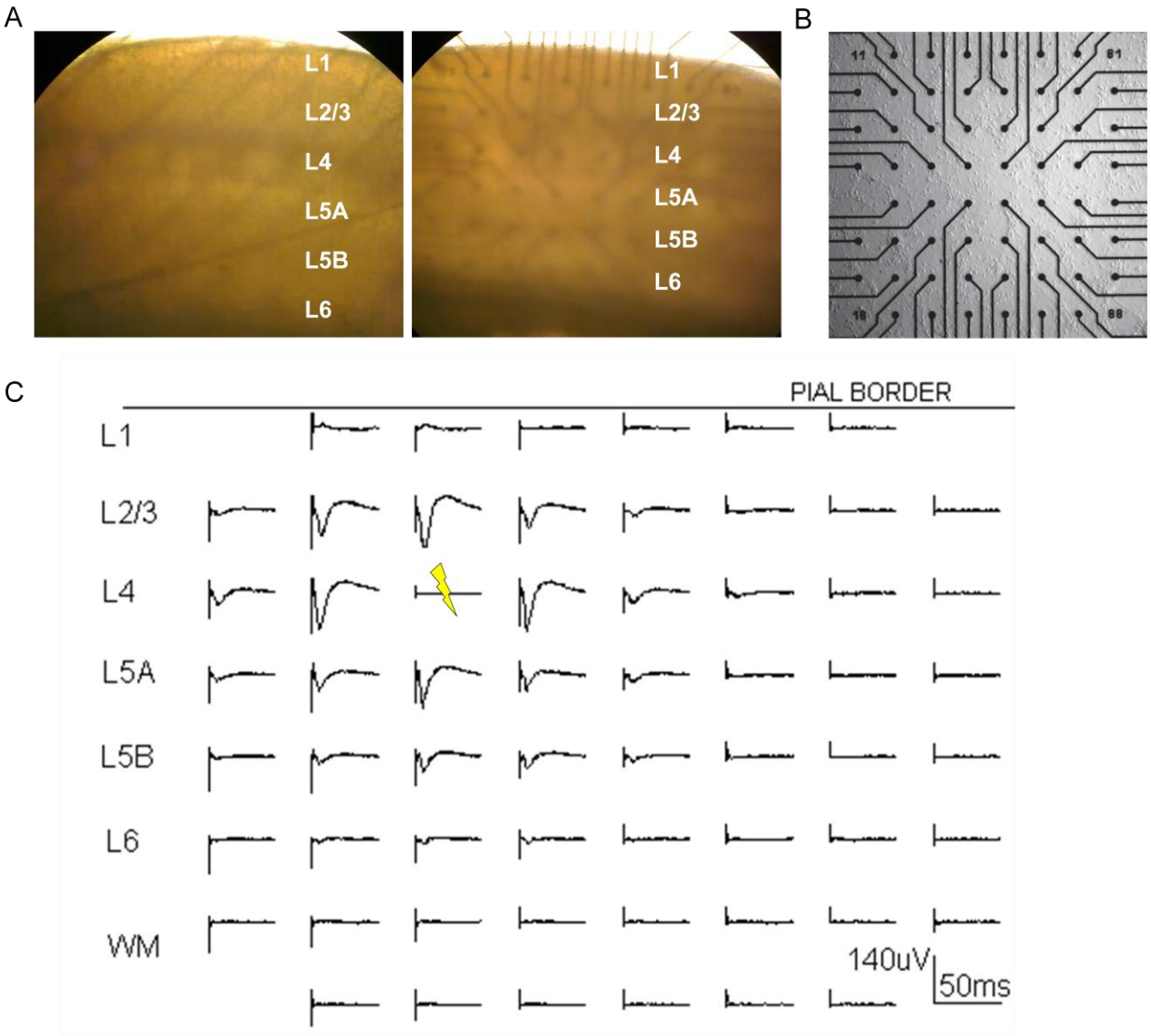

Figure 3.2. MEA recordings of evoked LFP responses. A) Photographs of an acute, unstained thalamocortical slice of mouse primary somatosensory cortex before (on the left) and after (on the right) positioning the slice on the MEA electrodes. The barrels in layer 4 are more clearly visible before positioning the slice. After positioning they appear on row 3 of the MEA chip. B) Electrodes layout in the 8X8 MEA grid. C) LFP responses (average of 15 trials) to a single stimulus delivered via an L4 electrode (marked by yellow symbol; 13 μA). In L1 the response consists of a positive deflection (P). Labels L1 to L6 indicate cortical layers. WM: white matter.

For recordings, slices were transferred into a MEA chip coated with poly-ornithine (500µg/ml), and held in place by either a hand-made platinum grid, or a stainless steel loop (HSG-5A, ALA Scientific Instruments) with nylon mesh. Slices were continuously perfused at 2.5 ml/min with oxygenated BBS or modified BBS ("mBBS"), as specified. mBBS contained: 125 NaCl, 3.5 KCl, 26 $NaHCO_3$, 1.25 NaH_2PO_4, 1 $CaCl_2$, 0.5 $MgCl_2$, 10 glucose, at pH 7.4 when bubbled with 95% O_2 and 5% CO_2. When using mBBS, slices were perfused for 20' in this solution before data acquisition. All experiments were performed at room temperature (21-24°C). The MEA was mounted on the stage of an Olympus BX51WI microscope and slices were viewed with a 10x objective. The baseline noise standard deviation in digitized voltage records was typically 2.9-3.8 µV in all electrodes. To facilitate the assignment of electrode traces to cortical columns and layers, slices were positioned on the MEA chip using a standard orientation with respect to MEA rows and columns (Figure 3.2) with the pial surface and the cortical layers always approximately parallel to the MEA rows. Layer 4 (L4) was identified from the presence of the characteristic barrels, appearing as translucent, clear areas separated by opaque bands, which were best visible before moving the slice onto the chip area. Layer 5 (L5) was also clearly identifiable as a continuous horizontal translucent clear band immediately below L4. After L4 identification, the slice was gently moved onto the chip and one MEA electrode was positioned in the upper half of L4; the corresponding MEA row (generally row 3 or 4) was noted. From upper L4, the next electrode row towards the pial surface was identified with layer 2/3 (L2/3), and the next row with layer 1 (L1), while when moving towards the ventricular surface, the first and second rows where identified with layers 5A (L5A) and 5B (L5B), and the third row with layer 6 (L6). Given the variable depth of cortical layers (Meyer et al., 2010b), the above correspondence between electrode rows (200 µm spacing) and cortical layers should be considered as approximate.

Photographs of the slice positioned on the MEA chip were taken with a digital camera, to roughly confirm the spatial relation of each MEA electrode to neocortical structures (Figure 3.2A). The identification of layers was not confirmed by further morphological analysis.

Individual barrels in adult mice thalamocortical slices are up to ~300 µm wide (see figures in: Harwell et al., 2005; Jan et al., 2008; Kaliszewska et al., 2011; Krook-Magnuson et al., 2008). A cortical column, i.e. the vertically-oriented region spanning the cortical layers and containing a single barrel (Lubke & Feldmayer, 2008), may variably include one or two columns of MEA electrodes. This may partly explain the asymmetry in signal propagation observed in some of our measurements of LFPs evoked by intra-cortical stimulation (see Results).

In recent years the use of standard pre-fabricated planar Micro-Electrode-Array (MEA) chips has become very popular. These chips can be flexibly employed with different electrical stimuli and

recording paradigms with wide applications to different types of tissue, and the complete equipment is available at a relatively affordable price. Most experiments using such MEA chips are carried out with dissociated cell cultures (Gullo et al., 2009; Plenz et al., 2011) that can be followed over several stages of development over days or weeks. Acute brain slices are seldom used because of the difficulty to position the slices in a reproducible way relative to the geometry of the underlying electrodes, as well as to establish reliable contacts between the tissue and the electrodes. Here we report successful multi-site recordings from acute slices of mouse somatosensory (barrel) cortex using standard commercial MEA equipment. The spatiotemporal characteristics of stimulus-induced LFPs fit with earlier observations (Wirth & Luscher, 2004; Bakker et al., 2009). More importantly we have been able to standardize both the experiments and the subsequent analysis such that rapid and informative comparisons can now be made between slices from different animal strains (e.g. with genetic modifications).

3.4 Stimulation

A part of this study was devoted to describing the LFPs evoked by electrical stimulation in L4. Biphasic current stimuli (200 μs overall length) with variable intensity (5-18 μA) were delivered through a MEA electrode (El_{st}) in L4, at the position of a putative barrel, using an isolated stimulator (ISO-01D-100, npi, Germany). A protocol consisting of an isolated stimulus alternated to a short train (5 stimuli, 50 Hz) was repeated every 20 s. The interval between single stimulus and train was generally 10 s, except in protocols designed to study recovery from synaptic depression, where three intervals - 2, 6 and 10 s – were investigated.

3.5 Data analysis

3.5.1 Evoked LFP analysis

LFPs evoked by periodic stimuli were recorded in BBS and digitized at 10 kHz (Figure 3.2C). In L2/3, the response consisted of a negative deflection (N) peaking at ~5 ms after the stimulus, followed by a slow positive deflection peaking at ~20-25 ms (Figure 3.3). The latter was correlated in size to the N response, and was most likely the result of the high-pass filter properties of our MEA amplifier (see Bakker et al., 2009), therefore it was not further examined. The recording stability was checked by monitoring the peak of the N response in L2/3 in the stimulated MEA column (Figure 3.4). In stable periods, averages of 15 responses were formed for all electrodes. At

the end of each recording, $CdCl_2$ (400 µM) was added to the bath saline to block voltage-dependent Ca^{2+} channels and synaptic transmission (Figures 3.4, 3.5). The average response in Cd^{2+} (i.e. the population spike arising from direct axonal excitation) was subtracted from the average response recorded in normal saline, to obtain the "synaptic LFP". All subsequent analysis was performed on synaptic LFPs. In some experiments, the evoked spike in Cd^{2+} was smaller than the corresponding spike in control, and occasionally it had a slightly longer delay from stimulus, therefore leaving a subtraction artifact in the synaptic LFP, which could extend up to ~2.5 ms after stimulus (Figure 3.4).

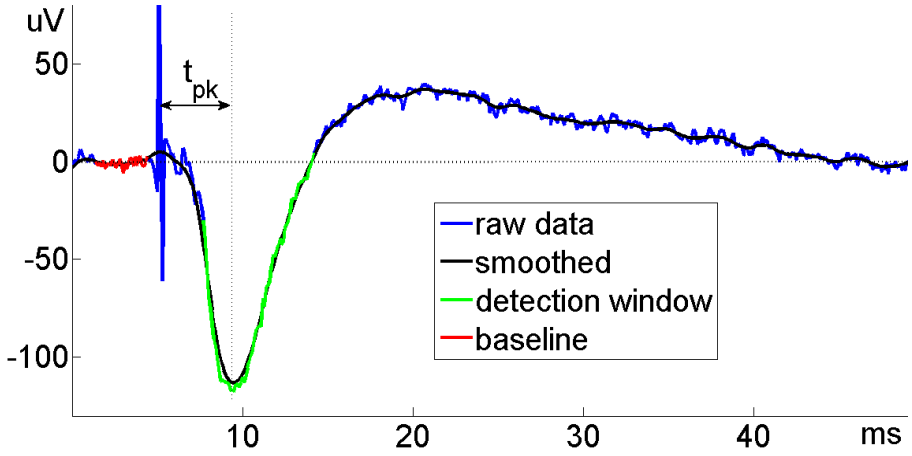

Figure 3.3. Measurement of the amplitude of the early negative (N) response. The blue trace is the average of 15 responses from the L2/3 electrode in the stimulated column. The amplitude of the response is calculated as the mean over a fixed 6.5 ms time window (from 2.8 to 9.3 ms after stimulus; in green) after subtraction of the mean baseline (in red). The vertical dotted line indicates the time of the minimum of a smoothed version of the trace in the same time window (in black). The latency from stimulus to this minimum (t_{pk}) is indicated.

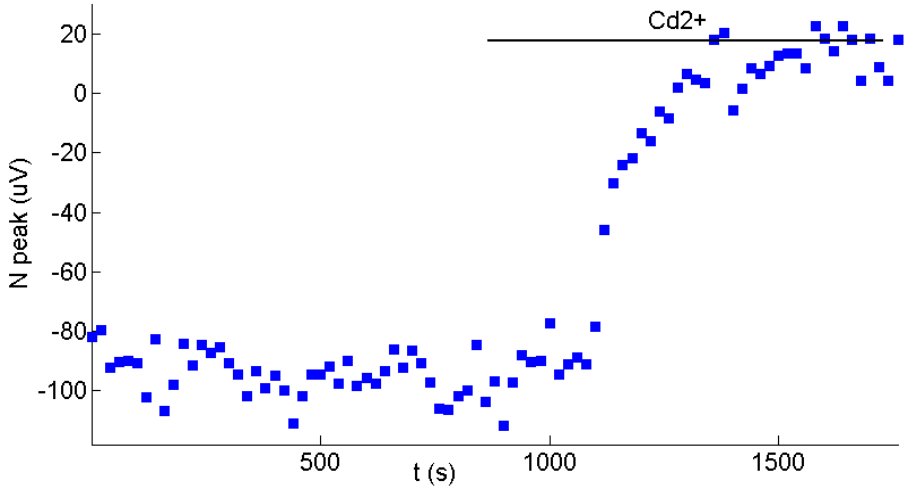

Figure 3.4. Time course of the negative N peak. Consecutive measurements of the N peak from an L2/3 electrode. During the time interval, indicated by the black bar, the slice is perfused with 400 µM Cd^{2+} to block synaptic transmission. After 7 min from the start of the perfusion the N response is completely abolished.

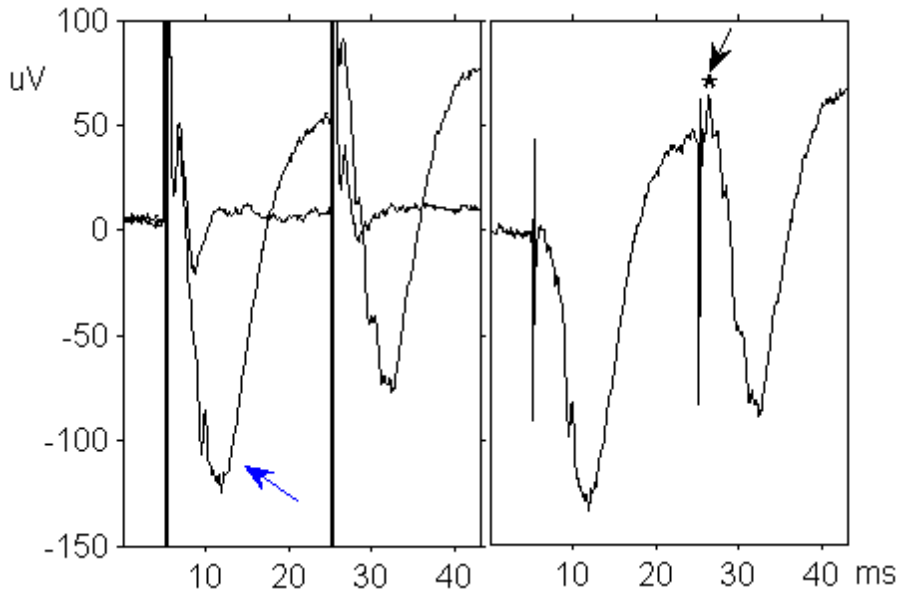

Figure 3.5. Evoked synaptic LFPs: subtraction of the Cd^{2+} resistant response. Left panel: superimposed averages of 15 responses obtained in control (indicated by the blue arrow) and 7 min after start of Cd^{2+} perfusion in the L2/3 electrode of the stimulated column. Their difference ("synaptic LFP") is shown in the right panel. The asterisk on the right panel indicates a badly corrected subtraction artifact (see text).

To evaluate the amplitude of the synaptic LFP we measured the mean response over a fixed 6.5 ms time window (from 2.8 to 9.3 ms after stimulus; Figure 3.3) on average traces, after subtraction of the mean baseline. The latter was calculated over 1 ms before stimulus (Figure 3.3, to avoid effects of the above artifact).

When measuring the size of the 5^{th} response at the end of a train, the baseline was evaluated in the last ms preceding the 5^{th} stimulus. This measurement should be considered an estimate of the degree of activation of mono- and polysynaptic contacts in the local circuit. The amplitude was measured on the eight electrodes surrounding El_{st}, positioned in the "stimulated" and in adjacent MEA columns. The time to peak of the N response (t_{pk}) was the delay from stimulus to the minimum of a smoothed version of the LFP (MATLAB filtfilt operation, with factors A=[1:w,w-1:-1:1] and B=w^2, w=8) in the same time window (Figure 3.3). In layers/electrodes presenting an isolated positive ("P") response (Figure 4.1B), t_{pk} was the delay to the maximal response in the same window.

The threshold for obtaining an LFP response was quite variable and precluded a unique choice of current stimulation intensity. This might be due to variable adhesion conditions of slices to the MEA chip and/or to variable slice viability. The stimulus was varied in order to obtain mean N responses, in L2/3 above the stimulating electrode, in the range 30-140 μV (peak responses between 50 and 180 μV). Quite commonly, the N response size displayed a fast 10-15% decrease after a few

stimuli, or, on the contrary, a late increase up to 10-20% developed after a few tens of stimuli. When this occurred, the average trace was formed from the stable period following the first few stimuli, or preceding the late increase, respectively (Figure 3.4). There was no significant correlation between the size of the mean N response and the intensity of the stimulating current, for either WT or KI mice (Figure 3.6). On average, the mean N size was similar in both strains (see Results). The range of stimulus intensity explored was 7-14 μA in WT and 2.5-18 μA in KI.

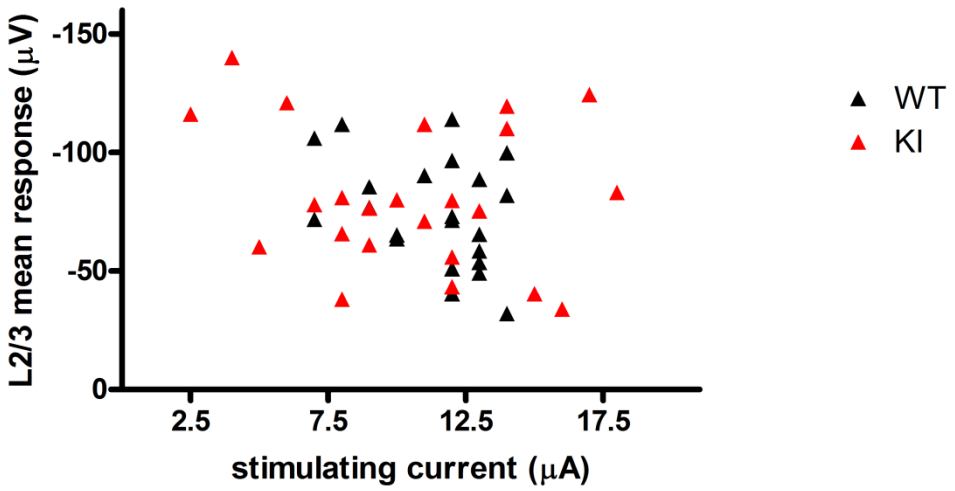

Figure 3.6. The mean response in L2/3 shows no correlation with the stimulus intensity, both for WT and KI.

3.5.2 Spontaneous LFP analysis

To quantitatively analyze spontaneous activity, we used a detection routine developed in house in the Matlab (Mathworks, Natick, Massachusetts, USA) software environment. For each electrode, the voltage trace was filtered to produce a moving average[1] by convolving it with a finite bell-shaped smoothing window (39 ms duration) that approaches a Gaussian with standard deviation 5.82 ms; the equivalent duration of the bell window (duration of a square window with the same corner frequency) was 19.5 ms. Deviations of the original voltage from this filtered trace were computed, squared, similarly filtered and decimated twice, to yield a running variance, $\sigma^2(t)$, over a 190 ms window, with a final sampling rate of 100 Hz. All subsequent parameters, characterizing an

[1] In time series analysis the moving-average model is a common approach for modeling univariate time series. The moving-average model is conceptually a linear regression of the current value of the series against current and previous terms. These terms at each point are assumed to be mutually independent and to come from the same distribution, typically a normal distribution, with location at zero and constant scale.

episode of spontaneous activity (up-state), were measured on the running standard deviation (σ) trace.

A putative up-state was detected when at least one trace, from any electrode, showed a σ value exceeding a certain threshold (Figure 3.7). The threshold was computed for each trace as the mean "basal" s.d. (σ_{bas}) of the trace, evaluated in periods without activity, plus 10 times its standard deviation. It should be noted that σ_{bas} was fairly constant across all electrodes of the MEA chip, so that the threshold ended up to be similar for all electrodes. Once a signal was detected in one electrode, any other electrode was considered to participate to the same episode if its σ trespassed the mean plus 5 times the s.d. of its σ_{bas}, and returned to baseline when σ returned below this level.

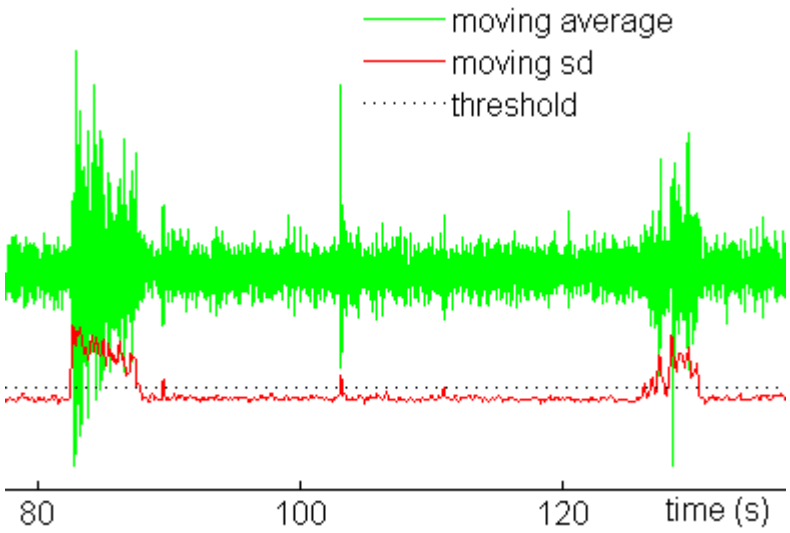

Figure 3.7. Up-states detection. The detection algorithm evaluates a running average (green trace) and a running standard deviation (s.d.; red trace) of the original voltage trace, and searches for threshold crossings. The threshold (horizontal dotted line) is calculated as the mean s.d. in resting periods (σ_{bas}) plus 10 times its standard deviation.

For each up-state, it was named "origin" the electrode in which the up-state was detected first (zero-time), and the delay to start of activity in the other electrodes was calculated from such zero-time. Occasionally, more than one origin was detected.

The “up-state duration” was measured from the time of first detection in the origin, to the time of end of the voltage fluctuation in the last participating electrode.

In each electrode participating to the up-state, the episode's "amplitude" was expressed as the maximum value attained by σ during the episode, normalized to the basal s.d.:

amplitude = $(\sigma/\sigma_{bas})\cdot 100$.

Given that, as mentioned, σ_{bas} was uniform across electrodes in the same MEA chip, the units of amplitude were also uniform in all traces. We defined as “up-state amplitude” the maximal amplitude (in units of % of σ_{bas}) across traces from all electrodes involved in a single episode. The “area per unit time” of an up-state in the i-th trace is an alternative measure of amplitude, computed

from the sum of the fractional deviations of σ from the basal s.d. σ_{bas}, during the up-state, divided by the duration of the up-state in electrode *i* (Δt_i):

$$\text{Area per unit time in electrode } i = \frac{1}{\Delta t_{up-state}} \frac{\sum_{up-state(} \sigma - \sigma_{bas)}}{\sigma bas}$$

The "up-state area per unit time" was defined as the maximal "area per unit time" across traces from all participating electrodes, and was expressed in units of % /s.
The values of duration, amplitude, area per unit time, delay and time of onset, measured in all 8x8 MEA electrodes, were saved in the corresponding cells of an 8x8 matrix for each up-state.

In order to exclude from our analysis contaminating spikes, spike bursts and isolated LFPs from the detected putative up-states (see Results) we required: i) an episode duration > 0.8 s in at least one electrode; ii) a minimum of 5 involved electrodes/episode; iii) an amplitude ≥ 20% σ_{bas} in at least one electrode. These requirements eliminated all isolated LFPs and the vast majority of spike bursts. However, spike bursts in ≥5 non-contiguous, sparse electrodes could still contaminate the up-state population. Therefore a further selection was performed by visually inspecting the delay, amplitude and duration matrices of all detected up-states, which were subdivided into 5 groups:
I) well-detected up-states, or isolated episodes with origin in one or a few contiguous electrodes of a non-lateral MEA column (columns 2-7; Figure 3.8A);
II) episodes with several non contiguous origins, and with delays progressively increasing around each origin: these were considered as two distinct superimposed up-states, arising nearly simultaneously in distinct cortical positions (Figure 3.8B);
III) up-states with delays progressively increasing around a given electrode, but with origin detected in a remote isolated electrode displaying an isolated spike burst temporally preceding the up-state (Figure 3.8C);
IV) up-states with apparent origin on the border columns of the MEA chip (column 1 or 8), which might be propagating from an origin in cortical regions outside the MEA (Figure 3.8D);
V) episodes with 5 or more sparse active electrodes, displaying short uncorrelated spike burst activity; these episodes did not represent a synchronized population activity, and were excluded from further analysis. We measured a global "frequency" of up-states by counting the episodes only in groups I to IV.

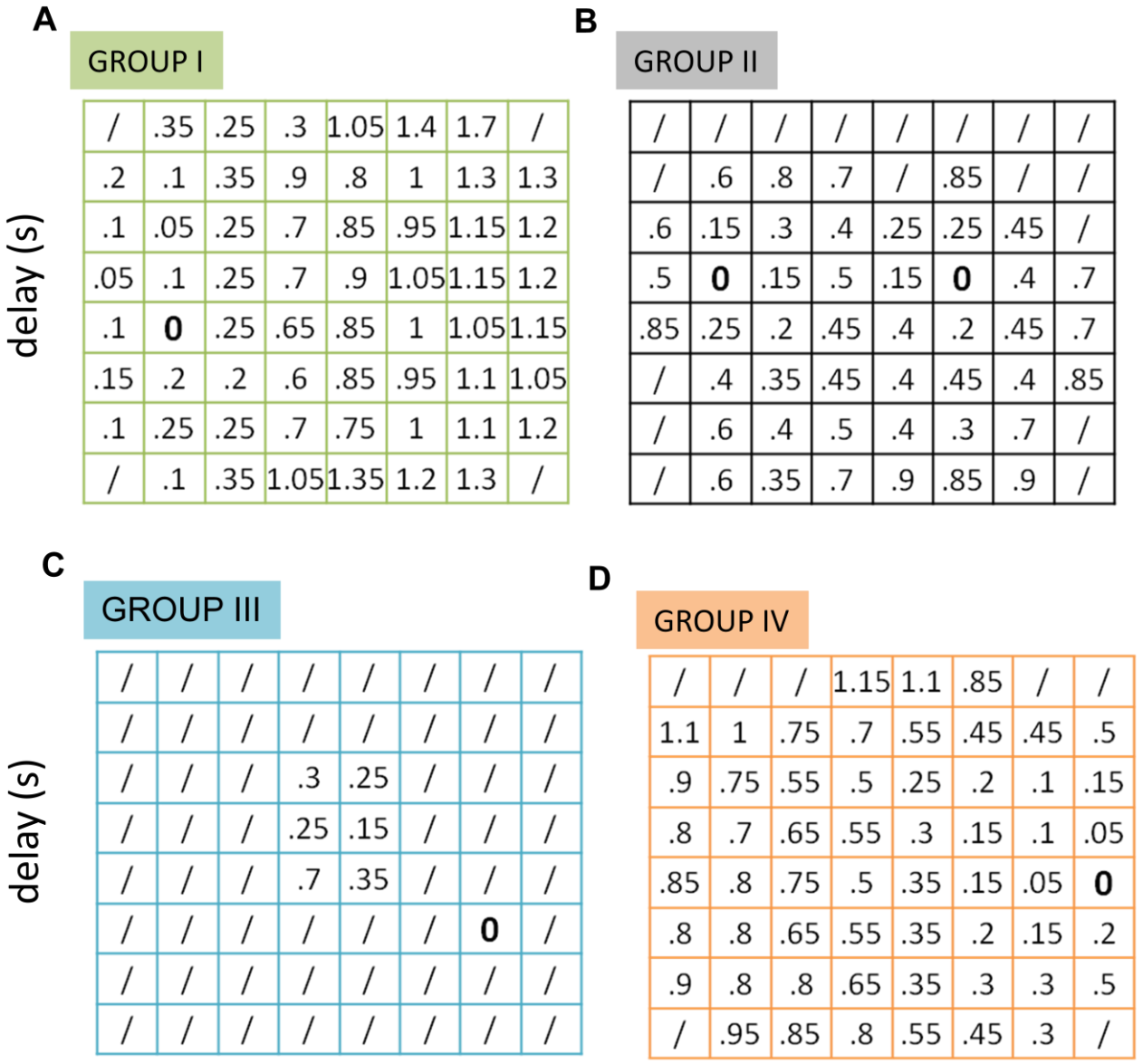

Figure 3.8. Delay matrix. For 4 exemplar episodes, the latency of activity detection with respect to detection in the origin ("delay"; in seconds) is plotted in a 8x8 matrix, representing the position of the electrodes in the MEA chip. "0" marks zero delay, i.e. the position of the origin. A) Example of a group I well-detected up-state. B) Example of a group II episode: two origins in two different slice regions: one on electrode 24, (amplitude: 103%) and the other on electrode 64 (amplitude 61%). C) Group III up-state. D) Group IV up-state (origin in column 8).

To explore up-state spatial propagation, we averaged across up-states delay, amplitude and durations around the origin (Figure 3.9). This was obtained by first remapping the delay, amplitude and duration matrix of each episode into 15x15 matrices, where the origin occupied the central position (row 8, column 8). When multiple adjacent origins were present, the matrix element with largest amplitude was chosen to be in the central (8,8) position. After remapping, an average matrix was obtained (for each parameter) by point-by-point averaging over all up-states. Separate averages were obtained for up-states with origin in each cortical layer so that matrix elements surrounding

the (8,8) position coherently represented defined layers and columns at progressively increasing distance from the origin. Only isolated up-states with origin in columns 2-7 (group I above) were included in this analysis, to avoid confusion from up-states with unidentified or ill-localized origin (groups III-IV) or from superimposed multiple episodes (group II).

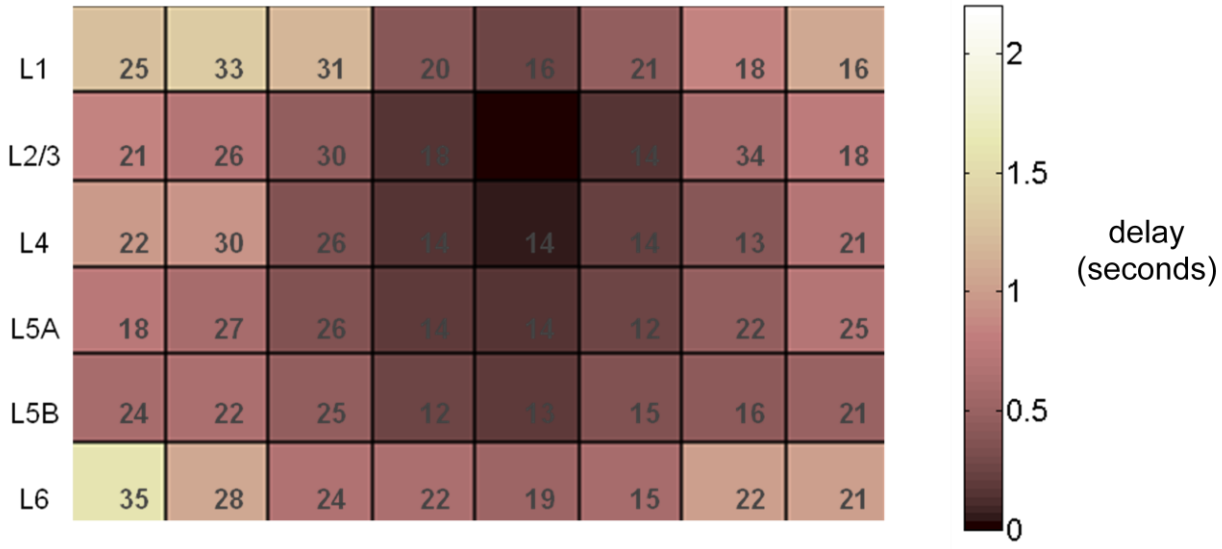

Figure 3.9. Average remapped delay matrix of up-states originating in L2/3 for WT experiments of the project described in Results (I). For each up-state of group I a "delay matrix" is obtained by reporting the delay of each episode into a 15x15 matrix, where the origin (delay=0) occupies the central position (row 8, column 8: in dark brown). The average delay matrix is obtained by averaging all matrices point-by-point. Delay (in seconds) in each position is color coded and the number in grey indicates the corresponding percentage standard error of the mean (100·s.e.m./mean). Cortical layers are marked on the left.

3.5.3 Statistical comparisons

For statistical comparisons, nonparametric methods were used unless otherwise specified, and two-tailed *p* values were computed using Prism software (GraphPad Software Inc.).

To compare the means of two groups of unpaired and paired values, the Mann–Whitney and Wilcoxon matched-pairs tests were used, respectively, unless specified. Repeated measures 1-way ANOVA was used for >2 groups of paired values. 2-way ANOVA with Bonferroni post-test comparisons were used to compare values depending on two independent factors. Differences were considered significant when the probability of the null hypothesis was < 0.05. P values < 0.01 or < 0.001 are marked in the text by two or three asterisks, respectively.

4. RESULTS (I): characterization of the R192Q migraine mouse model

This section reports an analysis of network excitability in the somatosensory cortex of knock-in (KI) mice (P17-P29) carrying the mutation R192Q in the CACNA1A gene coding for the P/Q Ca^{2+} channel type. Experiments have been performed in matched WT and KI mice, as described below.

4.1 Characterization of LFPs evoked by an isolated stimulus in layer 4 (L4)

Evoked responses were analyzed in 22 slices from 10 WT mice, and 23 slices from 10 KI mice. In both groups, the response to isolated stimuli delivered to the upper half of L4 consisted of an early "population spike", followed by a negative deflection peaking at ~5 ms from stimulus ("N peak"), always coupled to a slow positive deflection peaking at ~20-25 ms (see Methods, Figures 3.2 and 3.3), the latter being most likely related to the MEA filter properties. This pattern was observed in electrodes corresponding to supragranular, granular and infragranular layers around the stimulation electrode (El_{st}), with a decreasing amplitude at increasing distance across cortical columns (i.e. in the horizontal direction in the MEA chip).

The early population spike survived after bath perfusion with 400 µm Cd^{2+}, confirming its origin from direct axonal excitation, and was routinely subtracted from control responses (see Methods), yielding a "synaptic" response which is further described below. The synaptic LFP was nearly or completely abolished in all electrodes by bath perfusion of NBQX (2 µM; 15-20 min perfusion; n=6 WT slices, 4 animals) (Figure 4.1), confirming its dependence on activation of excitatory synapses. In some slices, the N deflection was composed of two or more closely spaced peaks, indicating the occurrence of synchronized monosynaptic and disynaptic/polysynaptic responses in the local neuronal population (e.g. see Figure 3.5). Given this complexity, the overall size of the N response was measured as the mean voltage over a fixed time window (from 2.8 to 9.3 ms after stimulus start) comprising one or more peaks (see Methods, Figure 3.3); the time of the maximal negative response in this interval provided the time-to-peak (t_{pk}).

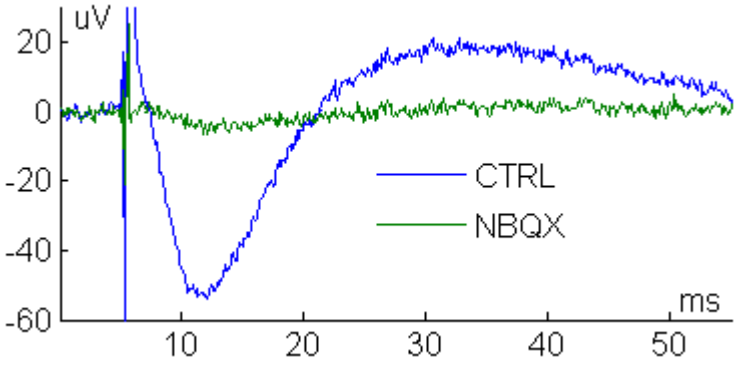

Figure 4.1. Average evoked response in control (in blue) and after 20 minutes bath perfusion of NBQX (2 µM; in green), from the L2/3 electrode in the stimulated column of a WT slice (P21 mouse). Note that NBQX nearly abolishes the synaptic LFP.

Generally, the N response was largest in layers 2/3 (L2/3) in the stimulated MEA column (i.e. in the first electrode above El_{st}), and/or in L4 in the two electrodes adjacent to El_{st}, and decreased when moving to infragranular layers (L5 and L6), in the stimulated as well as in adjacent columns (Figures 3.2, 4.2; Table 4.1); in some experiments, the response was barely visible in L5B and L6.

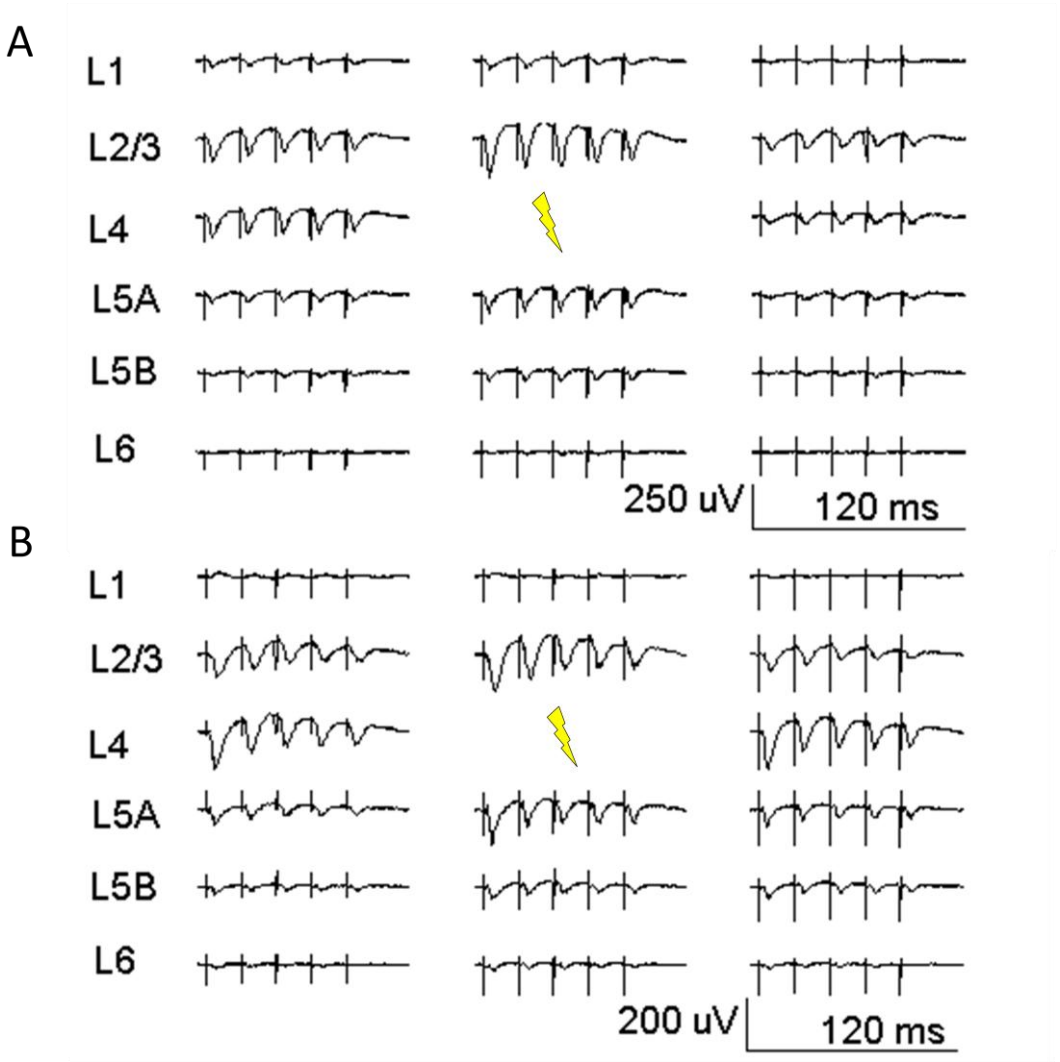

Figure 4.2. Two examples of synaptic LFP responses evoked by a train of 5 stimuli at 50 Hz in WT mice.
A.. In this example the N response is largest in L2/3 in the stimulated MEA column, i.e. the first electrode above the stimulus electrode (El_{st}, marked by yellow symbol here and in panel B; stimulus: 7 μA), and decreases when moving to the infragranular layers L5A, L5B and L6, in the stimulated as well as in adjacent columns. In L1, the evoked LFP consists of a negative deflection with very small amplitude. The ratio of the 5th over the 1st N response (N_5/N_1) reveals a clear depression in all layers. B. In another slice the N response is largest in L4 in the two electrodes adjacent to El_{st}. This is one of the 7 WT slices presenting in L1 an isolated positive deflection (P), peaking at ~7 ms from stimulus (13 μA in this example).

In most slices (15 of 22 WT slice; 16 of 23 KI slices), the evoked LFP in L1 consisted of a negative deflection with very small or null amplitude (Figure 4.2A). On the contrary, around a third of the slices (7 of 22 WT slices; 7 of 23 KI slices) presented an isolated positive deflection (P) in L1, which peaked at ~7 ms after the stimulus (Figure 4.2B), with clearly faster kinetics than the slow positive deflection coupled to the N response (compare Figure 4.2B, top traces, with Figure 3.3). In 3 WT slices and 3 KI slices, small isolated P signals were also visible in L5B and L6 (not shown).

In the stimulated column, the time-to-peak (t_{pk}; Figure 3.3) of the N response was shorter in L5A than in L2/3 (Table 4.2), both in WT and KI slices ($P<0.01$ and $P<0.001$, Wilcoxon matched pairs test for WT and KI experiments, respectively), suggesting a faster and/or more synchronous activation of the local network in L5A with respect to L2/3. In L2/3, t_{pk} in the left and right adjacent columns were larger than in the stimulated column (WT: $P<10^{-4}$, KI: $P=3\cdot10^{-4}$, repeated measures 1-way ANOVA), suggesting sequential activation of the local networks. In all layers, time-to-peak was similar in WT and KI mice.

Table 4.1. Synaptic LFPs. Average amplitude of the mean N responses (μV) in electrodes around the stimulating electrode ("stimulus"). A: absolute responses. B: values normalized to the largest response (occurring in L2/3 in the stimulated column) in each slice. Values (black: WT; red: KI) are expressed as mean ± sd (n: number of slices). L1 data are from a subset of experiments where an isolated positive deflection (P) was present (number of experiments marked by *).

A

	left adjacent column	stimulated column	right adjacent column
L1	**4.78** ± **2.29** (5*) **10.34** ± **8.65** (5*)	**7.67** ± **5.72** (7*) **13.69** ± **16.19** (7*)	**8.56** ± **8.13** (4*) **12.11** ± **8.17** (5*)
L2/3	**-34.73** ± **14.90** (21) **-32.17** ± **14.79** (21)	**-74.75** ± **22.76** (22) **-81.05** ± **30.53** (23)	**-32.71** ± **15.19** (21) **-31.00** ± **14.00** (21)
L4	**-39.02** ± **23.56** (20) **-39.41** ± **19.55** (21)	stimulus	**-41.48** ± **31.56** (21) **-45.80** ± **23.20** (21)
L5A	N.A.	**-37.06** ± **22.67** (18) **-41.00** ± **22.15** (21)	N.A.

B

L2/3	**0,46** ± **0,17** (21) **0,41** ± **0,16** (21)	**1** **1**	**0,43** ± **0,18** (21) **0,44** ± **0,22** (16)
L4	**0,52** ± **0,30** (20) **0,57** ± **0,46** (21)	stimulus	**0,58** ± **0,47** (20) **0,71** ± **0,48** (17)
L5A	N.A.	**0,53** ± **0,37** (18) **0,60** ± **0,53** (21)	N.A.

Table 4.2. Synaptic LFPs. Time-to-peak (ms) of the N responses in electrodes around the stimulated electrode (marked by "stimulus"). A: absolute t_{pk} values. B: t_{pk} normalized to L5A value in each slice, to better illustrate its increase in upper layers. Values (in black: WT; in red: KI) are expressed as mean ± sd (n: number of slices). Time-to-peak is shorter in L5A than in L2/3, both in WT and KI slices (see text).

A

	left adjacent column	stimulated column	right adjacent column
L1	**7.40 ± 0.85** (5) **7.15 ± 1.03** (5)	**6.91 ± 0.57** (7) **6.37 ± 1.72** (7)	**7.67 ± 0.46** (4) **6.61 ± 1.13** (5)
L2/3	**5.85 ± 1.07** (21) **6.26 ± 1.04** (21)	**5.39 ± 0.87** (22) **5.52 ± 0.91** (23)	**6.06 ± 0.93** (21) **6.50 ± 1.00** (21)
L4	**5.28 ± 1.18** (20) **5.23 ± 0.83** (21)	stimulus	**5.11 ± 0.64** (20) **5.30 ± 0.50** (20)
L5A	N.A.	**4.83 ± 0.71** (18) **4.83 ± 0.40** (21)	N.A.

B

L2/3	**1,22 ± 0,15** (17) **1,31 ± 0,17** (19)	**1,14 ± 0,12** (18) **1,17 ± 0,16** (21)	**1,29 ± 0,16** (17) **1,37 ± 0,25** (16)
L4	**1,05 ± 0,28** (18) **1,08 ± 0,15** (21)	stimulus	**1,02 ± 0,30** (18) **1,10 ± 0,12** (20)
L5A	N.A.	**1** **1**	N.A.

In a large fraction of the recordings, a visible asymmetry of the N response size in the two columns adjacent to the stimulated column was present. When measuring the ratio of the L2/3 response to the right and left of the stimulated column, values well below or above 1 were obtained in most cases (ratio < 0.8 or >1.2 in 17 of 22 WT slices and 12 of 22 KI slices), and similar degrees of asymmetry were present in L4 (ratio < 0.8 or >1.2 in 12 of 20 WT slices and 11 of 20 KI slices; Figure 4.3). This might be explained by considering geometrical and functional factors influencing local activity. Upon stimulation of an L4 barrel, maximal synaptic activation should be obtained inside the related cortical column, because most of the neuritic arborization of the stimulated

neurons is confined inside the column itself. Moreover, a single barrel and its functionally related column may have a horizontal width up to 300-350 μm (see Methods and references therein), therefore two adjacent electrodes from a MEA row, separated by 200 μm, may underlie a single barrel, in which case the opposite adjacent electrode would probably contact a septal region or an adjacent barrel, therefore reporting less intense activation.

The attenuation of the N response propagated laterally in L2/3, relative to its value in L2/3 in the stimulated MEA column, was also slightly, although not significantly, larger in KI than in WT animals (Figure 4.4). In L2/3, the ratio of mean N amplitude in one of the adjacent columns (chosen as the one with largest response) and in the stimulated column was 0.54 ± 0.03 in n=22 WT slices and 0.46 ± 0.03, in n=22 KI slices (mean ± s.e.m; P=0.115, Mann-Whitney test).

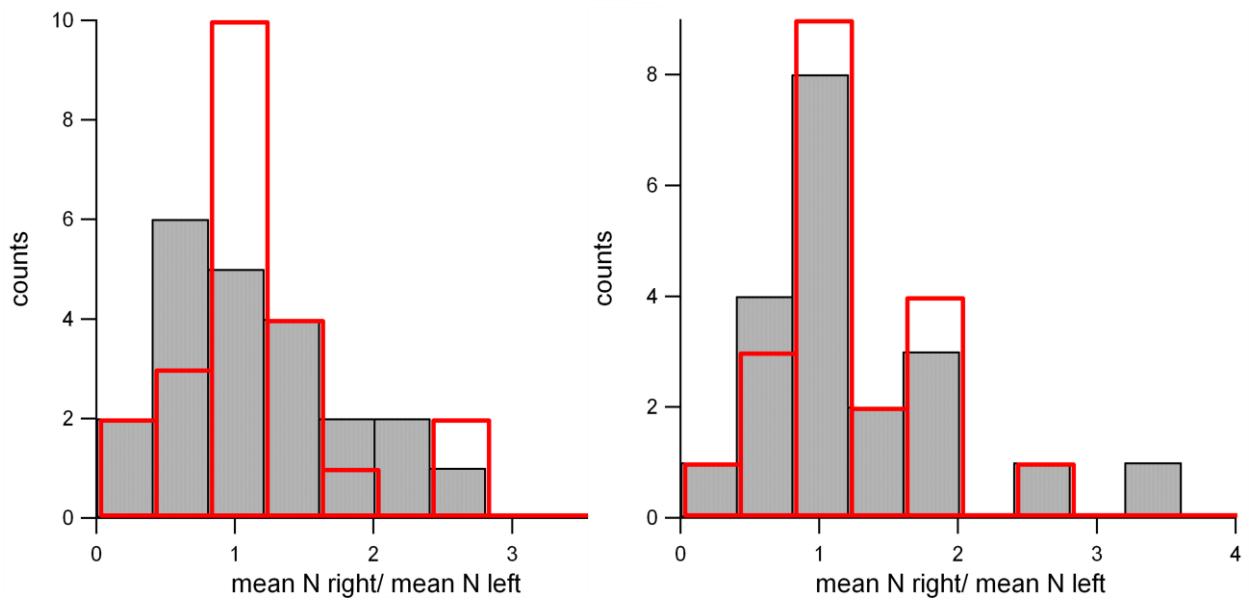

Figure 4.3. Asymmetry of N responses in L2/3 (left) and L4 (right). The distributions of the ratio of the N amplitude in the right adjacent column over the corresponding value in the left adjacent column, from 22 WT (in grey) and 22 KI (in red) slices. Notice that a large number of ratios are substantially smaller or larger than 1, indicating asymmetry between adjacent columns (see text).

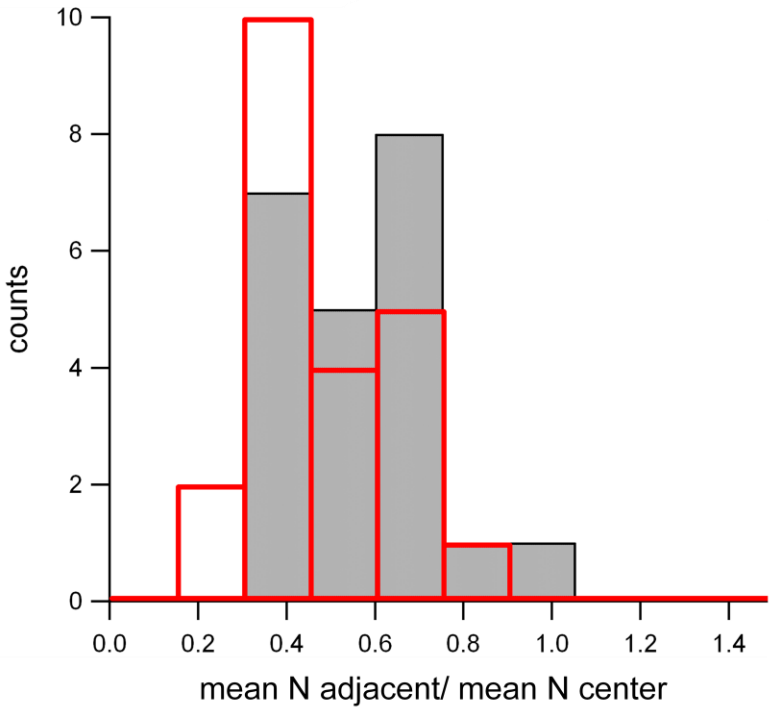

Figure 4.4. Attenuation of the N response in L2/3.
Distribution of the attenuation of the N response in L2/3 from 22 WT (in grey) and 22 KI (in red) experiments. The attenuation is the ratio of the N response in the adjacent L2/3 electrode with largest response, over the N response in L2/3 in the stimulated MEA column. Attenuation is slightly, although not significantly, larger in KI than in WT animals (see text).

4.2 Short-term plasticity after trains of stimuli in L4: larger depression of KI LFPs

It was shown that, upon stimulation with short trains, different excitatory and inhibitory synapses of the somatosensory cortex in WT animals have different, target-dependent short term plasticity behavior, going from strong depression to large facilitation (see Discussion). Moreover, differential effects of the R192Q mutation have been reported at different excitatory and inhibitory synapses (see Discussion).

The N signal observed in our study should reflect the combined presence of excitatory and inhibitory post-synaptic potentials (EPSPs/IPSPs) from a complex, undetermined mixture of partly facilitating and partly depressing synapses formed by axonal fibers activated by the stimulating MEA electrode in L4. Therefore, it is difficult to predict how the LFP should evolve along a train of stimuli, both in WT and in KI mice.

Upon trains of 5 stimuli at 50 Hz we analyzed the response in layers 2/3, 4 and 5A in the stimulated column and its first adjacent columns. The ratio of the 5th over the 1st N response (N_5/N_1) revealed in most cases a clear depression in all layers (Figure 4.2). In WT slices, depression in L2/3 (in the stimulated column) was correlated to the size of the first N response (see Figure 4.5 legend), while this was not the case in KI slices; no such correlation was observed in any other layer, in WT or in KI slices (Figure 4.5). Interestingly, depression was significantly more prominent in KI animals in

all layers (Table 4.3 and Figure 4.5). At the fifth stimulus of a 50 Hz train, depression in L2/3 was ~0.84 in WT and ~0.57 in KI slices, a result qualitatively similar to what observed with paired patch-clamp recordings at WT and KI L2/3 PC-FS synapses (Tottene et al., 2009, their Fig.7D). This suggests that these synapses contribute to the LFPs, although the depression observed here in LFPs is smaller than reported at PC-FS synapses, as if other synaptic types also contributed to the LFP response (see Discussion).

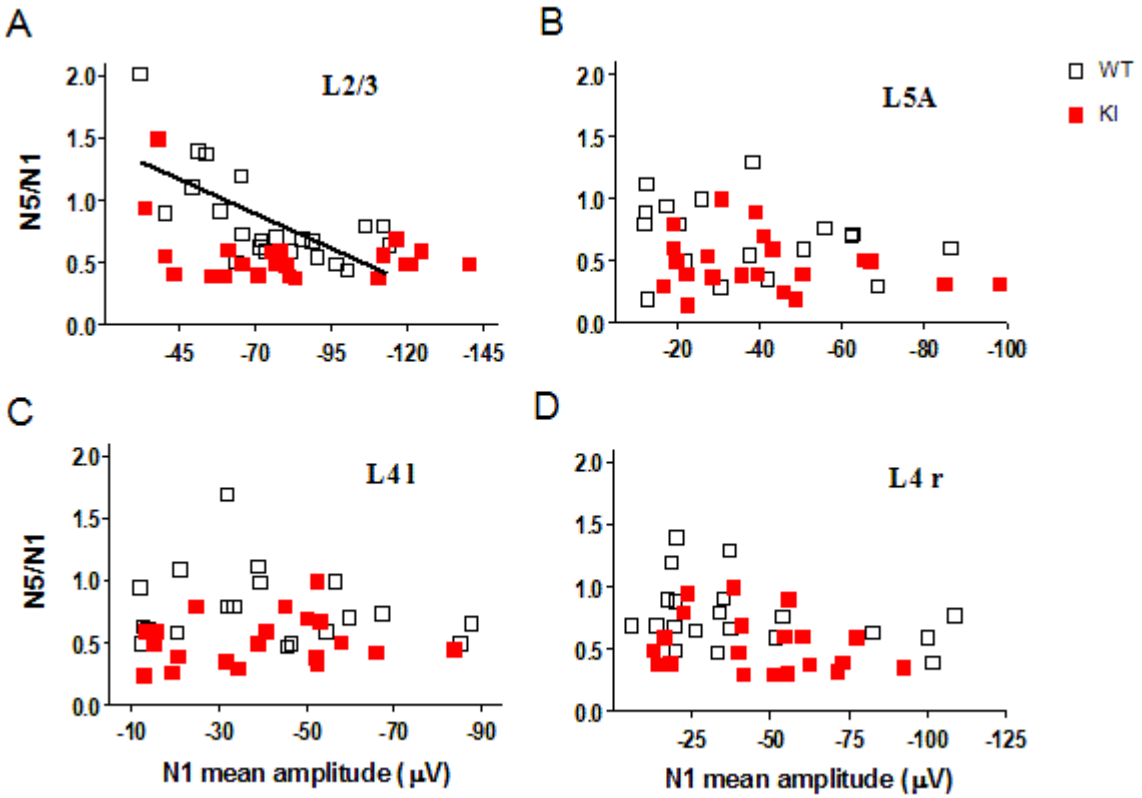

Figure 4.5. Short-term depression of N responses. The amplitude ratio of the 5th to the 1st N response (depression) is plotted versus the 1st response amplitude. In all layers depression appears to be greater in KI (red squares) than in WT (black squares) slices. A-D. Depression in L2/3 (panel A), L5A (panel B), in the first electrode to the left of the stimulating electrode (L4l: panel C), and first electrode to the right (L4r: panel D) in L4. In WT, but not in KI slices, depression in L2/3 in the stimulated column (panel A) is linearly correlated to the size of the first N response (R^2=0.449; P=0.0006). The corresponding regression line is shown. There is no correlation at the other locations.

The speed of recovery from depression may significantly influence network computation and the E/I balance (Abbott & Regehr, 2004). We studied the recovery of the N peak from depression induced by a train of 5 stimuli at 50 Hz, in L2/3. The amplitude of the N peak was measured at 2, 6 or 10 seconds after a train (Figure 4.6, Table 4.4) and its ratio to initial amplitude (amplitude of the first evoked response in the preceding train) was calculated. Recovery was significantly dependent

on time after the train ($P<10^{-4}$, 2-way repeated measures ANOVA), being still incomplete after 10 s (Table 4.4). Recovery was apparently (but not significantly, P=0.194), faster in KI mice (Figure 4.6, Table 4.4). More experiments, and possibly longer trains of stimuli, may be needed to completely clarify whether recovery from depression is altered in the cortical networks of KI mice.

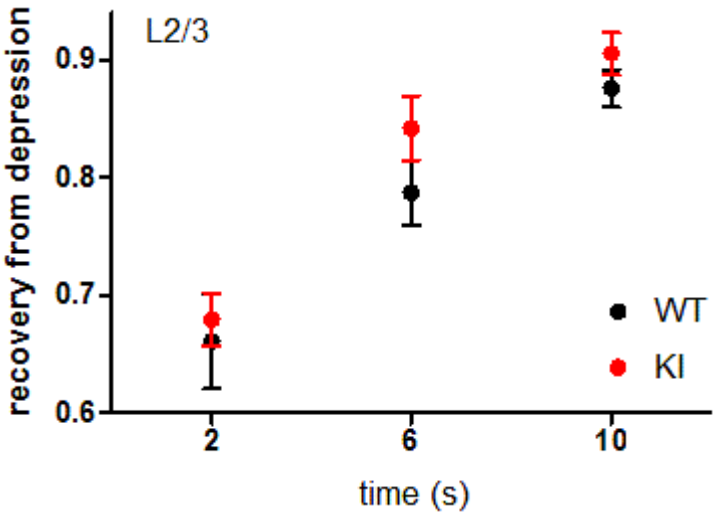

Figure 4.6.Recovery from depression in L2/3 of the stimulated column. The N response to an isolated test stimulus, normalized to the response to the first stimulus in the preceding train, is plotted for three different delays between train and test stimulus. Red and black symbols summarize results from n=11 KI slices and n=14 WT slices, respectively. Error bars: s.e.m.

Table 4.3. Depression of mean N response at 5th stimulus (50 Hz train). Mann Whitney tests confirm that in KI slices a significantly more prominent depression than in WT slices is present in all layers. Values (in black: WT; in red: KI) are expressed as mean ± sd (n).

	left adjacent column	stimulated column	right adjacent column
L2/3	**0.78 ± 0.35** (21) **0.57 ± 0.28** (21) **P = 0,005 ****	**0.84 ± 0.38** (22) **0.57 ± 0.25** (23) **P < 0,001 *****	**0.75 ± 0.24** (21) **0.55 ± 0.25** (21) **P = 0,003 ****
L4	**0.78 ± 0.30** (20) **0.51 ± 0.20** (21) **P = 0,002 ****	stimulus	**0.78 ± 0.26** (20) **0.54 ± 0.22** (20) **P = 0,005 ****
L5A	N.A.	**0.70 ± 0.30** (18) **0.48 ± 0.22** (21) **P = 0,032 ***	N.A.

Table 4.4. Recovery from depression of mean N response in L2/3. Response to a test stimulus, normalized to the response to first stimulus of the preceding train (5 stimuli at 50 Hz). The test stimulus is given with a delay of 2, 6 or 10 seconds after the train. In each electrode, recovery is significantly dependent on delay, though still incomplete after 10 seconds, and it appears to be faster in KI than in WT animals, though not significantly different upon a 2-way analysis of variance. Values (in black: WT; in red: KI) are expressed as mean ± sd (n).

	L2/3 left adjacent column	L2/3 stimulated column	L2/3 right adjacent column
2 s	**0,65 ± 0,14** (13) **0,62 ± 0,07** (9)	**0,66 ± 0,15** (14) **0,68 ± 0,07** (11)	**0,63 ± 0,15** (13) **0,65 ± 0,08** (10)
6 s	**0,81 ± 0,11** (13) **0,83 ± 0,08** (9)	**0,79 ± 0,10** (14) **0,84 ± 0,09** (11)	**0,78 ± 0,12** (13) **0,86 ± 0,14** (10)
10 s	**0,89 ± 0,06** (21) **0,94 ± 0,10** (21)	**0,90 ± 0,07** (22) **0,93 ± 0,07** (23)	**0,90 ± 0,10** (21) **0,93 ± 0,08** (21)

4.3 Spontaneous activity: up-states

Upon positioning a thalamocortical slice on the MEA chip, visual inspection of the MEA voltage recordings revealed variable patterns of spontaneous activity. Qualitatively, we classified this activity into three categories:

1) "up-states", or episodes involving simultaneously numerous electrodes in the chip, lasting a few seconds, and repeating at low rate (a few per minute). Up-states started from one (or a few contiguous) electrodes ("origin") and rapidly propagated to nearby electrodes in the MEA column of the origin ("primary column"), and in at least one or two nearby columns (Figure 4.7A);

2) "isolated LFPs": single biphasic deflections of 50-100 ms duration and 20-50 μV amplitude, appearing in one or a few electrodes (Figure 4.7B);

3) "spikes and spike bursts", rapid (in the ms range) biphasic deflections, putatively representing isolated spikes or bursts of spikes from a single or multiple neuronal units, appearing in one or a few contiguous or non-contiguous electrodes in any cortical layer (Figure 4.7B).

Spontaneous activity was detected using a threshold-crossing algorithm evaluating fluctuations of a running standard deviation (σ) of the voltage signal (see Methods).The algorithm allowed up-states to be effectively separated from isolated LFPs, spikes and spike bursts.

Up-states resembled the oscillations previously described in electrical extracellular recordings in cortical slices (Sanchez-Vives & McCormick, 2000; Rigas & Castros-Alamancos, 2007; Wester & Contreras, 2012.; Beltramo et al., 2013), and were, therefore, given the same name. However, they occurred at lower frequency (Figure 4.8), as may be expected given that our recordings were performed at room temperature, unlike more physiological temperature in the other studies. To increase membrane excitability and facilitate the occurrence of spontaneous activity, we routinely recorded from slices maintained in a modified BBS (mBBS; see Methods), with higher [K^+] and lower [Ca^{2+}] and [Mg^{2+}].

In our recordings, voltage traces were acquired in a large frequency band (10 Hz to 3 kHz). They included low frequency components (LFPs), typically interpreted as post-synaptic potentials, and higher frequency components (multi-unit activity, >500 Hz), typically interpreted as spikes (see footnote page 7, paragraph 1.1). Accordingly, in a single episode of spontaneous activity, large, slow oscillations (typically 70-100 ms for a single oscillatory cycle) generally superimposed to fast, small deflections in the ms range, most likely representing individual spikes from nearby neuron(s) (Figure 4.7). Given the attenuation below 10 Hz produced by the high-pass filter in the MEA

amplifiers, DC and very-low (<10 Hz) frequency components were cancelled, and slow oscillations in up-states appeared as biphasic waves around zero mean.

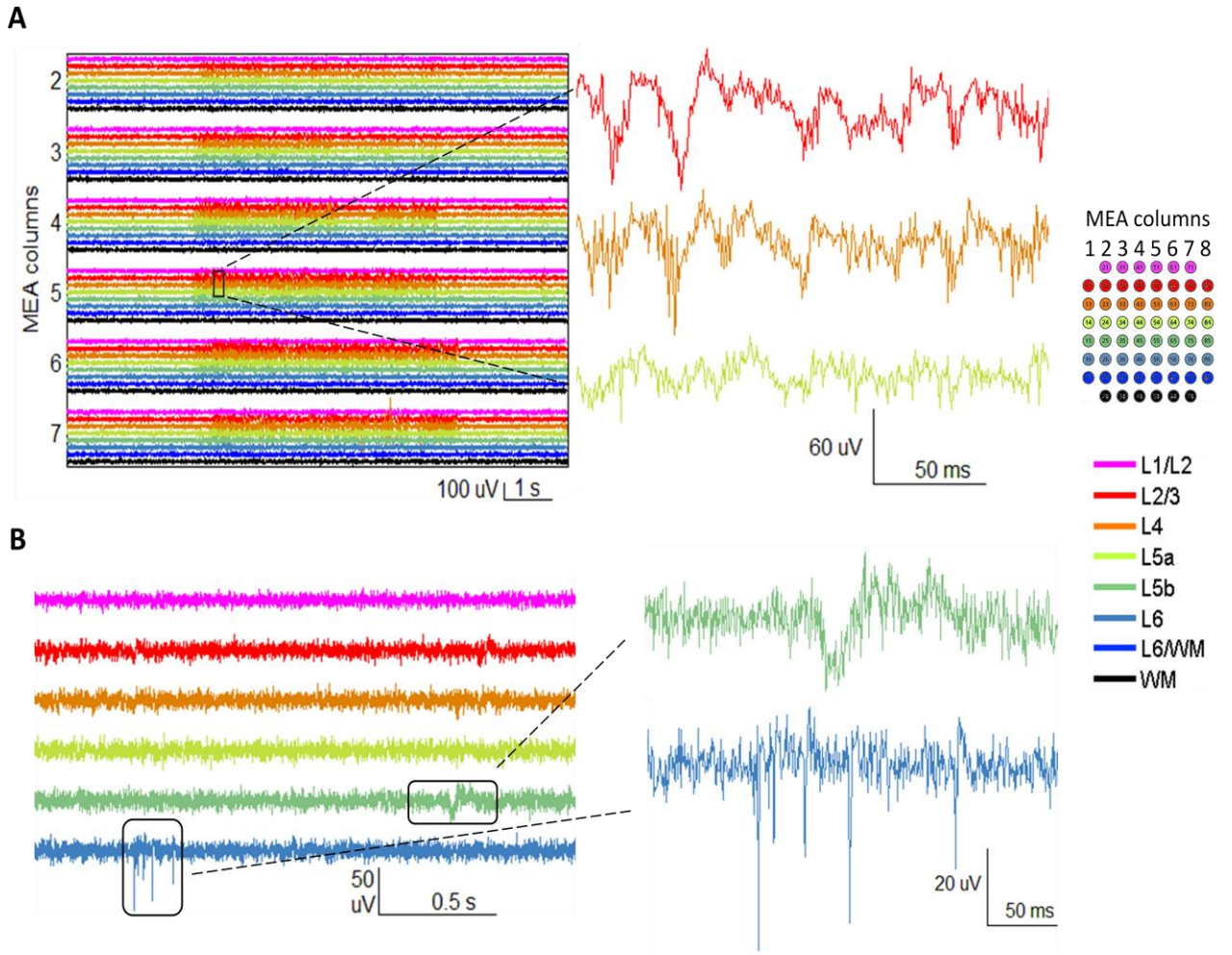

Figure 4.7. Spontaneous activity. A. Up-state lasting 5 seconds, starting from electrode 52 and propagating to nearby columns: three sample traces are enlarged in the inset. MEA columns numbers are indicated in the electrodes layout. B. An isolated LFP and spikes from one MEA column: enlarged in the inset. Cortical layers are color coded.

4.4 Up-states: frequency, layer of origin, strength and duration

Up-state frequency is higher in KI. Up-states were observed in most experiments (19 of 23 slices in 9 WT animals, and 18 of 25 slices in 9 KI animals). Their frequency was measured in accurately standardized conditions in a 15' time interval starting 20' after beginning slice perfusion with mBBS (2.5 ml/min). Nevertheless, the frequency of up-states was quite variable among experiments (Figure 4.8), with an average of 2.7 ± 0.16 min^{-1} in WT slices (n=19), and 3.2 ± 0.16 min^{-1} in KI slices (n=18) (mean ± s.e.m.). These average values were significantly different (P=0.013, Mann-Whitney test), indicating a stronger tendency of KI slices to produce spontaneous activity.

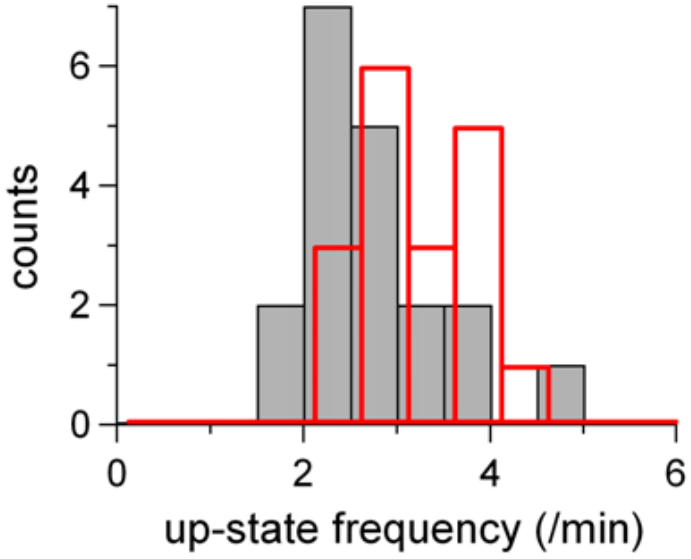

Figure 4.8. Frequency of up-states. Histogram of the frequencies measured in 19 WT (in grey), and 18 KI (in red) experiments.

Difference between WT and KI up-state origin. The mechanisms and site of initiation of spontaneous up-states, are thought to depend on the intrinsic properties of the various neuronal types in the cortical network and on the number and properties of their connections, and are still largely debated. To contribute to this debate, and to verify whether the R192Q migraine mutation influences the production of up-states, we wished to determine, for each episode, in which cortical layer the activity started first.

We defined as "origin" of the up-state the site corresponding to the MEA electrode where the episode was first detected. We analyzed 176 WT and 211 KI episodes (27% of all WT and 27% of all KI up-states) with well-identified origin inside the MEA chip (between MEA columns 2 and 7; group I episodes, see Methods). Up-states first detected in the lateral columns 1 or 8, which might have propagated from a cortical region outside the MEA chip, were excluded. In both WT and KI,

origins were found in any cortical layer, from L2/3 to L4, L5A and L5B (only very rarely in L1 or L6). However, the distribution of the layers of origin was different for the two strains (Figure 4.9): the probability of finding an origin in L2/3 was nearly 50% higher in KI with respect to WT animals ($P<0.01$, 2-way ANOVA with Bonferroni post-test). Accordingly, in KI mice the probability in L2/3 was significantly higher than in the infragranular layers ($P<0.001$) and in L4 ($P<0.01$). This shows that the KI cortical network in L2/3 is better suited to generate synchronized population activity than the WT one.

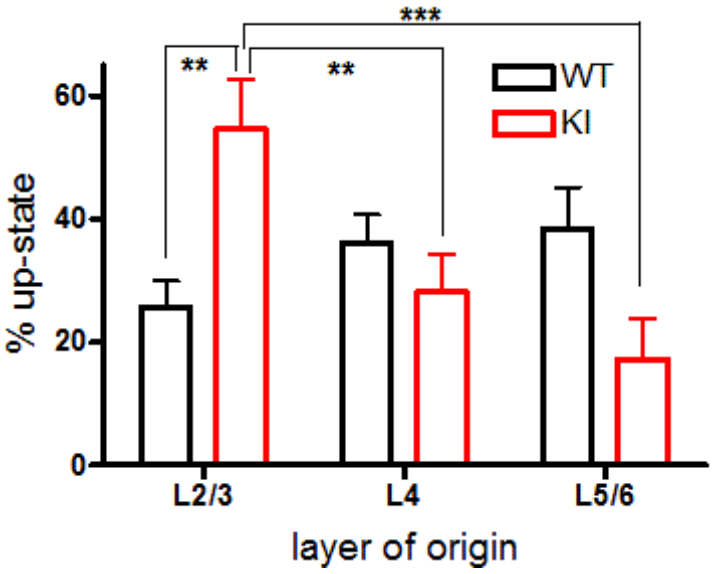

Figure 4.9. Up-states layer of origin. The percentage of up-states with origin in layers 2/3, 4 or 5/6 in 19 WT (in black; 176 total episodes), and 18 KI (in red; 211 total episodes) experiments. Bars represent means ± standard error of the mean. Brackets and stars indicate statistical significance (**: $P<0.01$; ***: $P<0.001$).

Difference between WT and KI up-state strength. For each up-state, we wished to measure a parameter related to the overall strength of the episode, and to localize the cortical layer where the strength was maximal. Given that in our recordings an up-state appears as a sequence of biphasic fluctuations over baseline voltage, to measure its strength, we computed the sum of the excess standard deviation of the voltage fluctuations along the up-state, which is related to the area under the up-state (see Methods), and we then divided this value by the duration of the episode, to yield an "area per unit time". Finally, in order to find the position in the cortex where the strength of neuronal activation was maximal, we looked for the maximal area per unit time across all MEA electrodes, which was called the "up-state strength", and the cortical layer where the area per unit time was maximal ("most active layer") was annotated.

Analysis of strength was again restricted to up-states of group I, with well-defined origin inside the MEA chip (see above). In WT the strength was 65.7 ± 48 % /s (n=176 up-states) and in KI 63.6 ± 38.3 % /s (n=211 up-states). In both strains the distributions were skewed, with a large number of small strengths (Figure 4.10). However, the two distributions were different, as shown by a

Kolmogorov-Smirnov test[1] (P=0.010): the median value was larger for KI events (50.6 % /s for KI versus 42.5 % /s for WT events) and an excess of intermediate values were observed in KI.

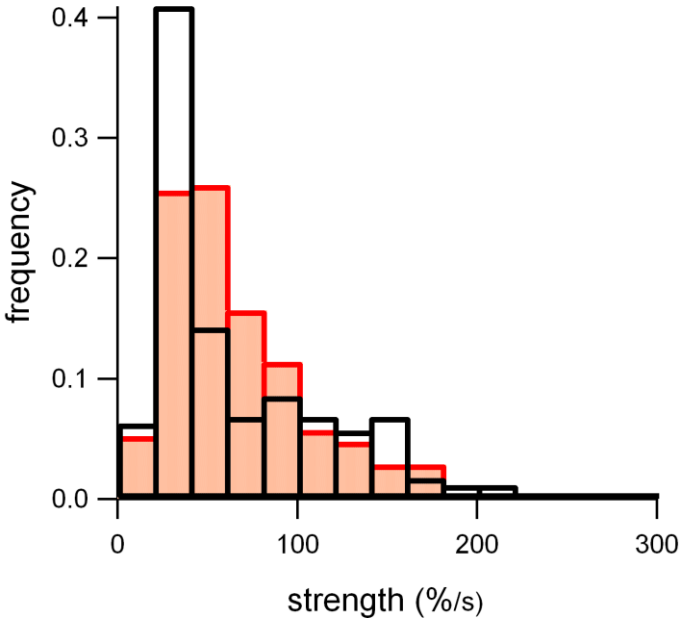

Figure 4.10. Strengths of up-states. Histogram of the max area per unit time of voltage fluctuations ("strength", %/s) measured in 176 up-states from 19 experiments in WT (black bars) and 211 up-states from 18 experiments in KI (red bars).

To better characterize the source of this difference, we explored the relation between the up-state strengths and the most active layers (Figure 4.11). Strengths were significantly dependent on the layer of maximal activation, (2-way ANOVA with Bonferroni post-test; P<0.0001), and moreover the roles of some layers were different in the two strains. For WT, up-state strengths were higher when the most active layer was in L4 than in L5A (P<0.01) or L5B (P<0.05), but not significantly different from L2/3. For KI, up-state strengths were significantly higher when the most active layer was in L2/3 than in L4 (P<0.001), L5A (P<0.001) or L5B (P<0.01); up-state strength measured in L2/3 appeared to be larger in KI than in WT, but this difference was not statistically significant (in WT relatively few up-states were most active in L2/3), while up-state strength measured in L4 was significantly smaller in KI than in WT (P<0.01). We conclude that KI local networks involved in up-states seem to display less, or less strong, synchronous activity in L4 than in L2/3, and than observed in L4 in WT.

[1] The KS-test seeks differences between two datasets; it is a non-parametric, distribution free test.

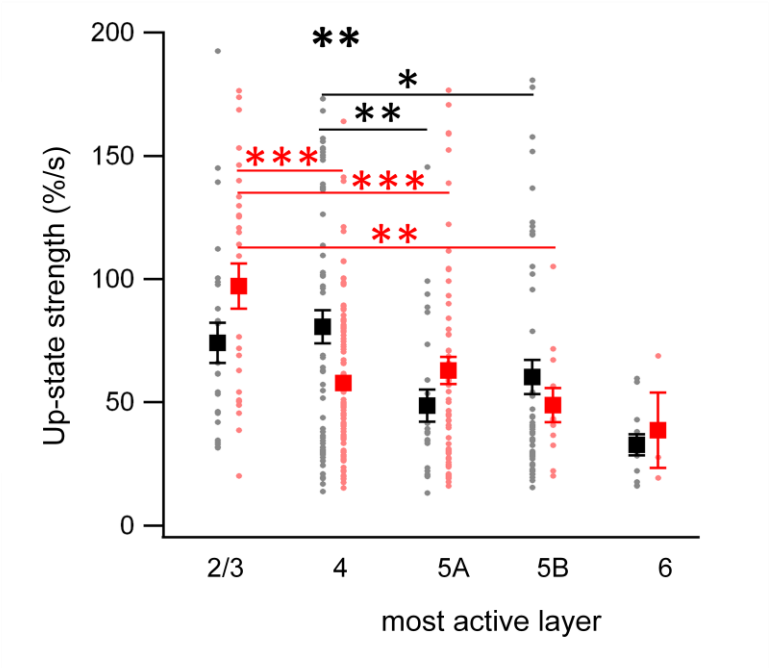

Figure 4.11. Up-state strength versus the most active layer. The maximal area of voltage fluctuations per unit time versus the layer in which maximal activation occurred ("most active layer"). Gray and red dots are from 176 WT and 211 KI up-states, respectively. Closed symbols (black: WT; red: KI) are the respective averages with standard error of the mean for each layer. The two asterisks on top show a significant difference between WT and KI strengths in L4. The other asterisks show statistical significance described in the text (see above).

Up-state duration. For each up-state with well-detected origin inside the chip area (group I episodes; see Methods), a total duration was measured as the time interval from first detection in the origin to return to baseline in the last involved electrode. The total duration was variable, spanning from a lower limit (imposed by the detection algorithm) of 0.8 s, up to many seconds (16.6 s). The overall mean duration was similar in the two strains: 4.38 ± 3.21 s in WT and 4.45 ± 2.96 s in KI mice. The respective distributions of durations were skewed, with a large number of short durations (Figure 4.12).

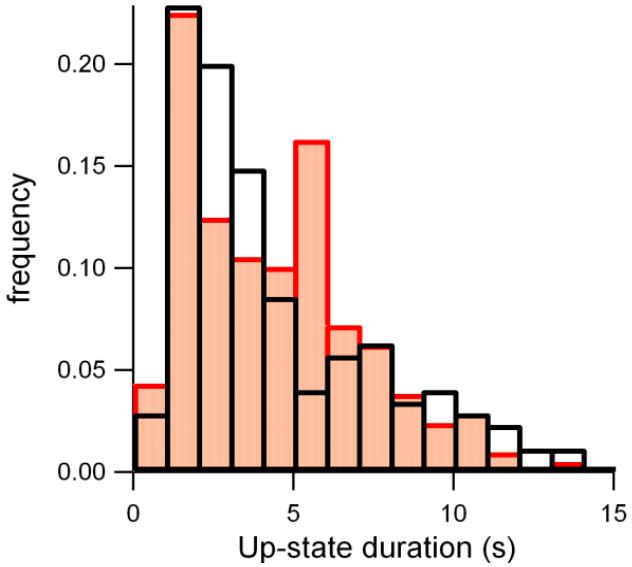

Figure 4.12. Up-state durations. Histogram of up-state durations in 176 up-states from 19 WT experiments (black bars) and 211 up-states from 18 KI experiments (red bars).

Kolmogorov-Smirnov test indicated a significant difference in the distribution of up-state durations (P=0.029), with a larger number of intermediate durations, and larger modal and median values in KI than in WT (mode: 1.15s in WT, 1.35s in KI; median: 3.35s in WT and 4.16s in KI).
We analyzed the possible relations between up-state duration and most active layer (Figure 4.13). Durations were significantly influenced by layer. WT durations were significantly longer in L4 than in L2/3 (P<0.01), L5A (P<0.05) and L5B (P<0.05). On the contrary, KI durations in L2/3 were not shorter than in L4, and they were longer than in L5B (P<0.05).

Overall, analysis of up-states strengths and durations reveals that while in WT slices the layer producing the longest and strongest up-states seems to be L4, in KI slices the longest, strongest up-states occur in L2/3, with L4 definitely displaying weaker activity than in WT.

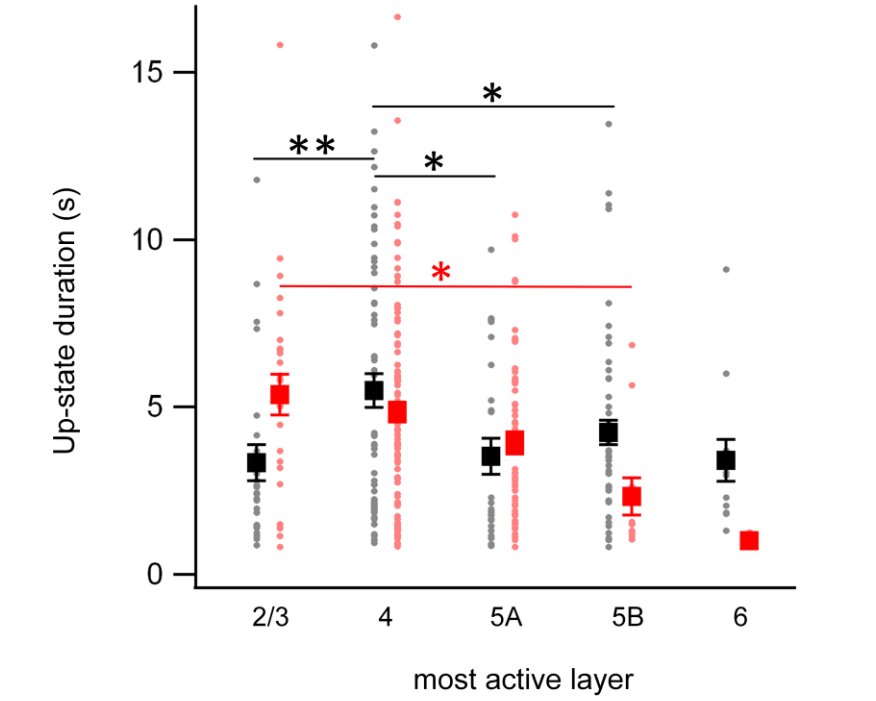

Figure 4.13. Up-state duration versus the most active layer. Grey and red dots are from 176 WT up-states and 211 KI up-states, respectively. Closed symbols (black: WT; red: KI) are the respective averages with standard error of the mean for each layer. Asterisks show statistical significance described in the text (see above).

4.5 Intracolumnar up-states propagation

Having characterized the "origin" of an up-state and the "most-active layer" (which often, but not necessarily, coincided), we examined how up-states propagate in the cortical network. The study of intralaminar propagation in the "horizontal" direction, parallel to the pial surface, was complicated by the evident asymmetry of propagation in the two opposite directions on the sides of the first activated MEA column (not shown), and was therefore abandoned. We rather concentrated on the propagation in the intracolumnar "vertical" direction inside the cortical column of origin. We separated up-states into subgroups according to their layer of origin, and we computed a parameter related to propagation velocity, i.e. the delay of up-state detection with respect to first detection in the origin, for each subgroup. We compared WT and KI delays for the two subgroups with origin in L2/3 ("Up_{23}") and L5A ("Up_{5A}"), by forming, for each up-state, a "delay matrix", with the origin (delay=0) at the center of a 15x15 array, and the remaining array positions containing the delay in the electrodes around the origin. Delay matrices were separately averaged for Up_{23} and Up_{5A}, and average delay matrices are reported in Figure 4.14 (standard errors of the mean are reported for each electrode in the respective matrix position). Only up-states with well-detected origin inside the MEA chip (group I up-states) were analyzed.

We found a significant difference between WT and KI intracolumnar propagation speeds. As regards Up_{23} events, propagating towards L5A, KI up-states propagated much slower, with a L2/3 to L5A delay of 0.14 ± 0.12 s in WT mice (n=43 events) and 0.23 ± 0.16 s in KI mice (n=106 events) (mean ± s.d. across experiments; P=0.001, Unpaired t test). On the contrary, for Up_{5A} propagating towards L2/3, KI up-states propagated faster, with a L5A to L2/3 delay of 0.26 ± 0.23 s in WT mice (n=28 events) and 0.12 ± 0.11 s in KI mice (n=16 events) (mean ± s.d.; P=0.028).

The speed of propagation of an up-state is most likely influenced in a complex way by the balance of excitatory and inhibitory recurrent local activity. A smaller (larger) speed might indicate a stronger (weaker) activation of local inhibitory circuits, and/or a weaker (stronger) activation of excitatory neurons. At the moment, it is not possible to distinguish between these possibilities, based on our data.

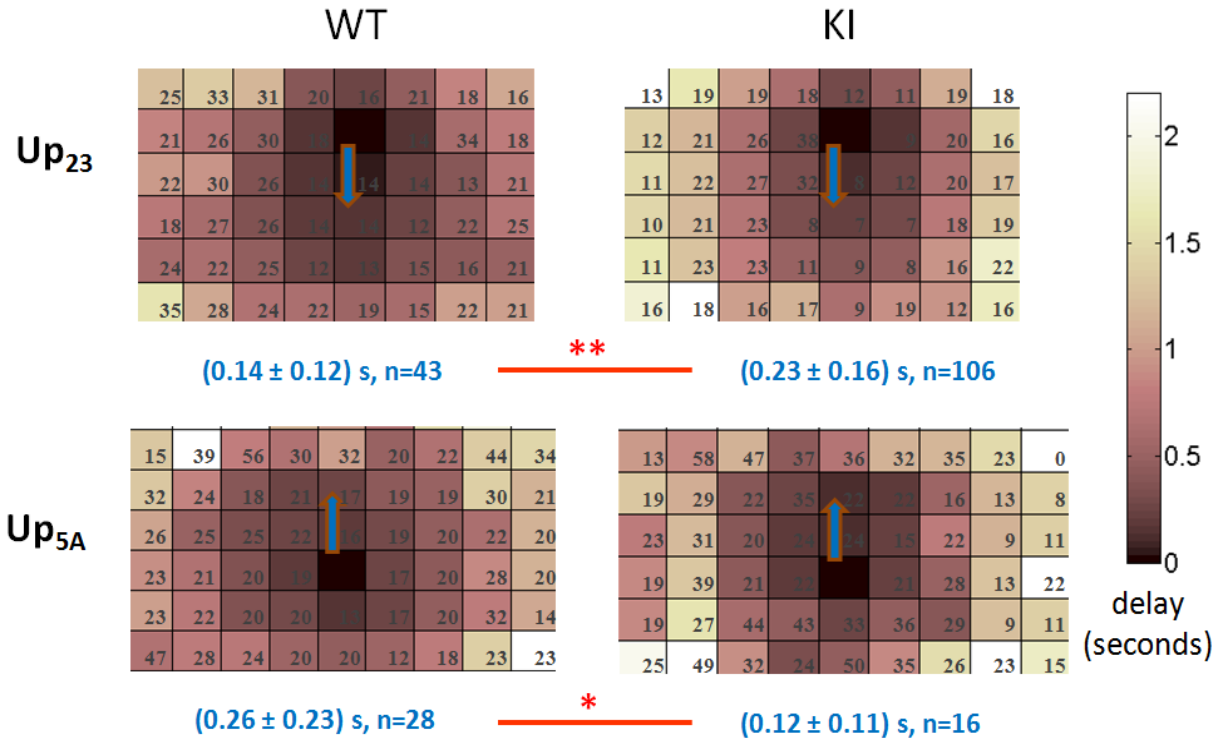

Figure 4.14. Different WT and KI intracolumnar up-state propagation delays. Color-coded matrices representing the average up-state detection delay after first detection in the origin in the other MEA electrodes. In each matrix, the origin is represented by the dark brown cell in the central column. Up_{23}: up-states with origin in L2/3. Up_{5A}: up-states with origin in L5A. The numbers below each matrix report the delay from the origin to the intracolumnar L5A (top) or L2/3 (bottom); the blue arrows point from the origin to the respective L5A or L2/3 electrodes. The number in grey in each cell represents the percentage standard error of the mean delay (100·s.e.m./mean). **: P<0.01; *: P<0.05.

5. RESULTS (II): characterization of the TKO epilepsy mouse model

In this section, a preliminary analysis of network excitability in the somatosensory cortex of Syn I/II/III triple knockout (TKO) mice at presymptomatic ages (P24-P36) is reported. A series of pilot experiments has been performed in matched WT and TKO mice, as described below.

5.1 Characterization of LFPs evoked by an isolated stimulus in layer 4 (L4)

Evoked responses were analyzed in 18 slices from 5 WT mice, and 15 slices from 5 TKO mice. In both groups the response to isolated stimuli delivered to layer 4 (L4) consisted of an early "population spike", followed by a negative deflection peaking at ~5 ms from stimulus ("N peak"). Short trains of 5 stimuli at 50 Hz evoked successively declining (depressed) N responses (Figure 5.1). These patterns, observed in electrodes corresponding to supragranular, granular and infragranular layers around the stimulation electrode (El_{st}), were similar to what previously described in paragraph 4.1.

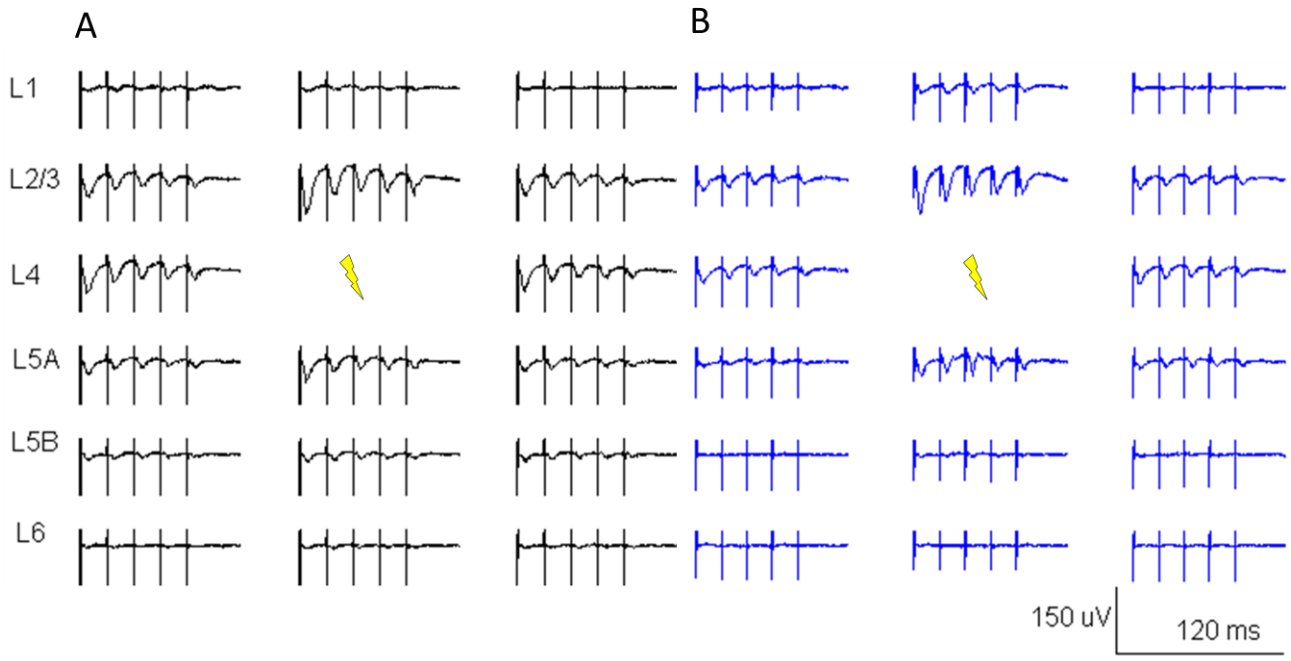

Figure 5.1 Evoked synaptic LFP responses in matched WT and TKO mice. A. Examplar WT experiment; stimulus intensity: 14 µA. B. Examplar TKO experiment; 13 µA. Stimulating electrodes are marked by yellow symbols. The ratio of the 5th over the 1st N response (N_5/N_1) reveals a clear depression in all layers in both examples. Cortical layers are indicated on the left.

The sizes of N responses in the stimulated column and in lateral columns were similar in WT and TKO mice, therefore presenting a similar spatial attenuation in both strains (Table 5.1).

Table 5.1. Synaptic LFPs. Average amplitude of the mean N response (µV) to an isolated stimulus in electrodes around the stimulating electrode ("stimulus"). A: absolute responses. B: values normalized to the largest response (occurring in L2/3 in the stimulated column) in each slice. Results (in black: WT; in blue: TKO) are expressed as mean ± sd (n).

A

	left adjacent column	stimulated column	right adjacent column
L2/3	**-26.70 ± 9.20** (18) **-26.20 ± 11.00** (15)	**-65.30 ± 14.40** (18) **-63.90 ± 26.60** (15)	**-36.00 ± 21.00** (18) **-33.83 ± 23.42** (15)
L4	**-24.80 ± 11.50** (17) **-27.00 ± 11.30** (15)	stimulus	**-36.40 ± 22.00** (17) **-40.70 ± 24.80** (15)
L5A	N.A.	**-23.90 ± 8.60** (15) **-25.00 ± 10.80** (14)	N.A.

B

L2/3	**0,42 ± 0,13** (18) **0,43 ± 0,17** (15)	**1** **1**	**0,54 ± 0,27** (18) **0,52 ± 0,21** (15)
L4	**0,39 ± 0,18** (17) **0,46 ± 0,21** (15)	stimulus	**0,57 ± 0,38** (17) **0,70 ± 0,49** (15)
L5A	N.A.	**0,37 ± 0,15** (15) **0,45 ± 0,29** (14)	N.A.

In the stimulated column, the time-to-peak (t_{pk}; see also Figure 3.3) of the N response was shorter in layer 5A (L5A) than in layer 2/3 (L2/3) (Table 5.2), both in WT and TKO slices ($P<0.001$, repeated measures 2-way ANOVA), suggesting a faster activation of the local network in L5A with respect to L2/3, similar to results described in the previous section (Table 4.2). Interestingly, a comparison between t_{pk} values in WT and TKO indicates a general faster network activation in TKO slices in all layers ($P=0.02$; Table 5.2).

Table 5.2. Synaptic LFPs. Time-to-peak (ms) of the N responses in electrodes around the stimulated electrode (marked by "stimulus"). A: absolute t_{pk} values. B: t_{pk} normalized to L5A value in each slice, to better illustrate its increase in upper layers. Values (in black: WT; in blue: TKO) are expressed as mean ± sd (n: number of slices). 2-way ANOVA shows that t_{pk} is shorter in L5A than in L2/3 of the stimulated MEA column, both in WT and TKO slices (see text). Moreover, in all positions t_{pk} is shorter in TKO than in WT (P=0.02).

A

	left adjacent column	stimulated column	right adjacent column
L2/3	**6.28 ± 0.98** (18) **5.61 ± 0.54** (15)	**5.49 ± 0.68** (18) **5.04 ± 0.39** (15)	**6.19 ± 0.96** (18) **5.63 ± 0.54** (15)
L4	**5.25 ± 0.93** (17) **4.94 ± 0.51** (15)	stimulus	**5.33 ± 1.02** (17) **4.70 ± 0.33** (15)
L5A	N.A.	**4.63 ± 0.48** (15) **4.23 ± 0.66** (14)	N.A.

B

L2/3	**1,36 ± 0,24** (15) **1,34 ± 0,18** (14)	**1,20 ± 0,19** (15) **1,20 ± 0,15** (14)	**1,34 ± 0,25** (15) **1,36 ± 0,17** (14)
L4	**1,15 ± 0,18** (15) **1,18 ± 0,14** (14)	stimulus	**1,12 ± 0,17** (15) **1,13 ± 0,13** (14)
L5A	N.A.	**1** **1**	N.A.

5.2 Short-term plasticity after trains of stimuli in L4

In presymptomatic TKO mice (up to 2-3 months of age), the genetic deletion of Syn I/II/III was shown to affect both excitatory and inhibitory synaptic transmission, with an enhancement of basal excitatory responses in the hippocampus and entorhinal cortex, and an impairment of inhibitory responses, which turns into an enhancement in the entorhinal cortex (but not in the hippocampus) at the onset of epilepsy (see paragraph 1.4.1). The mutation therefore seems to affect different synapses in different ways. The N signal observed in our study should reflect the combined presence of EPSPs and IPSPs from a variety of synapses formed by excitatory and inhibitory axonal

fibers activated by the stimulating MEA electrode in L4. Therefore, as in the case of the migraine R192Q mutation, the effect of the TKO mutation onto short-term plasticity is difficult to predict.

We analyzed the response to 50 Hz trains of 5 stimuli in layers 2/3, 4 and 5A in the stimulated and adjacent MEA columns. As mentioned, the ratio of the 5th over the 1st N response (N_5/N_1) revealed a clear depression in all layers (Figure 5.1) in most cases. Depression was similar in WT and TKO experiments, and no correlation between depression and the size of the first N response was observed in any layer (Table 5.3 and Figure 5.2).

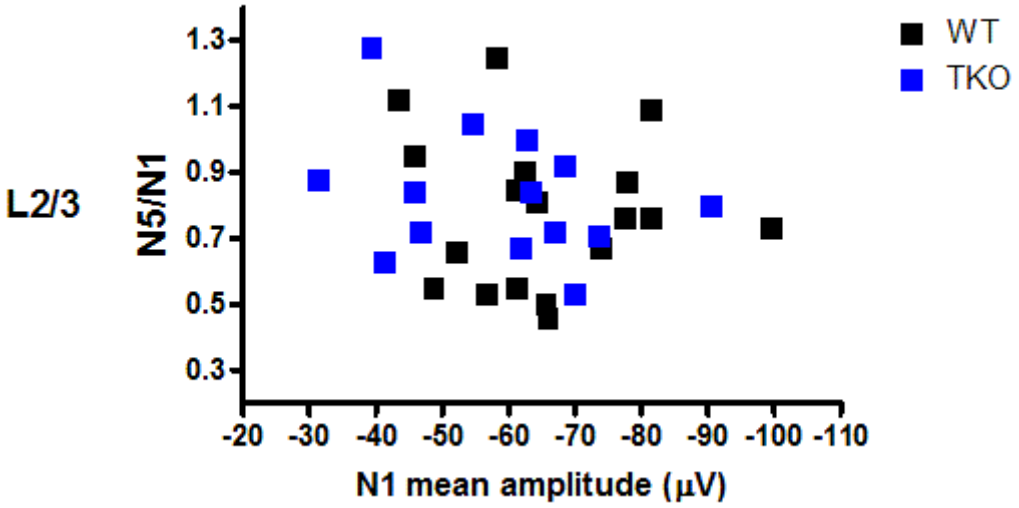

Figure 5.2 Short-term depression of N responses in L2/3. Similar depression in TKO and WT slices. No correlation is observed between depression values and mean amplitude of the response (black: WT; blue: TKO).

Table 5.3. Short-term depression of the mean N response to the 5th stimulus (50 Hz train). Depression is present in all layers both in WT and TKO slices. There are no differences in the amount of depression in the two strains. Results (black: WT; blue: TKO) are expressed as mean ± sd (n).

	left adjacent column	stimulated column	right adjacent column
L2/3	**0.85 ± 0.26** (18) **0.84 ± 0.19** (15)	**0.78 ± 0.23** (18) **0.80 ± 0.21** (15)	**0.80 ± 0.24** (18) **0.80 ± 0.24** (15)
L4	**0.95 ± 0.40** (17) **0.90 ± 0.27** (15)	stimulus	**0.79 ± 0.34** (17) **0.74 ± 0.21** (15)
L5A	N.A.	**0.81 ± 0.23** (15) **0.83 ± 0.20** (14)	N.A.

We also studied the recovery of the N peak from depression induced by a train of 5 stimuli at 50 Hz in L2/3 and in L5A. The peak of the N response to an isolated stimulus was measured at 2, 6 or 10 seconds after a train (Figure 5.3), and its ratio to the amplitude of the first evoked N response in the preceding train was calculated. Recovery was significantly dependent on the time interval after the train ($P<10^{-4}$, 2-way repeated measures ANOVA), being still incomplete after 10 s. Recovery was not significantly different in TKO and WT slices (2-way analysis of variance). More experiments, and possibly longer trains of stimuli, may be needed to completely clarify whether recovery from depression is altered in the cortical networks of TKO mice.

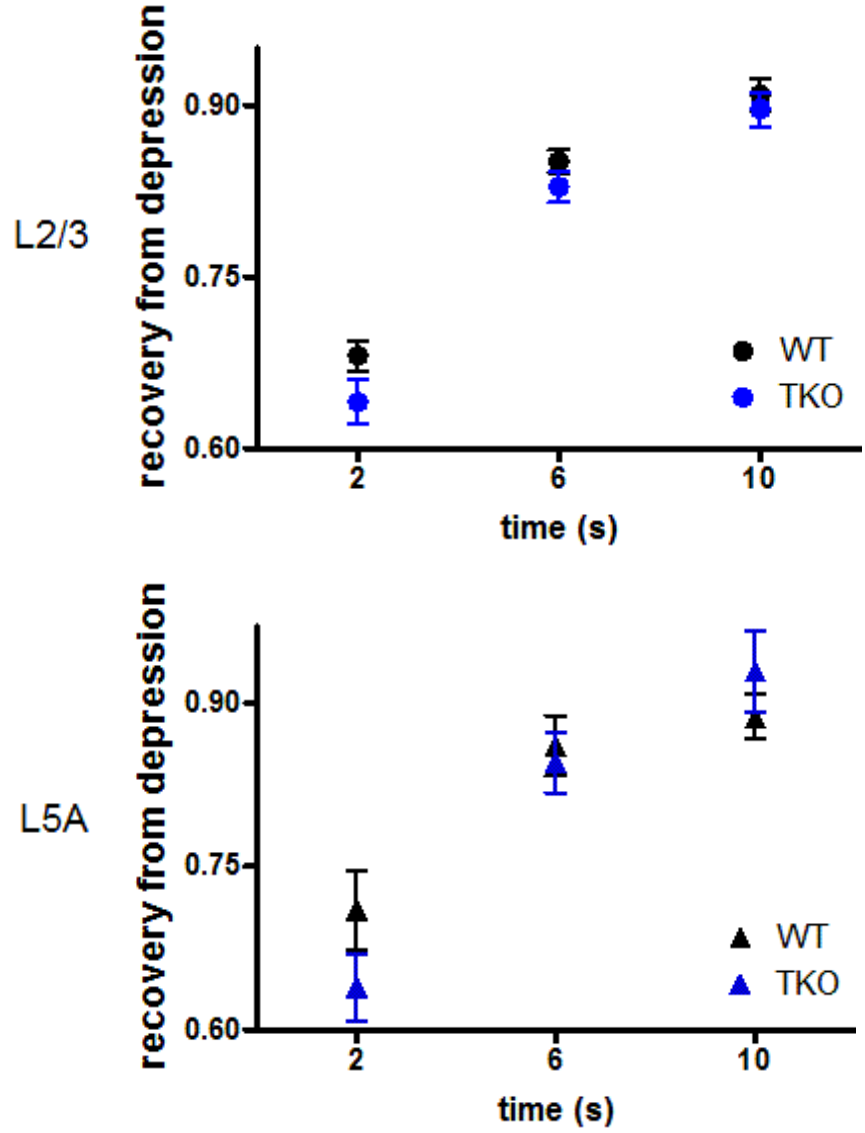

Figure 5.3 Recovery from depression in L2/3 and L5A. The ratio between the N response to an isolated test stimulus and the first N response in the preceding train is plotted for three different delays between train and the test stimulus. Blue and black symbols summarize results from n=15 TKO and n=18 WT slices, respectively, for L2/3, and n=14 TKO and n=15 WT slices, respectively, for L5A. Error bars: s.e.m.

5.3 Up-states: frequency and layer of origin

As reported in paragraph 4.3 for the case of WT and R192Q KI mice, variable patterns of spontaneous activity were present in MEA voltage recordings also for TKO and matched WT mice. Qualitatively, we classified this activity into three categories (up-states, isolated LFPs and spikes/spike bursts) as described in paragraph 4.3 (Figure 4.7).

To increase membrane excitability and facilitate the occurrence of spontaneous activity, we routinely recorded from slices maintained in a modified BBS (mBBS; see Methods), with higher $[K^+]$ and lower $[Ca^{2+}]$ and $[Mg^{2+}]$. In our recordings, voltage traces were acquired in a large frequency band (10 Hz to 3 kHz), and included both lower frequency components usually classified as "local field potentials" (LFPs; see page 7 footnote), and higher frequency components thought to report the occurrence of spikes (normally referred to as multi-unit activity, MUA, >500 Hz). Accordingly, in a single episode of spontaneous activity, large, slow oscillations (typically 70-100 ms for a single oscillatory cycle) were typically superimposed to fast, small deflections in the ms range, most likely representing individual spikes from the underlying neuron(s) (Figure 4.7).

Up-state frequency is higher in TKO mice. Up-states occurred in most experiments (11 of 16 slices in 5 WT animals, and 12 of 15 slices in 5 TKO animals). Their frequency was measured in accurately standardized conditions over a 15' time interval starting 20' after beginning slice perfusion with mBBS (2.5 ml/min). Up-states were detected using a threshold-crossing algorithm applied to the running standard deviation of the voltage traces (see Methods).

The frequency of up-states was quite variable among experiments (Figure 5.4). On average, up-state frequency was significantly larger in TKO than in WT slices (WT: 1.6 ± 0.18 min^{-1}; n=11 slices; TKO: 2.96 ± 0.18 min^{-1}; n=12 slices; mean ± s.e.m.; P=0.0005, Mann-Whitney test), indicating a stronger tendency of TKO slices to produce spontaneous activity.

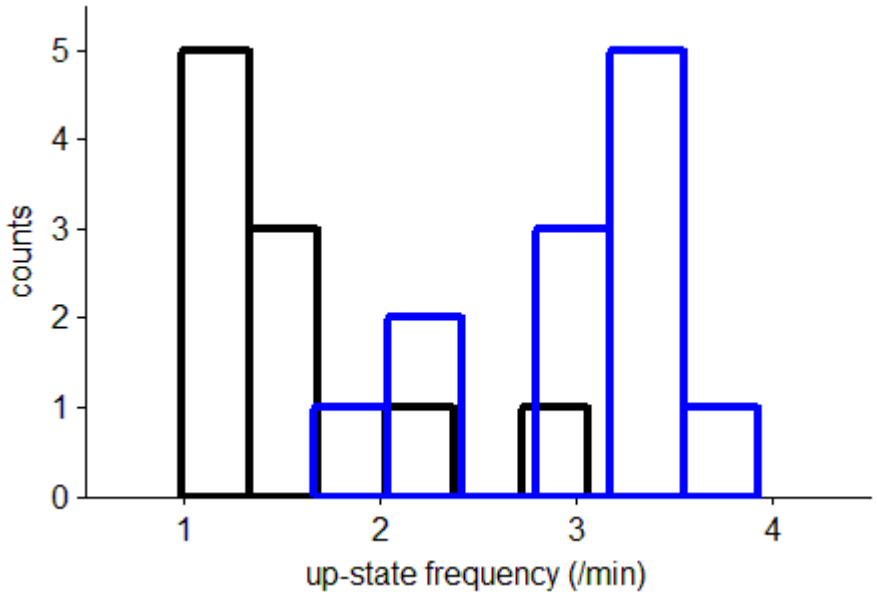

Figure 5.4. Up-states frequency is higher in TKO mice. Histogram of the frequencies of the 11 experiments in WT (black), and the 12 experiments in TKO (blue).

Up-state origin. The origin of TKO and WT up-states was examined for events with well-detected origin inside the MEA chip (group I up-states; see Methods). In WT the probability of finding the up-state origin in L2/3 was significantly higher than in L4 ($P<0.05$) or L5/6 ($P< 0.01$); in TKO the probability of finding the up-state origin in L4 was significantly lower than in L5/6 ($P<0.05$). However, the overall differences between strains were not significant, possibly due to the small numerosity of our preliminary observations. The higher probability of finding the origin of an up-state in L2/3 in WT mice is at odd with previously shown results (Figure 4.9), which were however obtained for younger animals. The reason for this discrepancy needs to be further clarified.

6. DISCUSSION (I)

We studied cortical neurotransmission in knock-in (KI) mice carrying a human FHM1 (R192Q) mutation in the *CACNA1A* gene. It has been demonstrated that these mice show increased P/Q-type Ca^{2+} current density in cortical pyramidal cells consequent to activation of mutant $Ca_V2.1$ channels at lower voltages (Tottene et al., 2009; van den Maagdenberg et al., 2004). KI mice show differential effects, in the somatosensory barrel cortex, on the function of excitatory synapses made by cortical L2/3 pyramidal cells (PCs) onto fast-spiking (FS) interneurons and somatostatin-positive (SOM+) interneurons, and of the reciprocal inhibitory synapses made by FS and SOM+ interneurons onto PCs (see below for details). These results suggested that cortical excitability and the excitatory/inhibitory balance might be altered in the somatosensory barrel cortex in KI.

We therefore performed and analyzed recordings of neuronal network activity from thalamocortical slices from matched KI and WT animals using planar MEAs. We characterized both local field potentials (LFPs) evoked by stimulation in L4 and spontaneous activity (up-states), and we found indications confirming the hypothesis of altered cortical excitability. In particular, we found that the R192Q FHM1 mutation leads to:

i) larger depression of LFPs, during 50 Hz trains of stimuli imparted in L4, in all layers in the stimulated MEA column and in nearby columns (putatively representing a functional cortical column);

ii) larger frequency of spontaneous up-states;

iii) a larger fraction of up-states originating in L2/3;

iv) a different dependency of up-state strength and duration on the cortical layer where maximal activation occurs;

v) a longer delay in up-state propagation from L2/3 to L5A, and a shorter delay in propagation from L5A to L2/3.

6.1 Larger depression of evoked LFPs in the somatosensory cortex of R192Q KI mice

LFPs evoked by trains of 5 stimuli at 50 Hz, applied in L4, were recorded in layers 2/3, 4 and 5A. In both WT and KI mice, responses were larger in L2/3, and nearly halved in L5A; they peaked earlier in L5A than in L2/3, and in the cortical column where stimulation was applied than in adjacent columns. Responses underwent clear depression in all layers (Figure 4.2) and in all layers depression was significantly more prominent in KI than in WT (Table 4.3 and Figure 4.5).

How are the LFPs recorded with MEA electrodes related to the synaptic and firing activity of the neuronal subtypes in the network? Qualitatively, the main factors influencing the amplitude of voltage signals are the density of neurons and synapses, their respective orientation (i.e., the lamination of the cortical structure), and the synchrony of their activation: large, synchronous population of synapses or firing neurons within laminated structures produce stronger signals (Johnston & Wu, 1994). Quantitatively, simultaneous extracellular recordings from multiple cortical depths should help interpreting the LFP in terms of the interaction among neurons across cortical layers within a functional column. The standard method for analyzing LFP signals recorded with a one-dimensional laminar multi-electrode array, inserted perpendicularly to the cortical surface, is to evaluate the distribution of the current source density (*csd*) across the cortical depth. Assuming constant extracellular conductivity and laminar homogeneity of the sources, the *csd* can be evaluated from the second spatial derivative of the LFP recorded at equidistant locations on the electrode array; the output of a *csd* analysis describes the LFP signal in terms of a spatially localized distribution of current sinks[1] and sources[2] (Nicholson and Freeman, 1975; Mitzdorf, 1985). However, the physiological significance of the *csd* analysis is limited because it does not clarify whether the sinks and sources belong to either the synaptic input or passive return[3] currents. For instance, a *csd* sink at a given location can correspond to either a local excitatory synaptic input or the return current of a remote inhibitory synaptic input. Moreover, the *csd* method measures the net transmembrane current contributed by all neuronal populations occupying a particular cortical location, and does not help in decomposing the signal into population-specific contributions.

On the other side, the numerical prediction of the waveform of extracellular voltage signals on the basis of a realistic model would require detailed knowledge of the morphology of the underlying neuronal elements, of the distribution and functionality of their connections, and of their intrinsic firing properties. A read-out of LFP waveforms in terms of activity of the underlying afferent pathways ("LFP generators") has been proposed for sufficiently well-laminated structures, such as the hippocampus (Makarova et al., 2011), but is much less practical for a less ordered structure such as the neocortex (Gratiy et al., 2011).

Overall, given the mathematical and interpretative complication of *csd* analysis, on one side, and the difficulty of producing a model and testing its numerical predictions, on the other, we did not attempt a quantitative interpretation of evoked LFPs in terms of the activity of the underlying synaptic components. Nevertheless, we propose qualitative considerations about their relation.

[1] Sink: by convention, a site on the neuronal membrane where positive charges enter the neuron.
[2] Source: location along the neuronal membrane where positive charges flow out of the neuron.
[3] Return current: a loop current that flows in the opposite direction, at a distance, to compensate for a sink or source current.

We found that, at the fifth stimulus of a 50 Hz train, depression of LFPs in L2/3 was ~0.84 in WT and ~0.57 in KI slices, a result qualitatively similar to the corresponding excitatory post-synaptic potential (EPSP) ratio observed with paired patch-clamp recordings (E_5/E_1) at WT and KI L2/3 PC→FS excitatory synapses (WT: ~0.42, KI: ~0.29, P11-P15 mice, Tottene et al., 2009, their Figure 7D), suggesting that these synapses contribute to the LFPs. However, depression at PC-FS synapses is larger than observed here in LFPs, both in WT and KI slices, suggesting that other synaptic types contribute to the LFP response. What is known about the behavior of other synapses? It was shown that, upon stimulation with short trains, different excitatory and inhibitory synapses of the somatosensory cortex in WT animals have different, target-dependent short term plasticity behavior, going from strong depression to large facilitation. As mentioned, at excitatory L2/3 PC→FS interneuron synapses, EPSPs evoked by short train of stimuli display significant short-term depression (Tottene et al., 2009, their Figure 7). On the contrary, at another excitatory synapse formed by PCs, the PC→SOM+ interneuron connection in L2/3, EPSPs display short-term facilitation (E_5/E_1 at 10 Hz: ~8; Pilati et al., 2013). At WT PC-PC recurrent synapses, the amplitude of the unitary excitatory postsynaptic current (EPSC) shows mild short-term depression: at the 4th stimulus of a 100 Hz train, E_4/E_1 was ~0.77 (Kapfer et al., 2007). Regarding inhibitory synapses, at the FS→PC synapse in L2/3, the inhibitory post-synaptic potential (IPSP) displays a marked depression, with a ratio of peak inhibitory amplitudes (I_5/I_1) at 10 Hz of ~0.45 (Tottene et al. 2009), while at the SOM+→PC synapse they show a relatively mild depression at 20 Hz (room temperature, Sessolo et al., 2011). This variability might be partly influenced by variable age of the animals, animal species, and recording conditions (P11-P15 in Tottene et al., 2009; P15-P19 in Pilati et al., 2013; both studies in mice at room temperature; P18-P28 rats at 32°C in Kapfer et al., 2007).

It is interesting to note that the studied effects of the R192Q mutation are different at different excitatory and inhibitory synapses. In L2/3, EPSPs evoked at PC→FS interneuron synapses by low-frequency stimuli are larger in KI, and display larger short-term depression than in WT synapses (Tottene et al., 2009). However, the effect of the mutation on PC synapses is target-dependent, as the EPSPs evoked at PC→SOM+ interneuron synapses by low frequency stimuli are larger in KI, but their short-term facilitation is unchanged in WT and KI (Pilati et al., 2013). Finally, the evoked IPSPs and their short-term plasticity behavior at the reciprocal FS→PC and SOM+→PC inhibitory synapses are unaffected by the mutation (Tottene et al., 2009; Pilati et al., 2013).

The contribution of inhibitory synapses to the N peak is expected to be minor, because excitatory neurons account for ~85% of the overall neuronal population (Beaulieu, 1993), and our protocol should produce random excitation of the underlying network, therefore activating mostly excitatory synapses. However, when a PC produces a train of APs, polysynaptic activation of the inhibitory network should increase during the train (e.g. see Kapfer et al., 2007), and potentially contribute more prominently to the N signal at late stimuli. If an inhibitory synapse were activated locally near a given electrode, it should produce a local current source and provide a positive voltage deflection, contributing to depress the N peak along the train. Therefore the larger depression in KI might depend on a stronger recruitment of the inhibitory system, occurring in parallel with the larger depression of excitatory synapses described by Tottene et al. (2009). At present we do not know how IPSPs contribute to the N signal, because pharmacological experiments with low doses of $GABA_AR$ antagonists provided erratic results (not shown). It is also possible that part of the responses, recorded in the various layers, does not result from the presence of independent active local sinks and sources, but rather represents sinks and sources arising from passive dipole effects correlated to remote synapses. More cellular experiments (patch-clamp or intracellular recordings) would be required to better understand the link between the basic properties of various classes of synapses and the local network activity, as observed with LFPs.

Whatever its origin, the larger N peak depression indicates that the local cortical network in KI animals strongly reacts to external stimuli in order to keep local excitation under control. It is interesting to note that all neocortical layers from L2/3 to L5A displayed a similarly depressing N response upon a 50 Hz train, and that for all layers depression was larger in KI. This suggests that in these layers the overall effect of the P/Q channel gain of function mutation is similar to that described in L2/3, namely the local network dampens excitation more strongly than in WT mice.

The speed of recovery from depression may significantly influence network computation and E/I balance (Abbott & Regehr, 2004). It was shown recently that recovery from depression induced by a long train of stimuli at 100 or 300 Hz is slightly but significantly faster in KI at the calyx of Held (Inchauspe et al., 2012).

Here, recovery from depression of LFPs evoked in the somatosensory barrel cortex by short 50 Hz trains was apparently, but not significantly, faster in KI than WT. More experiments, and possibly longer trains of stimuli, may be needed to completely clarify whether recovery from synaptic depression is altered in the cortical networks of KI mice. Such a conclusion would be in line with the known dependence of recovery on presynaptic Ca^{2+} (Dittman & Regehr, 1998; Stevens & Wesseling, 1998; Wang & Kaczmarek, 1998; Inchauspe et al., 2012).

6.2 Up-states are different in the somatosensory cortex of R192Q KI mice

A basic operation of cortical networks is the generation of self-maintained depolarized states. Spontaneous activity has been studied in the cortex in conditions of slow-wave sleep, anesthesia, or quiet wakefulness, where it consists of alternating up- and down-states, also termed slow oscillation (Steriade et al., 1993, 2001; Petersen et al., 2003; Wilson, 2008). The ability of cortical networks to generate persistent and recurring activities, even in the absence of subcortical inputs, suggests that this process may underlie perceptual influences on sensory information processing (Arieli et al., 1996; Kenet et al., 2003). In addition, slow oscillations are involved in the encoding of short-term memories (Marshall et al., 2006; Chen et al., 2013).

Sanchez-Vives and McCormick showed for the first time in 2000 that network oscillations can be maintained in neocortical slices. They demonstrated generation of the slow rhythm (< 1 Hz) in occipital and prefrontal slices of ferret neocortex, bathed in a medium mimicking the extracellular ionic composition *in situ*, at 35°C in an interface chamber. They recorded multiunit activity at high frequencies, i.e. spikes, and they observed a depolarized state associated with action potential activity at 2–10 Hz (in regular spiking neurons), followed by a hyperpolarized state, recurring with a periodicity of once every ~3 seconds (0.33 Hz). Following this pioneer study, up-states were observed with a variety of techniques *in vivo* and *ex vivo* (LFPs, MUA, single cell intracellular and patch-clamp recordings, voltage sensitive dyes and Ca^{2+} imaging; see paragraph 1.5.2).
Using thalamocortical slices of juvenile mice, and acquiring voltage traces in a large frequency band (10 Hz to 3 kHz), we recorded spontaneous up-states occurring at ~2.7 min^{-1} (0.045 Hz) in WT, and ~3.2 min^{-1} (0.053) in KI (Figure 4.8). The lower frequency is likely to be a consequence of performing experiments at room temperature, instead of physiological temperature as in previous slice recordings (Sanchez-Vives & McCormick, 2000; Rigas & Castros-Alamancos, 2007; Wester & Contreras, 2012), and of using a submerged chamber, where oxygen diffusion may be less efficient than in the interface chamber.
Interestingly, up-states were more frequent in KI than WT mice, suggesting that the KI somatosensory cortex is more excitable.

The mechanisms and site of initiation of up-states are thought to depend on the intrinsic properties of the various neuronal types in the cortical network and on the number and properties of their connections, and are still largely debated (see paragraph 1.5.2: Origin of up-states). To contribute to this debate, and to verify whether the R192Q migraine mutation influences the production of up-

states, we determined the up-state origin for each episode, i.e. the cortical layer where activity started first. Our results show that the origin of an up-state changes from one event to the other, and can be found in any cortical layer, from L2/3 to L5B in both WT and KI. This conclusion is in accordance with the result of Chauvette et al. (2010) obtained *in vivo* in the cat, where it was shown that, when using LFP recordings, the up-state might occur first at any depth in the cortex although with larger frequency in infragranular layers. It is interesting to note that previous studies using MUA recordings had reported that the up-state origin was exclusively found in L5 (e.g. Sanchez-Vives & McCormick, 2000), a result replicated using MUA in the work of Chauvette et al. (2010). To explain the apparent paradox, Chauvette et al. concluded that, even though the principal neurons in L5 tend to fire more than neurons in other layers, the up-state may start before any spike occurs: they actually show that cortical neurons *in vivo* are completely silent during a down-state, which suggests that the up-state must be initiated by spike-independent mechanisms. They propose that such mechanism be the subthreshold summation of excitatory miniature synaptic currents, as suggested by their multiple intracellular recordings. LFP recordings may detect subthreshold activity before any spike is produced (Kamondi et al., 1998; Gustafsson, 1984), and this would explain why LFPs and MUAs may give different results on the up-state origin. The principal neurons in L5 would be the first to fire, because of their intrinsic excitability properties, and because their large dendritic arbor receives a larger number of connections and consequently may sum up a larger number of minis. However, since there are more neurons in L2/3 than in any other layer (Markram 2004; Meyer et al., 2010a), the density of synapses is also likely to be higher in L2/3, which may explain why in some cases subthreshold mini activity is higher in L2/3, giving rise to up-states originating in L2/3. On the other side, L5 neurons are necessary to sustain and propagate the up-state, as shown by Beltramo et al. (2013) and Wester and Contreras (2011), because of their more frequent firing, and their larger impact on the surrounding network (Beltramo et al., 2013).

In conclusion, our results on up-state origin, obtained with combined LFP and MUA recordings, are compatible with the hypothesis of Chauvette and colleagues, that the up-state originates from subthreshold summation of spike-independent activity, putatively miniature synaptic activity, a phenomenon which may occur in any layer.

Interestingly, the distribution of the layer of origin is different for WT and KI mice (Figure 4.9): the probability of finding an origin in L2/3 is nearly 50% higher in KI with respect to WT animals. Accordingly, in KI the probability in L2/3 is significantly higher than in the infragranular layers and in L4. Overall, the KI cortical network in L2/3 appears better suited to generate synchronized

population activity than its WT counterpart, supporting the hypothesis that excitability is enhanced in the KI cortex and pointing to a possible preferential site (L2/3) for such difference.

We also noticed that KI slices showed a different dependency of up-state strength (a measure of the intensity of local field potential activity) and duration on the layer where maximal activity is found (Fig. 4.11 and 4.13). Moreover, the up-state propagated slowly between layers, and the speed was lower from supragranular to infragranular layers in KI mice, and conversely higher in the reverse direction. These observations cannot be directly reconnected to cellular and synaptic properties, given the relative paucity of information on the involvement of different types of neurons in up-states, and on the properties of their connections in WT and KI strains. However, it seems fair to say that L2/3 in KI mice is somewhat more excitable than in WT; further cellular studies are needed to confirm this hypothesis.

Psychophysical and neurophysiological studies have provided clear evidence that in the period between attacks migraineurs show hypersensitivity to sensory stimuli and abnormal processing of sensory information, characterized by increased amplitudes and reduced habituation of evoked and event-related potentials (Brighina et al., 2009; Pietrobon & Moskowitz, 2013). To understand the primary mechanisms of migraine attacks, it seems, therefore, essential to understand the mechanisms underlying the interictal abnormal processing of sensory information. Defective cortical up-states could be part of these mechanisms and even explain why the cortex of these patients undergoes a cortical spreading depression in response to migraine triggers such as intense, repetitive sensory stimulation.

7. DISCUSSION (II)

Deletion or loss-of-function mutations in the presynaptic proteins synapsins (Syns) generate an epileptic phenotype in mouse and man (Garcia et al. 2004). Mice lacking Syn I, Syn II, Syn I/II, or Syn I/II/III (TKO) are all prone to epileptic seizures starting at an age of 2-3 months (Gitler et al. 2004), a period of intense synapse maturation and refinement in which Syn I/II have already reached high expression levels (Cesca et al., 2010). A similar onset during childhood or adolescence is present in the epileptic patients affected by *SYN1* mutations (Garcia et al. 2004). Deletion of the synapsins, even of Syn I alone, causes a significant decrease in basal inhibitory transmission and in the number of vesicles in cultured inhibitory terminals (Gitler et al. 2004). Opposite, age-dependent effects on both excitatory and inhibitory synaptic transmission were recently shown in TKO mice. At presymptomatic age, an increased evoked excitatory postsynaptic current and impaired evoked inhibitory postsynaptic current amplitude were found (Farisello 2013; Ketzef & Gitler 2012), and 4-AP-evoked network interictal activity was shown to be enhanced in cortico-hippocampal slices of these mice before the onset of epilepsy (Boido et al., 2010).

Given these evidences, an imbalance between basal glutamatergic and GABAergic transmission was hypothesized at the network level. We therefore explored for the first time cortical neurotransmission in the somatosensory cortex of 4-5 weeks old TKO mice, by performing and analyzing recordings of neuronal network activity from thalamocortical slices from matched TKO and WT animals using planar MEAs.

We characterized local field potentials (LFPs) evoked by stimulation in L4 and spontaneous activity (up-states), and we found indications confirming the general hypothesis of altered cortical excitability also in our preparation. In particular, we found that Syns deletion leads to i) smaller time-to-peak of LFPs evoked by either a single stimulus or a train of stimuli in L4 (50 Hz) in all cortical layers; and ii) higher frequency of spontaneous up-states.

It is worth mentioning that our study was not directed at clarifying the causes that trigger an epileptic seizure, but rather describing the early changes occurring in network activity, due to a specific genetic lesion that leads to an epileptic phenotype later in development.

7.1 Smaller time to peak of evoked LFPs in the somatosensory cortex of TKO mice

The analysis of evoked LFP responses in the barrel cortex of WT and matched TKO mice suggested similar spatial attenuation properties, as the ratio of the size of N responses in adjacent columns versus the stimulated one were similar (Table 5.1). The time-to-peak of the N response was shorter

in TKO slices than WT in all layers (Table 5.2). Given the similar peak amplitudes, this result implies that the slope of the response was larger in TKO. This might be due to a larger number of involved neurons, to their more synchronous activation, or to larger post-synaptic currents in individual neurons. As an increased size of the readily-releasable pools in glutamatergic terminals has been reported in Syn I-/- (Chiappalone et al., 2009), and TKO mice (Farisello et al., 2013), larger excitatory postsynaptic currents, and a consequent massive excitation of nearby inhibitory neurons, upon electric stimulation, might be at the origin of the larger LFP slope. Whatever the precise cellular or synaptic mechanism, the TKO mutations produce a faster network activation, which is likely to be relevant for local input processing.

Synaptic depression during repetitive stimulation has also been hypothesized to contribute to seizure development, by causing an imbalance between the excitatory and inhibitory actions (Chiappalone et al., 2009). A derangement of short term plasticity paradigms, with enhanced facilitation of glutamatergic transmission and slow recovery from depression after a longer train, was actually reported in the CA1 region of acute hippocampal slices (Farisello et al., 2013). We attempted to study the effects of altered synaptic short-term depression on network responses in the barrel cortex, by applying the same protocol (trains of 5 stimuli at 50 Hz) that had unveiled a defective network in the migraine mouse model, and that we knew would generate a clear LFP depression in all layers (see Figure 5.1A). We analyzed the ratio of the 5th over the 1st N response (N_5/N_1) in layers 2/3, 4 and 5A in the stimulated column and its first adjacent columns (Figure 5.1; Table 5.3). We found that, at variance with the clear differences seen in single CA1 hippocampal neurons, LFP depression was similar in WT and TKO somatosensory cortices in all layers (Table 5.3 and Figure 5.2). We also studied the recovery from depression of the N response peak amplitude, by measuring the response to an isolated stimulus at 2, 6 or 10 seconds after a train (Figure 5.3), and calculating its amplitude ratio to the first evoked N response in the preceding train. Recovery was significantly dependent on the time interval after the train, and was not significantly different in TKO and WT mice after such short train of stimuli. More experiments, and possibly longer trains of stimuli, may be needed to completely clarify whether synaptic depression and recovery from depression are altered in the cortical networks of TKO mice.

7.2 Higher up-states frequency in the somatosensory cortex of TKO mice

The E/I balance has been shown to be involved in the basic mechanisms that underlie oscillatory waves (Shu et al., 2003; Atallah & Scanziani 2009), and thus its disruption is expected to lead to severe dysfunction. Given the alterations of excitatory and inhibitory transmission in the hippocampal and entorhinal cortices (see above), an alteration of the E/I balance, and consequently of spontaneous oscillatory waves, might also be present in the barrel cortex. We, therefore, investigated for the first time in TKO mice the spontaneous network activity in the somatosensory cortex. The up-state is readily detected in the field potential recording as a synchronous network event (see beginning of paragraph 6.2). Using thalamocortical slices of 4-5 weeks old mice, and acquiring voltage traces in a large frequency band (10 Hz to 3 kHz), we recorded spontaneous up-states occurring at ~1.6 min^{-1} in WT, and ~3 min^{-1} in TKO slices (Figure 5.8), that is, we found that in TKO mice the frequency of up-states is nearly doubled with respect to matched WT mice. This result points to a general greater excitability of TKO networks, not only in cortico-hippocampal slices, but also in the somatonsensory cortex.

The importance of fast GABAergic inhibition in controlling persistent activity has been described (Sanchez-Vives & McCormick, 2000; Shu et al., 2003). In L3 principal neurons of the rat entorhinal cortex *in vitro*, $GABA_A$ receptor-mediated inhibition appears to be critical for balancing up-states, while GABAergic inhibition via $GABA_B$ receptors seems to provide a powerful mechanism for termination of persistent network activity (Mann et al., 2009). Despite a role of GABAergic inhibition in initiating up-states has not been described yet, we can speculate that the reported impairment of inhibition (Farisello et al., 2013; Ketzef & Gitler, 2012) might contribute to the higher frequency of up-states detected in TKO slices. More experiments are needed to consolidate the characterization of up-states properties and propose hypotheses on their relations to functional synaptic changes.

It is important to note that Ketzef and Gitler (2012) found age-dependent changes in tonic inhibition and in the action potential duration, neither of which is likely to be directly determined by synapsins. The primary genetic lesion might then lead to unexpected functional changes during the latent period, which are instrumental in initiating epilepsy at a later stage. It will be therefore essential to investigate all the functional changes occurring even when they appear unrelated to synapsin deletion.

Future perspectives

Our study, using a chip that covers an area of 1.4 mm^2, allowed us to record network activity from hundreds of thousands of neurons. Known molecular alterations are expected to disrupt this network activity. Given the complexity of neuronal (and glial) communication, our results can only offer preliminary hints on how known synaptic alterations influence the network. Further investigations are needed; in fact, our results at this point cannot distinguish possible compensatory events, opposing the enhanced function of the P/Q type Ca^{2+} channel, or the deletion of Syns, from secondary effects of the genetic alterations. On the basis of the varied roles played by different subpopulations of interneurons (Isaacson & Scanziani, 2011), it is conceivable that specific changes in the function of subgroups of interneurons might affect network activity in considerably dissimilar ways. For this reason we aim at combining patch-clamp and MEA recordings in the future, to simultaneously observe single cell events and LFP signals.

We are now performing a spectral analysis of the spontaneous oscillations to better characterize the spatiotemporal properties of up- and down-states in WT and mutant mice. A subsequent development will be the study of the influence of external stimuli (e.g. direct activation of L4 or activation of thalamic afferents) on the generation of up-states. Furthermore, an effort will be made to perform experiments at physiological temperature.

REFERENCES

Abbott LF, Regehr WG (2004). Synaptic computation. *Nature* 431:796-803.

Agmon A, Connors BW (1991). Thalamocortical responses of mouse somatosensory (barrel) cortex in vitro. *Neuroscience* 41:365-79.

Amaral DG (2000). Chapter 17: The Anatomical Organization of the Central Nervous System. Principles of Neural Science, Kandel ER, Schwartz JS, Jessell TM. *McGraw-Hill.*

Antal A, Lang N, Boros K, NitscheM, Siebner HR, Paulus W (2008). Homeostatic metaplasticity of the motor cortex is altered during headache-free intervals in migraine with aura. *Cereb. Cortex* 18:2701–5.

Arieli A, Sterkin A, Grinvald A, Aertsen A (1996). Dynamics of ongoing activity: explanation of the large variability in evoked cortical responses. *Science* 273, 1868–1871.

Ascoli GA, Alonso-Nanclares L, Anderson SA, Barrionuevo G, Benavides-Piccione R, Burkhalter A, et al. (2008). Petilla terminology: nomenclature of features of GABAergic interneurons of the cerebral cortex. *Nat. Rev. Neurosci*. 9:557–568.

Atallah BV, Scanziani M (2009). Instantaneous modulation of gamma oscillation frequency by balancing excitation with inhibition. Neuron 62:566–577.

Aurora SK, Wilkinson F (2007). The brain is hyperexcitable in migraine. *Cephalalgia* 27:1442–53.

Ayata C, Jin H, Kudo C, Dalkara T, Moskowitz MA (2006). Suppression of cortical spreading depression in migraine prophylaxis. *Ann. Neurol.* 59:652-661.

Bacci A, Sancini G, Verderio C, Armano S, Pravettoni E, Fesce R, Franceschetti S, Matteoli M (2002). Block of Glutamate-Glutamine Cycle Between Astrocytes and Neurons Inhibits Epileptiform Activity in Hippocampus. *J Neurophysiol* 88:2302-2310.

Bakker R, Schubert D, Levels K, Bezgin G, Bojak I, Kötter R (2009). Classification of cortical microcircuits based on micro-electrode-array data from slices of rat barrel cortex. *Neural Netw.* 22:1159-68.

Beaulieu C (1993). Numerical data on neocortical neurons in adult rats, with special reference to the GABA population. *Brain Res.* 609:284-292.

Beggs JM, Plenz D (2003). Neuronal avalanches in neocortical circuits. *J. Neurosci.* 23:11167–11177.

Beltramo R, D'Urso G, Dal Maschio M, Farisello P, Bovetti S, Clovis Y, Lassi G, Tucci V, De Pietri Tonelli D, Fellin T (2013). Layer-specific excitatory circuits differentially control recurrent network dynamics in the neocortex. *Nat. Neurosci.* 16(2):227-34.

Benfenati F, Valtorta F, Chieregatti E, Greengard P (1992). Interaction of free and synaptic vesicle-bound synapsin I with F-actin. *Neuron* 8:377-86.

Binzegger T, Douglas RJ, Martin KA (2004). A quantitative map of the circuit of cat primary visual cortex. *J. Neurosci.* 24:8441–8453.

Boido D, Farisello P, Cesca F, Ferrea E, Valtorta F, Benfenati F, Baldelli P (2010). Cortico-hippocampal hyperexcitability in synapsin I/II/III knockout mice: age-dependency and response to the antiepileptic drug levetiracetam. *Neuroscience* 171:268–328.

Brighina F, Palermo A, Fierro B (2009). Cortical inhibition and habituation to evoked potentials: relevance for pathophysiology of migraine. *J. Headache Pain* 10:77–84.

Buzsaki G (2010). Neural syntax: cell assemblies, synapsembles, and readers. *Neuron* 68:362–385.

Buzsaki G, Anastassiou CA, Koch C (2012). The origin of extra- cellular fields and currents–EEG, ECoG, LFP and spikes. *Nat.Rev. Neurosci.* 13:407–420.

Cash SS, Halgren E, Dehghani N, Rossetti AO, Thesen T, Wang C, Devinsky O, Kuzniecky R, Doyle W, Madsen JR, et al. (2009). The human K-complex represents an isolated cortical down-state. *Science* 324:1084-1087.

Castro-Alamancos MA (2009). Cortical up and activated states: implications for sensory information processing. *Neuroscientist* 15:625–634.

Catterall WA, Few AP (2008). Calcium channel regulation and presynaptic plasticity. *Neuron* 59, 882-901.111.

Catterall WA, Perez-Reyes E, Snutch TP, Striessnig J (2005). International Union of Pharmacology. XLVIII. Nomenclature and structure-function relationships of voltage-gated calcium channels. *Pharmacol. Rev.* 57:411-425.

Ceccaldi PE, Grohovaz F, Benfenati F, Chieregatti E, Greengard P, Valtorta F (1995). Dephosphorylated synapsin I anchors synaptic vesicles to actin cytoskeleton: an analysis by videomicroscopy. *J. Cell. Biol.* 128:905-12.

Ceruti S, Villa G, Fumagalli M, Colombo L, Magni G, Zanardelli M, Fabbretti E, Verderio C, van den Maagdenberg AM, Nistri A, Abbracchio MP (2011). Calcitonin gene-related peptide-mediated enhancement of purinergic neuron/glia communication by the algogenic factor bradykinin in mouse trigeminal ganglia from wild-type and R192Q $Ca_V2.1$ Knock-in mice: implications for basic mechanisms of migraine pain. *J. Neurosci.* 31:3638–3649.

Cesca F, Baldelli P, Valtorta F, Benfenati F (2010). The Synapsins: key actors of synapse function and plasticity. *Prog Neurobiol.* 91: 313–348.

Charles A, Brennan K, (2009). Cortical spreading depression-new insights and persistent questions. *Cephalalgia*, 29(10):1115-24.

Charles A. 2010. Does cortical spreading depression initiate a migraine attack? Maybe not. *Headache* 50:731-33.

Chauvette S, Volgushev M, Timofeev I (2010). Origin of active states in local neocortical networks during slow sleep oscillation. *Cerebral Cortex* 20:2660-2674.

Chen X, Rochefort NL, Sakmann B, Konnerth A (2013). Reactivation of the same synapses during spontaneous up states and sensory stimuli. *Cell Rep*. 4(1):31-39.

Chiappalone M, Casagrande S, Tedesco M, Valtorta F, Baldelli P, et al. (2009). Opposite changes in glutamatergic and GABAergic transmission underlie the diffuse hyperexcitability of synapsin I-deficient cortical networks. *Cereb. Cortex* 19:1422–1439.

Citri A, Malenka RC (2008). Synaptic plasticity: multiple forms, functions, and mechanisms. *Neuropsychopharmacology* 33: 18–41.

Compte A, Reig R, Descalzo VF, Harvey MA, Puccini GD, Sanchez-Vives MV (2008). Spontaneous high-frequency (10–80 Hz) oscillations during up states in the cerebral cortex *in vitro. The Journal of Neuroscience* 28(51):13828 –13844.

Conte A, Barbanti P, Frasca V, Iacovelli E, Gabriele M, et al. (2010). Differences in short-term primary motor cortex synaptic potentiation as assessed by repetitive transcranial magnetic stimulation in migraine patients with and without aura. *Pain* 148:43–48.

Coppola G, Pierelli F, Schoenen J (2007). Is the cerebral cortex hyperexcitable or hyperresponsive in migraine? *Cephalalgia* 27:1427–39.

Cossart R, Aronov D, Yuste R (2003). Attractor dynamics of network UP states in the neocortex. *Nature*, 423:283–288.

Dalkara, T., Zervas, N.T., and Moskowitz, M.A. (2006). From spreading depression to the trigeminovascular system. *Neurol. Sci.* 27 Suppl 2:S86-90.

De Curtis M, Gnatkovsky V (2009) Reevaluating the mechanisms of focal ictogenesis: The role of low-voltage fast activity. *Epilepsia* 50:2514–2525.

DeFelipe J, Lopez-Cruz PL, Benavides-Piccione R, Bielza C, Larranaga P, Anderson S, et al. (2013). New insights into the classification and nomenclature of cortical GABAergic interneurons. *Nat. Rev. Neurosci*. 14:202–216.

de Kock CP, Bruno RM, Spors H, Sakmann B (2007). Layer- and cell-type-specific suprathreshold stimulus representation in rat primary somatosensory cortex. *J Physiol.* 15;581:139-54.

de Vries B, Frants RR, Ferrari MD, van den Maagdenberg AM (2009). Molecular genetics of migraine. *Hum. Genet*. 126, 115-132.

Dittman JS, Regehr WG (1998). Calcium dependence and recovery kinetics of presynaptic depression at the climbing fiber to Purkinje cell synapse. *J Neurosci.* 18:6147–6162.

Dodick DW (2008). Examining the essence of migraine—is it the blood vessel or the brain? A debate. *Headache* 48:661–67.

Douglas RJ, Martin KA (2004). Neuronal circuits of the neocortex. *Annu Rev Neurosci* 27:419-451.

Dugué GP, Dumoulin A, Triller A, Dieudonné S (2005). Target-dependent use of co-released inhibitory transmitters at central synapses. *J. Neurosci.* 25(28):6490-8.

Ertel EA, Campbell KP, Harpold MM, Hofmann F, Mori Y, Perez-Reyes E, Schwartz A, Snutch TP, Tanabe T, Birnbaumer L, et al. (2000) Nomenclature of voltage gated calcium channels *Neuron* 25:533–535.

Farisello P, Boido D, Nieus T, Medrihan L, Cesca F, Valtorta F, Baldelli P, Benfenati F (2013). Synaptic and extrasynaptic origin of the excitation/inhibition imbalance in the hippocampus of synapsin I/II/III knockout mice. *Cerebral Cortex* 23:581-593.

Feldman DE (2009). Synaptic mechanisms for plasticity in neocortex. *Annu Rev Neurosci* 32:33-55.

Fellin T, Halassa MM, Terunuma M, Succol F, Takano H, Frank M, Moss SJ, Haydon PG (2009). Endogenous non neuronal modulators of synaptic transmission control cortical slow oscillations in vivo. *Proc. Natl. Acad. Sci. U S A* 106(35):15037-42.

Fioretti B, Catacuzzeno L, Sforna L, Gerke-Duncan MB, van den Maagdenberg AM, Franciolini F, Connor M, Pietrobon D (2011). Trigeminal ganglion neuron subtype-specific alterations of $Ca_V2.1$ calcium current and excitability in a Cacna1a mouse model of migraine. *J. Physiol.* 589:5879–5895.

Fishell G, Rudy B (2011). Mechanisms of inhibition within the telencephalon: "Where the wild things are". *Annu. Rev. Neurosci.* 34:535–567.

Fisher RS, Boas WVE, Blume W, Elger C, Genton P, Lee P, Engel J (2005). Epileptic seizures and epilepsy: definition proposed by the International League Against Epilepsy (ILAE) and the International Bureau for Epilepsy (IBL). *Epilepsia* 4**:**470-472.

Fino E, Packer AM, Yuste R (2013). The logic of inhibitory connectivity in the neocortex. *Neuroscientist* 19:228-37.

Frankel WN (2009). Genetics of complex neurological disease: challenges and opportunities for modeling epilepsy in mice and rats. *Trends Genet.* 25:361–367.

Gabernet L, Jadhav SP, Feldman DE, Carandini M, Scanziani M (2005). Somatosensory integration controlled by dynamic thalamocortical feed-forward inhibition. *Neuron* 48:315–327.

Garcia CC, Blair HJ, Seager M, Coulthard A, Tennant S, Buddles M, Curtis A, Goodship JA (2004). Identification of a mutation in synapsin I, a synaptic vesicle protein, in a family with epilepsy. *J Med Genet.* 41:183-186.

Giannandrea M, Guarnieri FC, Gehring NH, Monzani E, Benfenati F, Kulozik AE, Valtorta F (2013). Nonsense-mediated mRNA decay and loss-of-function of the protein underlie the X-linked epilepsy associated with the W3566× mutation in Synapsin I. *PLoS ONE* 8(6):e67724.

Gitler D, Takagishi Y, Feng J, Ren Y, Rodriguiz RM, Wetsel WC, Greengard P, Augustine GJ (2004). Different presynaptic roles of synapsins at excitatory and inhibitory synapses. *J. Neurosci.* 24:11368-80.

Glickfeld LL, Atallah BV, Scanziani M (2008). Complementary modulation of somatic inhibition by opioids and cannabinoids. J. Neurosci. 28:1824–1832.

Gratiy SL, Devor A, Einevoll GT, Dale AM (2011). On the estimation of population-specific synaptic currents from laminar multielectrode recordings. *Front Neuroinform.* 5:32.

Gullo F, Maffezzoli A, Dossi E, Wanke E (2009). Short-latency cross- and autocorrelation identify clusters of interacting cortical neurons recorded from multi-electrode array. *J. Neurosci. Methods* 181, 186–198.

Gustafsson B (1984). Afterpotentials and transduction properties in different types of central neurones. *Arch Ital Biol.* 122(1):17-30.

Gutnik MJ & Crill WE (1995). The cortical neuron as an electrophysiological unit. In: The Cortical Neuron, edited by Gutnick MJ and Mody I. New York: *Oxford Univ. Press*, p. 33–51.

Haider B, Duque A, Hasenstaub AR, McCormick DA (2006). Neocortical network activity in vivo is generated through a dynamic balance of excitation and inhibition. *J Neurosci*. 26:4535–4545.

Haider B, McCormick DA (2009). Rapid neocortical dynamics: cellular and network mechanisms. *Neuron* 62(2):171–189.

Harwell C, Burbach B, Svoboda K, Nedivi E (2005). Regulation of cpg15 expression during single whisker experience in the barrel cortex of adult mice. *J Neurobiol.* 65(1):85-96.

Hasenstaub A, Shu Y, Haider B, Kraushaar U, Duque A, McCormick DA (2005). Inhibitory postsynaptic potentials carry synchronized frequency information in active cortical networks. *Neuron* 47:423–435.

Hebb D. The organization of behavior: a neuropsychological theory. *New York: Wiley*; 1949.

Hsu D, Chen W, Hsu M, Beggs JM (2008) An open hypothesis: Is epilepsy learned, and can it be unlearned? *Epilepsy & Behavior* 13:511–522.

Inchauspe CG, Urbano FJ, Di Guilmi MN, Forsythe ID, Ferrari MD, van den Maagdenberg AM, Uchitel OD (2010). Gain of function in FHM-1 $Ca_V2.1$ knock-in mice is related to the shape of the action potential. *J. Neurophysiol.* 104:291–299.

Inchauspe CG, Urbano FJ, Di Guilmi MN, Ferrari MD, van den Maagdenberg AM, Forsythe ID, Uchitel OD (2012). Presynaptic $Ca_V2.1$ calcium channels carrying familial hemiplegic migraine mutation R192Q allow faster recovery from synaptic depression in mouse calyx of Held. *Neurophysiol.* 108:2967–2976.

Isaacson JS, Scanziani M (2011). How inhibition shapes cortical activity. *Neuron* 72:231–243.

Jan TA, Lu L, Li CX, Williams RW, Waters RS (2008). Genetic analysis of posterior medial barrel subfield (PMBSF) size in somatosensory cortex (SI) in recombinant inbred strains of mice. *BMC Neurosci.* 9:3.

Johnston D, Wu SM (1994). Foundations of Cellular Neurophysiology. *Bradford Books*.

Jones IL, Livi P, Lewandowska MK, Fiscella M, Roscic B, Hierlemann A (2011). The potential of microelectrode arrays and microelectronics for biomedical research and diagnostics. *Anal. Bioanal. Chem.* 399:2313–2329.

Kaliszewska A, Bijata M, Kaczmareck L, Kossut M (2011). Experience-Dependent Plasticity of the Barrel Cortex in Mice Observed with 2-DG Brain Mapping and c-Fos: Effects of MMP-9 KO. *Cereb Cortex.* 22(9):2160-70.

Kamondi A, Acsády L, Wang XJ, Buzsáki G (1998). Theta oscillations in somata and dendrites of hippocampal pyramidal cells in vivo: activity-dependent phase-precession of action potentials. *Hippocampus* 8(3):244-61.

Kandel ER, Siegelbaum SA (2000). Chapter 12: Synaptic Integration. Chapter 14: Transmitter Release. Principles of Neural Science, Kandel ER, Schwartz JS, Jessell TM. *McGraw-Hill.*

Kapfer C, Glickfeld LL, Atallah BV, Scanziani M (2007). Supralinear increase of recurrent inhibition during sparse activity in the somatosensory cortex. *Nat. Neurosci.* 10:743–753.

Kenet T, Bibitchkov D, Tsodyks M, Grinvald A, Arieli A (2003). Spontaneously emerging cortical representations of visual attributes. *Nature* 425, 954–956.

Kerr JN, Greenberg D, Helmchen F (2005). Imaging input and output of neocortical networks in vivo. *Proc. Natl. Acad. Sci. USA* 102:14063–14068.

Ketzef M, Gitler D (2012). Epileptic synapsin triple knockout mice exhibit progressive long-term aberrant plasticity in the entorhinal cortex. *Cereb Cortex*. doi: 10.1093/cercor/bhs384 [Epub ahead of print].

Krook-Magnuson EI, Li P, Paluszkiewicz SM, Huntsman MM (2008). Tonically Active Inhibition Selectively Controls Feedforward Circuits in Mouse Barrel Cortex. *J Neurophysiol.* 100(2): 932–944.

Kullmann DM, Lamsa K (2008). "Roles of distinct glutamate receptors in induction of anti-Hebbian long-term potentiation". *J. Physiol. (Lond.)* 586 (6): 1481–6.

Lübke J, Feldmeyer D (2007). Excitatory signal flow and connectivity in a cortical column: focus on barrel cortex. *Brain Struct. Funct.* 212:3–17.

MacLean JN, Watson BO, Aaron GB, Yuste R (2005). Internal dynamics determine the cortical response to thalamic stimulation. *Neuron* 48:811– 823.

Makarova J, Ibarz JM, Makarov VA, Benito N, Herreras O (2011). Parallel readout of pathway-specific inputs to laminated brain structures. *Front Syst Neurosci.* 5:77.

Mann EO, Kohl MM, Paulsen O (2009). Distinct roles of $GABA_A$ and $GABA_B$ receptors in balancing and terminating persistent cortical activity. *J. Neurosci.* 29:7513–7518.

Mao BQ, Hamzei-Sichani F, Aronov D, Froemke RC, Yuste R (2001). Dynamics of spontaneous activity in neocortical slices. *Neuron* 32:883–898.

Markand ON (2003). Pearls, perils, and pitfalls in the use of electroencephalogram. *Semin. Neurol*. 23:7-46**.**

Markram H, Toledo-Rodriguez M, Wang Y, Gupta A, Silberberg G, Wu C (2004). Interneurons of the neocortical inhibitory system. *Nat. Rev. Neurosci.* 5:793–807.

Marshall L, Helgadóttir H, Mölle M, Born J (2006). Boosting slow oscillations during sleep potentiates memory. *Nature* 444, 610–613.

Massimini M, Huber R, Ferrarelli F, Hill S, Tononi G (2004). The sleep slow oscillation as a traveling wave. *J Neurosci.* 24:6862--6870.

Messlinger K (2009). Migraine: where and how does the pain originate? *Exp. Brain. Res.* 196:179-193.

Metherate R, Ashe JH (1993). Ionic flux contributions to neocortical slow waves and nucleus basalis mediated activation: whole-cell recordings in vivo. *J. Neurosci.* 13:5312–5323.

Meyer HS, Wimmer VC, Oberlaender M, de Kock CP, Sakmann B, Helmstaedter M (2010a). Number and laminar distribution of neurons in a thalamocortical projection column of rat vibrissal cortex. *Cereb. Cortex* 20:2277–2286.

Meyer HS, Wimmer VC, Hemberger M, Bruno RM, de Kock CP, Frick A, Sakmann B, Helmstaedter M (2010b). Cell type-specific thalamic innervation in a column of rat vibrissal cortex. *Cereb. Cortex* 20:2287–2303.

Mitzdorf U (1985). Current source-density method and application in cat cerebral cortex: investigation of evoked potentials and EEG phenomena. *Physiol. Rev.* 65:37–100.

Nicholson C, Freeman JA (1975). Theory of current source-density analysis and determination of conductivity tensor for anuran cerebellum. *J. Neurophysiol.* 38:356–368.

Nunez PL, Srinivasan R (2006). Electric Fields of the Brain: The Neurophysics of EEG. Oxford: *Oxford University Press*.

Petersen CC, Hahn TT, Mehta M, Grinvald A, Sakmann B (2003). Interaction of sensory responses with spontaneous depolarization in layer 2/3 barrel cortex. *Proc Natl Acad Sci USA.*, 100(23):13638-43.

Petersen CC (2007). The functional organization of the barrel cortex. *Neuron* 56:339–355.

Pettersen KH, Hagen E, Einevoll GT (2007). Estimation of population firing rates and current source densities from laminar electrode recordings. *J. Comput. Neurosci.* 24:291–313.

Pietrobon D (2013). Calcium channels and migraine. *Biochim. Biophys. Acta*. 1828:1655-65.

Pietrobon D (2005a). Migraine: new molecular mechanisms. *Neuroscientist* 11:373-386.

Pietrobon D (2005b). Function and dysfunction of synaptic calcium channels: insights from mouse models. *Curr. Opin. Neurobiol.* 15:257–65.

Pietrobon D (2007). Familial hemiplegic migraine. *Neurotherapeutics* 4:274-284.

Pietrobon D (2010a). $Ca_V2.1$ channelopathies. *Pflüg. Arch.* 460:375–93.

Pietrobon D (2010b). Insights into migraine mechanisms and $Ca_V2.1$ calcium channel function from mouse models of familial hemiplegic migraine. *J. Physiol.* 588:1871–78.

Pietrobon D, Moskowitz MA (2013). Pathophysiology of migraine. *Annu. Rev. Physiol.* 75:365-91.

Pietrobon D, Striessnig J (2003). Neurobiology of migraine. *Nat. Rev. Neurosci.* 4:386-398.

Pilati N, Forli A, Sessolo M, Pietrobon D (2013). Differential effect of familial hemiplegic migraine mutations on excitatory and inhibitory synaptic transmission between cortical pyramidal cells and somatostain-expressing interneurons. *XV National Congress of the Italian Society of Neuroscience*. Abstract.

Plenz D, Stewart CV, Shew W, Yang H, Klaus A, Bellay T (2011). Multi-electrode array recordings of neuronal avalanches in organotypic cultures. *Journal of Visualized Experiments*, (54), e2949. doi:10.3791/2949.

Poduri A, Lowenstein D (2011). Epilepsy genetics - past, present, and future. *Curr. Opin. Genet. Dev.* 21:325-32.

Poulet JF, Petersen CC (2008). Internal brain state regulates membrane potential synchrony in barrel cortex behaving mice. *Nature* 454 (7206):881-5.

Rajakulendran S, Graves TD, Labrum RW, Kotzadimitriou D, Eunson L, Davis MB, Davies R, Wood NW, Kullmann DM, Hanna MG & Schorge S (2010). Genetic and functional characterisation of the P/Q calcium channel in episodic ataxia with epilepsy. *J. Physiol.* 588:1905–1913.

Rigas P, Castro-Alamancos MA (2007). Thalamocortical Up states: differential effects of intrinsic and extrinsic cortical inputs on persistent activity. *The Journal of Neuroscience* 27(16):4261– 4272.

Russell JF, Fu YH, Ptáček LJ (2013). Episodic neurologic disorders: syndromes, genes, and mechanisms. *Annu. Rev. Neurosci.* 36:25–50.

Sanchez-Vives MV, McCormick DA (2000). Cellular and network mechanisms of rhythmic recurrent activity in neocortex. *Nat. Neurosci.* 3:1027–1034.

Sessolo M, Conti R, Merighi A, Pietrobon D (2011). P/Q- and N-type calcium channels cooperate to control neurotransmitter release at the excitatory and reciprocal inhibitory synapses between layer 2/3 pyramidal cells and somatostatin-expressing interneurons of the mouse somatosensory cortex. *Washington, DC: Society for Neuroscience Online*. Abstract.

Shew WL, Plenz D (2013). The Functional Benefits of Criticality in the Cortex. *Neuroscientist* 19:88-100.

Shu Y, Hasenstaub A, McCormick DA (2003). Turning on and off recurrent balanced cortical activity. *Nature* 423:288–93.

Silberberg G, Markram H (2007). Disynaptic inhibition between neocortical pyramidal cells mediated by Martinotti cells. *Neuron* 53:735–46.

Siniatchkin M, Sendacki M, Moeller F, Wolff S, Jansen O, et al. (2011). Abnormal changes of synaptic excitability in migraine with aura. *Cereb. Cortex* 22:2207–16.

Steriade M, Nuñez A, Amzica F (1993). A novel slow (< 1 Hz) oscillation of neocortical neurons in vivo: depolarizing and hyperpolarizing components. *J Neurosci.*13(8):3252-65.

Steriade M, Timofeev I, Grenier F (2001). Natural waking and sleep states: a view from inside neocortical neurons. *J. Neurophysiol.* 85(5):1969-85.

Stevens CF, Wesseling JF (1998). Activity-dependent modulation of the rate at which synaptic vesicles become available to undergo exocytosis. *Neuron* 21:415–424.

Timofeev I, Grenier F, Bazhenov M, Sejnowski TJ, Steriade M (2000). Origin of slow cortical oscillations in deafferented cortical slabs. *Cereb Cortex* 10:1185–1199.

Tsien RW, Lipscombe D, Madison D, Bley K, Fox A (1995). Reflections on calcium channel diversity, 1988–1994. *Trends Neurosci* 18:52–54.

Tottene A, Conti R, Fabbro A, Vecchia D, Shapovalova M, Santello M, van den Maagdenberg AM, Ferrari MD, Pietrobon D (2009). Enhanced excitatory transmission at cortical synapses as the basis for facilitated spreading depression in CaV2.1 knockin migraine mice. *Neuron* 61:762-773.

Turrigiano G (2011). Too many cooks? Intrinsic and synaptic homeostatic mechanisms in cortical circuit refinement. *Annu. Rev. Neurosci.* 34:89-103.

Valtorta F, Benfenati F, Greengard P (1992a). Structure and function of the synapsins. *J. Biol. Chem.* 267:7195-8.

Valtorta F, Greengard P, Fesce R, Chieregatti E, Benfenati F (1992b). Effects of the neuronal phosphoprotein synapsin I on actin polymerization. I. Evidence for a phosphorylation-dependent nucleating effect. *J. Biol. Chem.* 267:11281-8.

van den Maagdenberg AM, Pietrobon D, Pizzorusso T, Kaja S, Broos LA, Cesetti T, van de Ven RC, Tottene A, van der Kaa J, Plomp JJ, et al. (2004). A *Cacna1a* knockin migraine mouse model with increased susceptibility to cortical spreading depression. *Neuron* 41:701-710.

Vecchia D, Pietrobon D (2012). Migraine: a disorder of brain excitatory inhibitory balance? *Trends Neurosci*., 35(8):507-20.

Wang LY, Kaczmarek LK (1998). High frequency firing helps replenish the readily releasable pool of synaptic vesicles. *Nature* 394:384–388.

Waters J, Helmchen F (2006). Background synaptic activity is sparse in neocortex. *J Neurosci.* 26:8267–8277.

Welch KM (2005). Brain hyperexcitability: the basis for antiepileptic drugs in migraine prevention. *Headache* 45(Suppl 1):S25–S32.

Wester JC, Contreras D (2012). Columnar interactions determine horizontal propagation of recurrent network activity in neocortex. *The Journal of Neuroscience* 32(16):5454 –5471.

Wilent WB, Contreras D (2005). Dynamics of excitation and inhibition underlying stimulus selectivity in rat somatosensory cortex. *Nat. Neurosci.* 8:1364–1370.

Wilson C (2008). Up and down states. *Scholarpedia Journal* 3(6):1410.

Wimmer VC, Bruno RM, de Kock CP, Kuner T, Sakmann B (2010). Dimensions of a projection column and architecture of VPM and POm axons in rat vibrissal cortex. *Cereb. Cortex* 20:2265–2276.

Wirth C, Luscher HR (2004). Spatiotemporal evolution of excitation and inhibition in the rat barrel cortex investigated with multielectrode arrays. *J Neurophysiol.* 91:1635–1647.

Zucker RS, Regehr WG (2002). Short-term synaptic plasticity. *Annu. Rev. Physiol.* 64:355–405.